Lecture Notes in Electrical Engineering 741

Zahriladha Zakaria
Seyed Sattar Emamian *Editors*

Advances in Electrical and Electronic Engineering and Computer Science

Springer

Lecture Notes in Electrical Engineering

Volume 741

The book series *Lecture Notes in Electrical Engineering* (LNEE) publishes the latest developments in Electrical Engineering - quickly, informally and in high quality. While original research reported in proceedings and monographs has traditionally formed the core of LNEE, we also encourage authors to submit books devoted to supporting student education and professional training in the various fields and applications areas of electrical engineering. The series cover classical and emerging topics concerning:

- Communication Engineering, Information Theory and Networks
- Electronics Engineering and Microelectronics
- Signal, Image and Speech Processing
- Wireless and Mobile Communication
- Circuits and Systems
- Energy Systems, Power Electronics and Electrical Machines
- Electro-optical Engineering
- Instrumentation Engineering
- Avionics Engineering
- Control Systems
- Internet-of-Things and Cybersecurity
- Biomedical Devices, MEMS and NEMS

For general information about this book series, comments or suggestions, please contact leontina.dicecco@springer.com.

To submit a proposal or request further information, please contact the Publishing Editor in your country:

China

Jasmine Dou, Editor (jasmine.dou@springer.com)

India, Japan, Rest of Asia

Swati Meherishi, Editorial Director (Swati.Meherishi@springer.com)

Southeast Asia, Australia, New Zealand

Ramesh Nath Premnath, Editor (ramesh.premnath@springernature.com)

USA, Canada:

Michael Luby, Senior Editor (michael.luby@springer.com)

All other Countries:

Leontina Di Cecco, Senior Editor (leontina.dicecco@springer.com)

**** This series is indexed by EI Compendex and Scopus databases. ****

More information about this series at http://www.springer.com/series/7818

Zahriladha Zakaria · Seyed Sattar Emamian
Editors

Advances in Electrical and Electronic Engineering and Computer Science

Springer

Editors
Zahriladha Zakaria
Faculty of Electronic Engineering
and Computer Engineering
Centre for Telecommunication
Research and Innovation
Universiti Teknikal Malaysia Melaka
Melaka, Malaysia

Seyed Sattar Emamian
Sigma Research and Consulting
Delft, Zuid-Holland, The Netherlands

ISSN 1876-1100 ISSN 1876-1119 (electronic)
Lecture Notes in Electrical Engineering
ISBN 978-981-33-6489-9 ISBN 978-981-33-6490-5 (eBook)
https://doi.org/10.1007/978-981-33-6490-5

This Springer imprint is published by the registered company Springer Nature Singapore Pte Ltd.
The registered company address is: 152 Beach Road, #21-01/04 Gateway East, Singapore 189721, Singapore

Preface

This book presents a compilation of research works covering the fields of computer science, electrical and electronic engineering. All manuscripts in this volume were presented during the 2nd International Conference on Computer Science, Electrical and Electronic Engineering 2020 (ICCEE 2020) which was conducted through a virtual presentation on 18 August 2020. This conference holds a vital role in as a catalyst in seeking wisdom, sharing thoughts and opinions to promote better understanding of engineering and information technology and to strive for quality research towards Fourth Industrial Revolution (IR 4.0).

The editor(s) of the proceeding would like to express the utmost gratitude and thanks to all reviewers in the technical team for making this volume a success.

Delft, The Netherlands — Dr. Seyed Sattar Emamian
Melaka, Malaysia — Prof. Dr. Zahriladha Zakaria

Acknowledgments

The editors would like to thank all the members of the local organizing committee who helped organize the 2nd International Conference on Computer Science, Electrical and Electronic Engineering 2020 (ICCEE 2020), which was conducted through a virtual presentation on 18 August 2020. We would like to thank the colleagues and staff members at the institutions and organizations that served as partners for the international conference. Their support in organizing a successful conference has helped the editors to gather ideas and papers presented in this book. The editors are grateful to all the speakers who attended the conference and shared from their wealth of experience some exciting findings who have further propelled us to publish this book.

The editors also appreciate various people, including the production team at Springer, who helped and contributed to the creation of this book. We thank all the authors and contributors who presented at the conference and sent us their papers for peer-review. The editors would like to thank and appreciate the peer-reviewers for their suggestions, comments, efforts and time spent to go over all the papers. The creation of this book has helped us to become a formidable team. The process has been enjoyable, challenging, inspiring and more peaceful than we ever thought. We thank you all!

Delft, The Netherlands — Dr. Seyed Sattar Emamian
Melaka, Malaysia — Prof. Dr. Zahriladha Zakaria

Contents

A Mobile Augmented Reality Interface on Additive Manufacturing

Yih Bing Chu and Chee Wah Chang

Abstract The increasing customized and complexity of products makes the handling of additive manufacturing becomes more sophisticated. Amidst the growing demands of personalized product, interpretation of input from customer to the specification of product is now a challenge for the industry. In view of this, augmented reality (AR), a technology which projects virtual content of target object on real world scenery can be used to interpret the design information and project the detail onto display accordingly. Through visual interaction, the technical information on additive manufacturing can be easily visualised and flow of the process can be managed and planned on preliminary before actual production. This helps prevent the misunderstanding of information conveyed through verbal communication and subsequently satisfactory of the product fabricated is of definite guarantee. As such, a mobile AR interface to visualise additive manufacturing is proposed. In this work, cloud database is integrated to the AR system to enable online information retrieval on the product material. Overall, a prototype system has been developed and evaluation of the usability of the AR interface has been conducted. The mobile application is essential to guide operators and could possibly be used to design additive manufacturing process.

Keywords Augmented reality · Additive manufacturing · Mobile visualisation · Assisted maintenance · Virtual simulation

1 Introduction

Additive manufacturing (AM) is a process to fabricate parts or products from a 3 dimensional (3D) digital model by depositing the material in layer by layer custom. With the aid of computer-aided-design (CAD) technology, design of a complex 3D structure can then be transformed into a digitalized data for computerized printing

Y. B. Chu (✉) · C. W. Chang
Tunku Abdul Rahman University College, Kuala Lumpur, Malaysia
e-mail: allan.chu.y.b@gmail.com

Z. Zakaria and S. S. Emamian, *Advances in Electrical and Electronic Engineering and Computer Science*, Lecture Notes in Electrical Engineering 741,
https://doi.org/10.1007/978-981-33-6490-5_1

[1]. Manufacturing that incorporates AM aims to minimize the cost of production results from customized fabrication of tailored-made products. Progressively, the technique allows fast printing of complex structures with lower material wastage and subsequently improves the yield of production [2]. Till date, AM has gained much popularity since its first inception in the 1980s. Nowadays, the technology can be found in application such as medical [3, 4], electronics [5], mechanical assembly [6], automotive industry [7] and so on.

Despite the appealing image of AM in the era of industry 4.0, the market is consistently challenged by the continuous changes of customer demand [8]. Generally, these changes are unpredictable and varied through time. Although characterization can be performed to model the specification of customer, mapping the data to the specific production batch for customized fabrication can be very complex. Moreover, in addition to the competitive and fast-growing market, manufacturers are in short to coordinate their manufacturing platform to match these changes in real time. Hence, there is a need to standardize the manufacturing process to be responsive to changes in customer demand and ultimately ensuring customer satisfaction.

Augmented reality (AR) is an emerging technology that creates visual perception of physical object in real-world environment via computer techniques. Particularly in manufacturing, AR helps improve customer satisfaction, creates a much interactive user interface, assist in understanding complex manufacturing operations and also improve efficiency of production plant [9–12]. Recently, researchers have demonstrated a working AR to output context aware information to support maintenance and assembly process [10, 13]. The proposed AR interface is able to improve efficiency of the manufacturing process by means of adaptive knowledge transfer to the worker in real time. Equally, if the information is readily accessible and visualised to customer, uncertainties to the desired specification of the finished product can be managed prior to actual fabrication. This enables the fabrication of customized product in batch production settings and in addition reduces the expenses needed for a similar fabrication in a customized manufacturing plant. On the other hand, with the augmented visualisation of product, customer can then customize the process of additive manufacturing based on own preference and thus improve customer satisfaction.

In view of this, development of an augmented interface to visualise AM process of personalized product is both strategic and advantageous. Therefore, the objective of this research is to design and create a user-oriented augmented display to interface AM for fabrication. Specifically, firebase, a mobile development platform is integrated to the proposed AR for remote data retrieval of AM. In this paper, an implementation of cloud database integrated AR to personalize product is presented. At the same instance, the virtual reality system serves as a visual interpretation, simulation tool as well as modeling platform to characterize 3D prototyping of customized product.

The remainder of this paper is structured as follows: Sect. 2 outlines the related works; Sect. 3 describes the initial implementation of the augmented reality system on Ender 3 3D printer; Sect. 4 demonstrates an evaluation of the augmented reality

system in a real-world application; Sect. 5 draws the conclusions, limitations and future improvement of the work.

2 Related Works

The term "augmented reality" was first coined by Caudell and Mizell when their developed an experimental AR system on wiring harnesses [14]. Throughout the decade, it can be observed that AR has been increasingly used for researches in manufacturing industry. In research, the group of A. Y. C. Nee and S. K. Ong has been actively committed to the development of AR system. In 2012, Zhu et al. [15] have developed an authorable context-aware AR system to aid maintenance operator. Using marker based tracking method, the AR content is generated on mobile user interface in real time. Overall, the proposed system enabled the operators to update the rendered AR content on-site and successfully implemented in a CNC milling machine a year later [16]. During the same year, Wang et al. [17] from this group have introduced an interactive AR interface to aid manual assembly of knuckle joint. To augment the assembly sequence accordingly, the group adjust the orientation of the virtual joint based on the orientation of hand movement. This omits the necessity of an auxiliary computer-aided design (CAD) information and reduce the preparation time upon actual assembly. After another year, Fang et al. [18] have presented an AR interface to plan robot path. An Euclidean distance based method has been developed to interface human command to virtual robot in AR environment. Till recently, Wang et al. [9] demonstrated an ubiquitous AR for shop floor planning. In this work, genetic algorithm has been used for dynamic task scheduling of shop floor in real time. The proposed AR system will assign maintenance task to on-site operator should the machine experience breakdown.

Aside that, AR solution has been explored to customize design for children footwear [19]. In this work, marked stocking is used for augmenting virtual footwear on the foot of customer. The environment is consistently captured by a KINECT sensor and as such enabled real time foot tracking of customer. Never the less, maintenance is still the major focus for most AR researches [20]. It is found that the augmented content helps reduce the maintenance time and hence leading to an improved efficiency. Interestingly, some researches claimed that by projecting the augmented content on large screen, the augmented instructions managed to help reduce the completion time of maintaining a motorbike engine [21]. Furthermore, some researchers even converted the maintenance instruction as standard symbol for visualisation [22]. Overall, the researches on AR are mainly augmented on a marked object and are focused on overlapping the information on a real time recorded environment background.

This paper focuses on development of an AR system to visualise additive manufacturing. As mobile devices are used in this work, sophisticated setup such as high end camera and headset is omitted. Moreover, since edge detection is employed to track the target object, physical markers that require precise settings

can be excluded as well. This work presents an interactive mobile interface featuring two modes of visualisation: first mode is to augment maintenance instructions onto the virtual manufacturing station. Second mode observes a virtual simulation scene for the additive manufacturing process. The development of AR system in this work is performed using Unity 3D and Vuforia for their robust tracking capability. In addition, Firebase is integrated to the AR to augment specific content from the server onto the mobile screen. For simplicity, Ender 3 3D printer is setup as the additive manufacturing station for this work.

3 Results

The work proposes development and implementation of an augmented interface on mobile devices. The augmented virtual model should visualise maintenance, simulation of additive manufacturing process and contain the integration of cloud server for information retrieval. In this work, One Plus 5 was used to run the developed mobile application. The architecture of the proposed system is illustrated in Fig. 1.

3.1 Target Tracking

The first part of the work is focused on tracking or recognition of target object to be displayed onto the mobile screen. In view of the aforementioned advantages, this paper demonstrated edge detection method instead of the marker based solution.

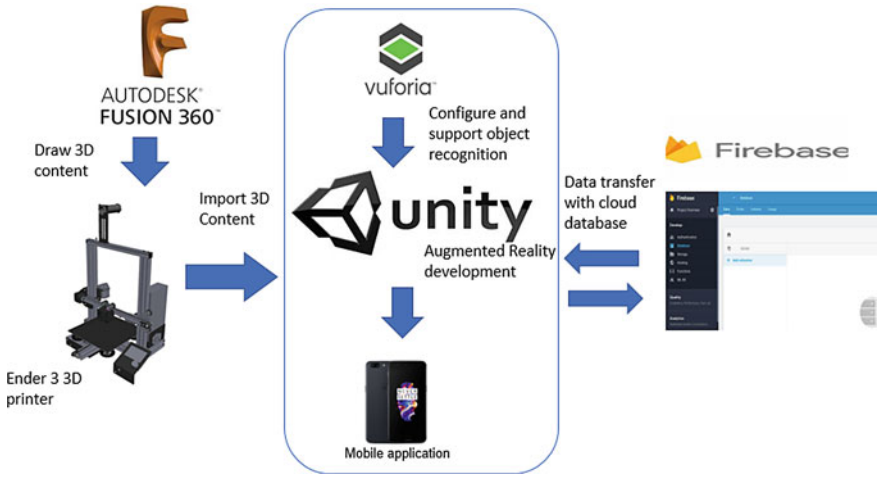

Fig. 1 Architecture of the proposed augmented reality interface

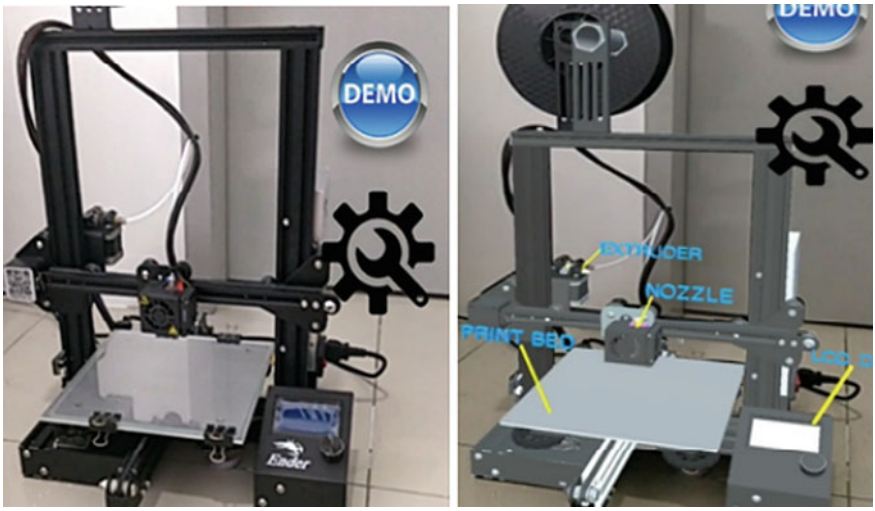

Fig. 2 The AR interface prior to object tracking (left) and after target recognition (right)

Figure 2 (left) presents the AR scene prior to target tracking. Once the edges set in the AR system matches physical outline of the machine, virtual model of the setup will overlap the actual station in real time. To create a much realistic AR scene, the edge layout is rendered invisible on the AR scene [23].

Secondly, the work focused on creating the virtual object of the manufacturing station. To project the virtual model of the target station, the 3D digitalized content of the machine is required. In this work, Autodesk Fusion 360 was used to design and construct the 3D content of the manufacturing station. Based on Fig. 1, Vuforia engine is integrated to enable object recognition and robust tracking onto the Unity 3D development platform. The virtual model shown in Fig. 2 (right) is the 3D content drawn using Fusion 360.

3.2 Assisted Maintenance

This section visualises the maintenance and servicing of the 3D printer. Generally, the maintenance information is augmented as text on the AR scene to suggest solution for the particular maintenance activities. The instructions provided on the maintenance activities are based on the possible causes of failure and its corresponding resolve action. In cases of breakdown, the activities shown on the augmented instructions should be conducted. Instead of manual diagnostic, the AR system illustrated graphical presentation of the augmented command for assisted maintenance. Since the time for lookup of manual is reduced, the downtime of maintenance is also decreases and hence leading to higher efficiency of additive

manufacturing. To improve the interaction with user, the augmented content is presented with symbol, textual and intuitive presentation. While symbol and textual describes the maintenance information as augmented logo and instruction respectively, intuitive presentation allows better understanding of the maintenance instructions with projected graphical content.

4 System Implementation

The intuitive presentation of the maintenance instruction is realized with object transformation of the manufacturing station. To convert manufacturing station from position 1 to position 2, an object transformation matrix is applied.

$$\boldsymbol{O} = \boldsymbol{T} * \boldsymbol{o} \tag{1}$$

$\boldsymbol{O}$ is the new coordinate of object after oriented
$\boldsymbol{T}$ is the transformation matrix
$\boldsymbol{o}$ is the original position or orientation of object in world coordinate.

The transformation matrix $\boldsymbol{T}$ consists of a 3 × 3 rotational matrix r and translational vector t.

$$\boldsymbol{O} = \begin{bmatrix} \boldsymbol{r}_{11} & \boldsymbol{r}_{12} & \boldsymbol{r}_{13} & \boldsymbol{t}_x \\ \boldsymbol{r}_{21} & \boldsymbol{r}_{22} & \boldsymbol{r}_{23} & \boldsymbol{t}_y \\ \boldsymbol{r}_{31} & \boldsymbol{r}_{32} & \boldsymbol{r}_{33} & \boldsymbol{t}_z \end{bmatrix} * \begin{bmatrix} \boldsymbol{X} \\ \boldsymbol{Y} \\ \boldsymbol{Z} \\ 1 \end{bmatrix} \tag{2}$$

The system calculates the destination coordinate of the target object based on the transformation matrix. The outcome of this stage observes the object oriented in the AR scene. This approach omits complicated mapping of marker frame and the need for calibration of high-tech camera.

4.1 Maintenance of Nozzle

The maintenance operation of the nozzle is consisting of 3 steps. Figure 3 shows the maintenance scene of the proposed AR system. The operation involved unlocking the casing and fan cover to reach the nozzle. Graphical content of the parts and servicing steps were projected onto the AR scene. Servicing of the nozzle is essential since the filament for printing often clog at the nozzle and causes breakdown of the machine. In order to validate the developed AR mobile interface, a group of engineers aged within 22–29 years old were requested to perform the

maintenance task using the AR system. A survey which scaled from 1 (disagree) to 10 (agree) was given to the engineers and none of them had any experience on using AR for visualisation. Since manual lookup is omitted with the application of AR, the time on performing the task is expected to be shorten and hence increasing the efficiency of the maintenance task. Figure 4 shows the response of participants on the effectiveness of the AR system in improving efficiency of the maintenance operation.

Based on the response, it is worth noticing that all of the participants agreed on using the proposed AR system in improving the efficiency of maintenance. It was also found that the participants are more confident on servicing the nozzle using the AR system. In view of this, the developed AR interface is proved to be useful especially in training new staff on the aforementioned task.

4.2 Virtual Simulation

This section presents a virtual scene for user to visualise the additive manufacturing process. Figure 5 presents the virtual simulation scene for the additive manufacturing process. The AR scene allows user to visualise the process from various angles by dragging the screen in accordance to the finger movement. For simplicity,

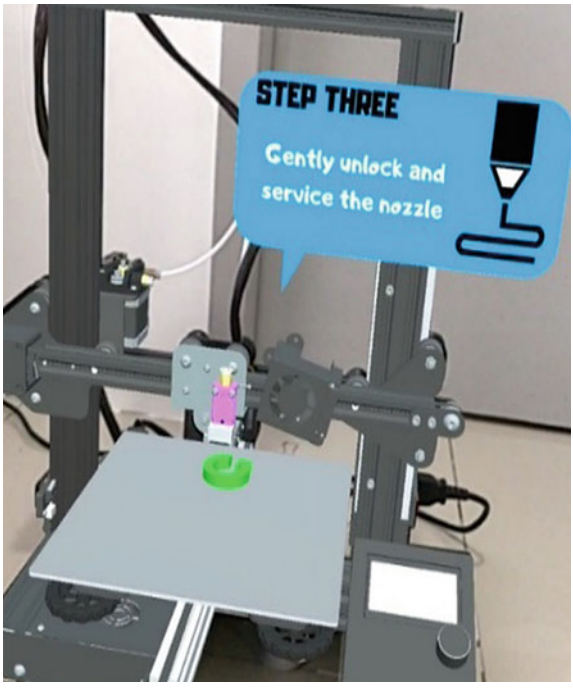

Fig. 3 Augmented reality presentation of the maintenance task

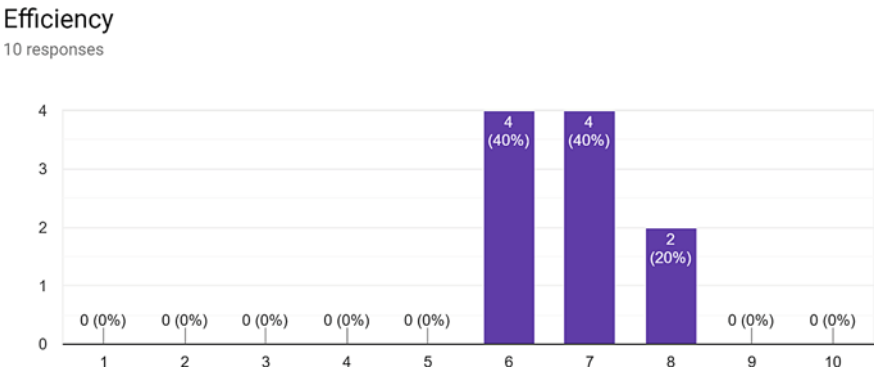

Fig. 4 Response of participants on the effectiveness of the developed AR system

this section simulates the product in shape of a 1000 cm^3 sized cubic. The rate of filament insertion in this simulation was set at 6.67 filament/sec and the filament size as well as printing height is of 0.2 mm^3.

The virtual model can easily be dragged into the station for simulation. However, due to the technical setting of the development platform, the 3D content

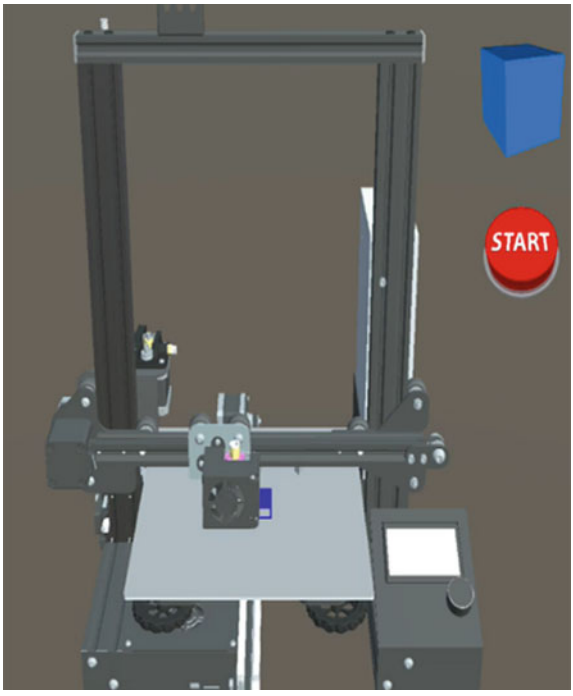

Fig. 5 Virtual simulation scene of the additive manufacturing process

cannot be automatically loaded into the virtual scene, and hence the virtual model to be visualised on simulation should be integrated into the platform in advanced.

Some technical difficulties were faced during the simulation. Foremost, the AR system experiences lagging upon simulation of the virtual models onto the scene which may be caused by the low memory or processing power of the mobile device used. Thus, for smoother operation, only one model (blue cube) is simulated on the AR scene. This section is important as it provides visualisation on the additive manufacturing pathway and the number of steps required to print the product. The information is especially useful to plan and design the manufacturing process with respect to the product requirement. A similar survey which is scaled from 1 (agree) to 10 (disagree) was given to the participants to assess their experience in using the AR interface. From the survey, it can be evaluated that the mobile AR interface is easily used and comfortable for usage to user. The participants also responded that, the AR system assisted them to properly visualise the technical aspect of the fabrication and the desired product feature prior to actual fabrication. Figures 6 and 7 shows the response of participants on the feature and conveniency of the developed AR system respectively. As the AR provides virtual simulation, misunderstanding of product enquiry and wrong fabrication of unwanted product can be prevented. The AR interface is compatible for installation on mobile device and convenient for visualisation at any time. Never the less, further standardization of the AR interface and simulation on sophisticated product is still required in the future.

4.3 Cloud Database

In this work, the AR interface is integrated with a cloud database for online information retrieval. Figure 8 presents the context ontology for the cloud database service.

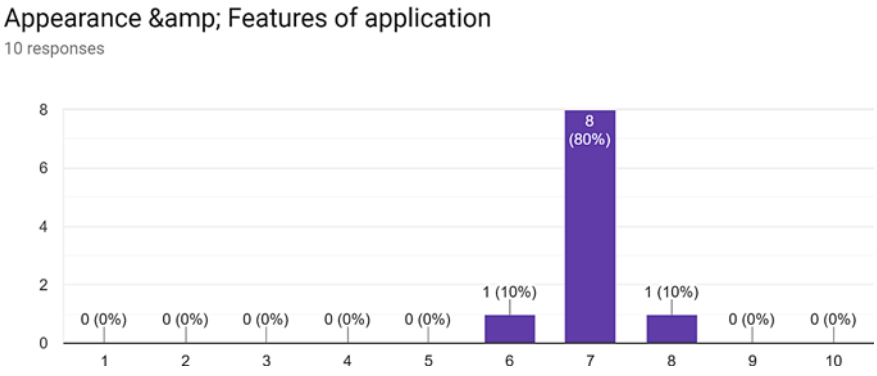

Fig. 6 Response of participants on the appearance and feature of the developed AR system

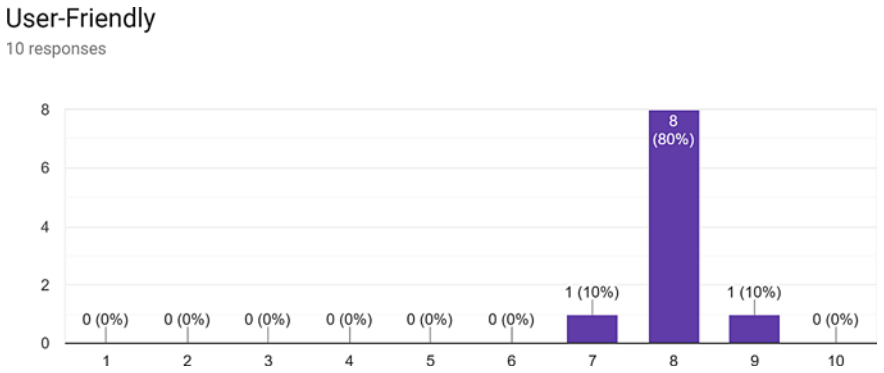

Fig. 7 Response of participants on the conveniency of the developed AR system

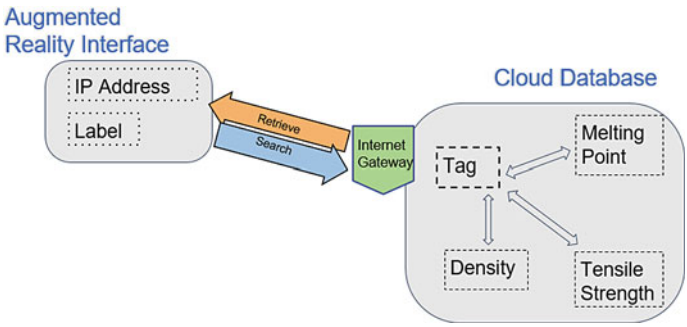

Fig. 8 Context ontology of the cloud database service

An internet connection is required to access the content in database. For better user experience, the internet address to retrieve the information has been preliminary hardcoded into the AR system. User is required to key in the name of the product material on the search bar in order to activate this operation. The label in the AR scene should match the tag referring to the respective information and output the information onto the mobile screen accordingly. For implementation purpose, only basic information of the product material such as melting point, tensile strength and density were programmed into the mobile application. Once a valid entrance has been keyed, the developed application will automatically retrieve the information from cloud. Figure 9 shows the coding used to retrieve information from the cloud database to the developed AR system.

The above work presents an implementation of a markerless mobile AR interface to visualise additive manufacturing. There are two important contributions; (1) assisted maintenance on the 3D printer using the developed AR interface, (2) virtual simulation of the additive manufacturing process. The developed AR allows retrieval of technical information related to the manufacturing process from a

```
        private void GetDataFromFirebase()
{  RestClient.Get<filamentInfo>(url: "https://unitytest2bbdd.firebaseio.com/" +
          searchFilament.text + ".json").Then(onResolved: response =>
              {
                 user = response;
                 UpdateScore();
              }); }
```

Fig. 9 Code to automatically retrieve information from the cloud database

dedicated cloud database. The integration is meant for implementing Industry 4.0 into the AR technology. Never the less, further development and research is still required in order to develop and standardize the use of AR in the manufacturing industry. The developed AR is able to visualise the additive manufacturing process of desired product on own try-on. Overall, credits to the mobile framework, the developed mobile AR interface omit the use of expensive camera and sophisticated maker alignment. Based on the survey, the mobile application developed is in agreement useful in terms of improving efficiency and in guiding staff especially to first-time learner. On the whole, the proposed AR system has been developed and the functions have been tested accordingly.

5 Conclusions

In the presented work, AR was implemented to visualise additive manufacturing process. The proposed approach incorporated virtual simulation for user to visualise the production. In addition, database was integrated into the AR for data transfer purposes. As there is a growing interest of manufacturing trend shifting to product customization, the developed AR system may serve as solution to interpret customer demand into product specifications. Based on the evaluation, although AR is not dominantly used in manufacturing, it may prove helpful in the field of design for additive manufacturing. Especially in the consultation stage, the use of AR can help avoid misunderstanding in the product requirement which may lead to additional costs for reproducing the product.

Future work will focus on expanding the feature of AR. Expansion to include new materials such as biomaterials, metals and alloys and their specification in additive manufacturing is anticipated. The development of AR on additive manufacturing of highly customized product for various functions and applications is also part of the research interest. By looking at the system performance, research on hardware which supports the AR is also important. The research on testing and application of AR in additive manufacturing still require further standardization.

References

1. Chergui A, Hadj-Hamou K, Vignat F (2018) Production scheduling and nesting in additive manufacturing. Comput Ind Eng 126:292–301
2. Culmone C, Smit G, Breedveld P (2019) Additive manufacturing of medical instruments: a state-of-the-art review. Addit Manuf 27:461–473
3. Javaid M, Haleem A (2018) Additive manufacturing applications in medical cases: a literature based review. Alexandria J Med 54(4):411–422
4. Javaid M, Haleem A (2019) Current status and challenges of additive manufacturing in orthopaedics: an overview. JCOT 10(2):380–386
5. Tan HW, Tran T, Chua CK (2016) A review of printed passive electronic components through fully additive manufacturing methods. Virtual Phys Prototyping 11(4):271–288
6. Sossou G, Demoly F, Montavon G, Gomes S (2018) An additive manufacturing oriented design approach to mechanical assemblies. J Comput Des Eng 5(1):3–18
7. Leal R, Barreiros FM, Alves L, Romeiro F, Vasco JC, Santos M, Marto C (2017) Additive manufacturing tooling for the automotive industry. Int J Adv Manuf Tech 92:1671–1676
8. Roblek V, Mesko M, Krapez A (2016) A complex view of industry 4.0. SAGE Open 6(2):1–11
9. Wang X, Yew AWW, Ong SK, Nee AYC (2020) Enhancing smart shop floor management with ubiquitous augmented reality. Int J Prod Res 58(8):2352–2367
10. Erkoyuncu JA, Amo IFD, Mura MD, Roy R, Dini G (2017) Improving efficiency of industrial maintenance with context aware adaptive authoring in augmented reality. CIRP Ann Manuf Techn 66(1):465–468
11. Flavián C, Ibáñez-Sánchez S, Orús C (2019) The impact of virtual, augmented and mixed reality technologies on the customer experience. J Bus Res 100:547–560
12. Syberfeldt A, Danielsson O, Holm M, Wang L (2015) Visual assembling guidance using augmented reality. Procedia Manuf 1:98–109
13. Osorio-Gomez G, Vigano R, Arbelaez JC (2016) An augmented reality tool to validate the assembly sequence of a discrete product. IJCAET 8(1–2):164–178
14. Bottani E, Vignali G (2019) Augmented reality technology in the manufacturing industry: a review of the last decade. IISE Trans 51(3):284–310
15. Zhu J, Ong SK, Nee AYC (2013) An authorable context-aware augmented reality system to assist the maintenance technicians. Int J Adv Manuf Tec 66:1699–1714
16. Zhu J, Ong SK, Nee AYC (2015) A context-aware augmented reality assisted maintenance system. Int J Comput Integ M 28(2):213–225
17. Wang ZB, Ong SK, Nee AYC (2013) Augmented reality aided interactive manual assembly design. Int J Adv Manuf Tech 69:1311–1321
18. Fang HC, Ong SK, Nee AYC (2014) A novel augmented reality-based interface for robot path planning. Int J Interact Des Manuf 8:33–42
19. Luh YP, Wang JB, Chang JW, Chang SY, Chu CH (2013) Augmented reality-based design customization of footwear for children. J Intell Manuf 24:905–917
20. Mourtzis D, Zogopoulos V, Vlachou E (2017) Augmented reality application to support remote maintenance as a service in the robotics industry. Procedia CIRP 63:46–51
21. Fiorentino M, Uva AE, Gattullo M, Debernardis S, Monno G (2014) Augmented reality on large screen for interactive maintenance instructions. Comput Ind 65(2):270–278
22. Scurati GW, Gattullo M, Fiorentino M, Ferrise F, Bordegoni M, Uva AE (2018) Converting maintenance actions into standard symbols for augmented reality applications in industry 4.0. Comput Ind 98:68–79
23. Brito PQ, Stoyanova J (2018) Marker versus markerless augmented reality. which has more impact on users? Int J Human-Comput Int 34(9):819–833

Safety Risk Assessment and Warning System at Engineering Laboratory Through IoT Technologies

Seerla Kanagarajoo Betharajoo, Sivajothi Paramasivam, and H. S. Chua

Abstract Common contributing factors associated to accidents or near-misses in laboratories arises due to risks related to improper use or maintenance of laboratory test equipment and machine. Hence, maintenance and regular inspection of laboratory test equipment and machine are essential parts of safety activity. The project exploits dominance of Internet of Things (IoT) used in many applications to leverage combination of networks and radio frequency identification (RFID) tags technologies to gauge safety risks associated with laboratory inventory in an automated manner. Thus, this paper makes the following contributions:(1) developed an automated inventory laboratory management system that enable test and measurement equipment and machine to be traceable by RFID technology (2) generated an analysis output using informatics as a diagnostic component to improve safety risks presented by test and measurement equipment and machine and (3) developed a graphical user interface that served as the graphical output in monitoring and controlling safety status. Critical issues associated with safety risks which include maintenance schedules, calibration dates, outdated equipment and inventory of equipment are gauged by this system. Subsequently it successfully provides graphical notification on each issue which reflects intact, caution and warning status with green, yellow and red colour codes respectively. In addition, graphical information highlights percentage of progress to stress the severity of the evaluated issue to the technical personnel. This smart system initiates electronic-mail notification to prompt proactive actions to be taken by the technical personnel in a timely manner to mitigate potential accidents or near-misses within the laboratory settings.

Keywords Inventory management · Engineering laboratory · Internet of things · RFID · Networks · Safety risk

S. K. Betharajoo · S. Paramasivam (✉) · H. S. Chua
School of Engineering, University of Wollongong Malaysia KDU, Glenmarie Campus, Shah Alam, Selangor, Malaysia
e-mail: siva@kdu.edu.my

Z. Zakaria and S. S. Emamian, *Advances in Electrical and Electronic Engineering and Computer Science*, Lecture Notes in Electrical Engineering 741,
https://doi.org/10.1007/978-981-33-6490-5_2

1 Introduction

As teaching and research activities are becoming more complex; academic institutions are aware of and acknowledge that experiments have not always been done without laboratories accidents and near-misses. The reason being problems with test equipment and machine may present in many ways during laboratories session which potentially pose safety hazard such as danger of electrical shock, and some equipment can cause physical cuts and emit dangerous sparks. Common contributing factors associated to laboratories accidents or even near-misses arises due to risks related to improper use or maintenance of laboratory test equipment and machine. Hence, maintenance and regular inspection of laboratory test equipment and machine are essential parts of safety activity.

As technology has advanced, test and measurement equipment are developed for measuring ever more complex parameters to ever increasing levels of precision and accuracy. Thus, these come at an increased cost and large investment for both acquisition and maintenance. The situation is further compounded as majority of acquired test and measurement equipment of advanced technologies and developing materials introduce new safety and quality risks that has high potential to create harm to stakeholders involving academic staffs, technicians, students, apprentices, administrative staffs, short term visitors as well as vendors and suppliers if not properly used or maintained [1].

Studies have indicated that in many engineering teaching and research laboratory settings safety culture has been the prime focus to prevent accidents or injuries as these occur through lack of knowledge of safety risks involving test and measurement equipment and machine. According to a student was killed by a machine–shop equipment while carrying out experiments in the laboratory [2, 3]. An alarming finding revealed that laboratory accidents, both in teaching and research laboratories, represented 18.4% of the total incidents reported at Iowa State University from 2001 to 2014, and dominantly victims involve students and employees [4]. Consequently, gravely emphasizes that academic laboratories are more dangerous because of the lacklustre attitude approach towards safety specifically in maintaining functional quality of various test and measurement equipment and machine in an effective and systematic manner.

Laboratory management is a very important element specifically in ensuring safety aspect of academic and research laboratory activities. Most cases in the past event where accidents in laboratory happened are due to the failure of keeping track those faulty and non-functional test and measurement equipment and machine, which are also closely related to the poor inventory and maintenance system.

It is against this backdrop that this paper makes the following contributions: (1) developed an automated inventory laboratory management system that enable test and measurement equipment and machine to be traceable by RFID technology (2) generated an analysis output using informatics as a diagnostic component to improve safety risks presented by test and measurement equipment and machine and (3) developed a graphical user interface that served as the graphical output in

monitoring and controlling safety status. Thus, it is envisaged that efficient inventory maintenance and control implementation would yield a high degree of accountability in detecting risks and safety related to use of test and measurement equipment and machine.

2 Academic Laboratories—Significance on Assessment of Resources

Laboratory is as an integral part of academic resource in engineering education as it forms as the primary vehicle where basic experimental skills are learnt by systematically performing a set of prescribed and suitably designed experiments. As such, these laboratories supporting various engineering disciplines houses an array of hand tools, test and measurement equipment and machine.

In these settings, students are to carry out experiments by making all the required connections of the laboratory equipment, and then they manually operate tools and machinery in order to execute experimental exercises. Thus, prompts a query whether usage of various test and measurement equipment and machine meets the desired safety compliance in preventing accident or severe injuries during laboratories session [1].

In this connection, safety risks associated with array of hand tools, test and measurement equipment and machine being used have received the most attention in the laboratory safety. As shown in Table 1, the most common equipment-related hazards in laboratories come from devices powered by electricity devices for work, materials driven by compressed gases or chemical and rotating equipment and machines or tools for cutting and drilling which account for the greatest frequency of laboratory accidents and injuries [5].

In light of the severity of the given cases, risk assessment on safety hazards within academic and research laboratory settings are the responsibility of all stakeholders specifically the technical support team who are tasked to ensure tools, test equipment and machines are always in healthy working conditions [9]. Consequently, safety risk can be identified in the event laboratory personal may

Table 1 A partial list of laboratory accidents at academic institutions (2006–2019) [6–8]

Year	Institution	Accident description
2006	Cleveland State University, USA	Staff died of electrocution of electrical device
2007	Indian Institute of Science, India	Researcher died of laboratory explosion
2009	Army Base—Iraq	Staff died of electrocution by machine
2011	Yale University, USA	Undergraduate died by rotating axis of lathe machine
2019	Technion, Israel Institute of Technology	Staff died due to explosion during materials experiments

notice or notified subtle changes such as drift in quality control or calibrator values, or obvious flaws in equipment function. This also entails soliciting feedback from co-workers and colleagues to improve safety and the process as there will be many errors and problems occurring that may go undetected. Thus, proper maintenance work of test and measurement equipment and machine in the laboratory is necessary to ensure accurate and reliable usage for experimental activity and learning needs with acceptable degree of safety aspect.

Thus, these arrays of resources require efficient and aptly smart system with a provision of monitoring and early alerting mechanism of flaws in equipment function or related issues that has direct bearing on addressing laboratories accidents and near-misses. As such, it is imperative that these academic resources are well maintained, serviced, tracked and recorded accurately in proper time schedule [10].

Engineering and research–related laboratory environment may involve a wide variety of safety hazards which include unguarded machinery and moving machinery parts; electrical hazards from test and measurement equipment and machine as well as malfunction and outdated equipment. In this relation, realization of development of safety control measures involving test and measurement equipment and machine in the inventory systems should be maintained and serviced periodically to ensure that laboratory services consistently meet the needs of teaching and learning situations at all times.

Conversely, the analysis of a well-defined scope of work in evaluating element of risk assessment that has direct bearing on safety hazard issues involve:

- maintaining good-quality tools, devices, equipment and machine
- removing and disposing of outdated equipment from use
- schedule calibration and performance evaluation
- perform maintenance work of equipment
- identifying equipment for repair work due to breakdowns and failures
- sustaining quality compliance on record keeping.

Well-designed laboratory facility that houses all the test and measurement equipment and machine adequately alone is insufficient to address improvement effort on safety risk to minimize or eliminate exposures of accident or injuries to laboratory personnel, community and environment. In fact, the laboratory management system, in its quest to formulate improvement effort on safety assessments and mitigation plans; documents and records of laboratory set ups are essential part of the inventory system.

Consequently, in order to retain and develop safe work performance within the engineering laboratory settings; use of informatics forms as a highly desirable solution to evaluate the risks presented by safety hazards.

In this relation, leveraging on development of Internet of things, quality assessment of inventory tracking and maintenance monitoring and early alerting mechanism can be automated by computerizing using cloud architecture and radio frequency identification (RFID) technology. The reason being the advanced

technology of RFID provides an efficient mode of assessing the risk revolving various equipment as it manage and communicate information on inventory details and specifications. In fact, RFID has gain increased attention recently for its use on remote storage and retrieval of data for many applications such as warehouses, production shop floors, logistics companies, distribution centers and retailers [11].

In addition, the graphical representation provides unique colour code indicator which uses colour codes to reflect status of the test and measurement equipment based on the level of risk and safety. In this relation, red colour is interpreted that it is in a critical level which will indicate on the service or is beyond repair condition. The yellow colour signifying a warning sign that the equipment service is almost due for service and maintenance. As of green, it is safe to operate the test and measurement equipment.

Thus, this entails embracing smart technology to automate and rely on an information system in critical decision making which is viewed as an effort on modernizing the quality system which has direct bearing on safety aspect of stakeholders.

3 Methodology

Although the laboratory adheres to basic safety regulations, this study is intended to further enhance improvement on safety risk of the test and measurement equipment through usage of informatics and RFID technology [12]. On the informatics section, visual basic is used to design and develop the GUI interface to relay vital information related to status of the test and measurement equipment via network. There will be two prong of monitoring whereby the first is to monitor on the safety risk status related to each test and measurement equipment in terms of maintenance and usage and the second is on the inventory management in meeting quality compliance on record keeping.

Basically, it keeps track of the equipment due date in terms of calibration date, maintenance date, retirement date and the list of equipment in the inventory. It alerts the lab support team if the date is approaching closer to due date.

3.1 Project Design and Settings

The layout design and installation of RFID system was tested in Electrical and Electronics Systems Laboratory which is located at the second floor of the University Campus. This particular laboratory houses many test and measurement equipment of different brands as well as technical specification. The complete floor layout of the laboratories under the School of Engineering is shown in Fig. 1.

The RFID antenna is mounted beside the exits of the laboratory whereby a pair of brackets are used to hold the antenna at an angle of 45° position to capture the

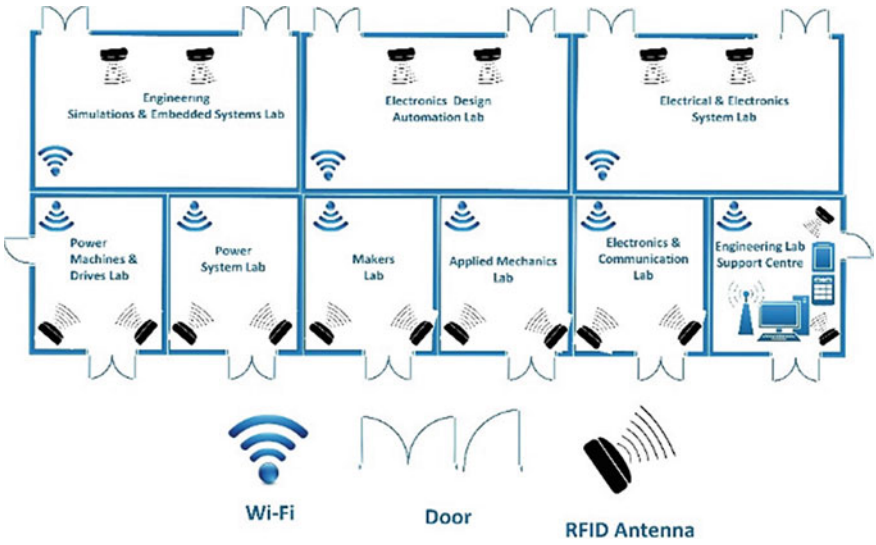

Fig. 1 Floor plan of all engineering laboratory system

best frequency range for the tags on the equipment. This particular laboratory houses 36 different test and measurement equipment which are tagged with a unique identification. The frequency range for this set up falls within 865–867 MHz frequency. A proposed distance between the two brackets are 2 m range and the height is in 2.5 m. A single reader is used and operate on a wireless mode to capture the data from the RFID antenna. This will well cover the area of the workstation containing the said number of equipment [13].

In the operational mode, the RFID reader performs a real time scan to check the availability of the test and measurement equipment at its designated workstation. In fact, a routine check on a timely manner is done to ensure their presence for inventory management. This is done by tracking the RFID tag which consist a unique identity for each equipment. This is shown in Fig. 2.

Fig. 2 The actual view of RFID antenna in electrical and electronic laboratory

Dominantly, the process involves, detection of a passive tag where by information in the tag will be read and send to RFID reader. In turn, it will be transmitted to the wireless link communication port. The data is transmitted via wireless router to a client computer in the engineering lab support centre which is located about four meters away. The data will updated in the client computer which is supported by a graphical user interface. The system configuration enables the users to access into the informatics system to do data retrieval or modification of data for analysis. The flow chart of this mechanism is shown in Fig. 3.

This entails the system to generate an analysis output using informatics as a diagnostic component by checking critical information pertaining to safety risk of various test and measurement equipment at the workstation. In fact, all this are able to be monitored using network and subsequently prompts vision base notifications onto the client computer of the laboratory support team.

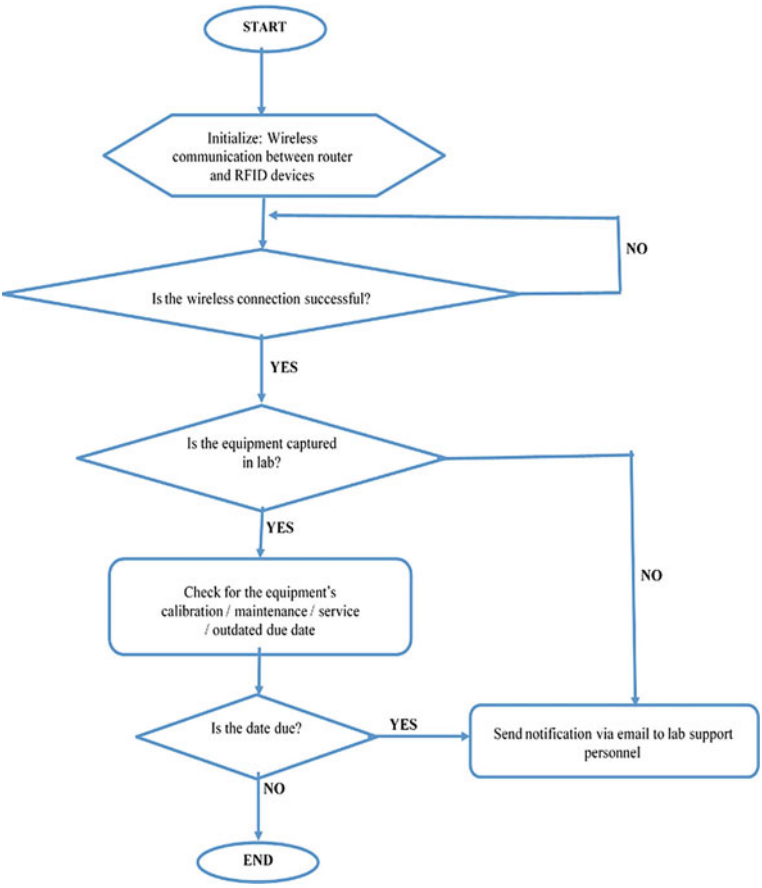

Fig. 3 The flowchart of the system

In addition the system updates the inventory database and eventually triggers a warning alert as part of security measure to notify if in the event of the equipment is absent at the workstation. As indicated, the system design uses a database to exhibit graphical output of safety risk status of test and measurement equipment that is not functioning and is beyond repair status, or when it is outdated lifespan and should be replaced and to the extent of calibration due of each equipment that are in the calibration list of the database.

3.2 *Database Design Settings*

The database system authorized to act both as an administrator and the user rights. In administrator mode, it permits to do all function including add or remove users and to update the inventory status, which includes borrowing out of the laboratory tools. In the user mode, it only permits to check the database, borrowed out of tools and receive the tools after usage of experimental session. In ensuring effective system control, only the administrator and assigned users have access rights.

Figure 4 shows the graphical user interface of logging in and main menu of the created the database system design.

As shown in Fig. 5, there will be four sub menus. Each sub menu has a database that performs the coded relating to its category. In fact, acts as a platform to view various relevant details which include the stock check to the borrowed details by authorized stakeholders. Critically, it also keeps track of maintenance, service and calibration due dates of each test and measurement equipment to the extent of the retiring due date.

In this graphical representation, critical details of the equipment's safety risk status is verified and assessed to reflect the condition of the equipment such that when it is faulty, is it a beyond repair status or under repair status. This is shown in Fig. 5.

In calibration alert page, calibration due dates will be checked and prompts timely indication to the relevant superior. Similarly, in the maintenance and service menu, dates would be checked on routine maintenance schedules and initiates alerting signal on a timely manner. This applies to the retiring (beyond lifespan) report.

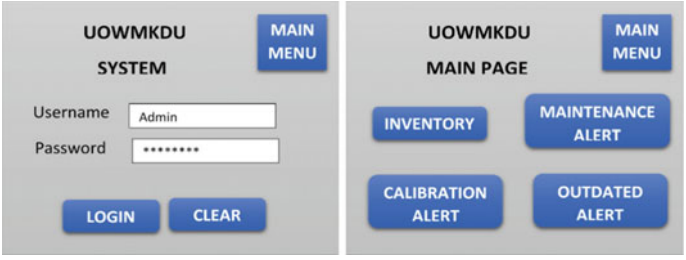

Fig. 4 Login page and main page

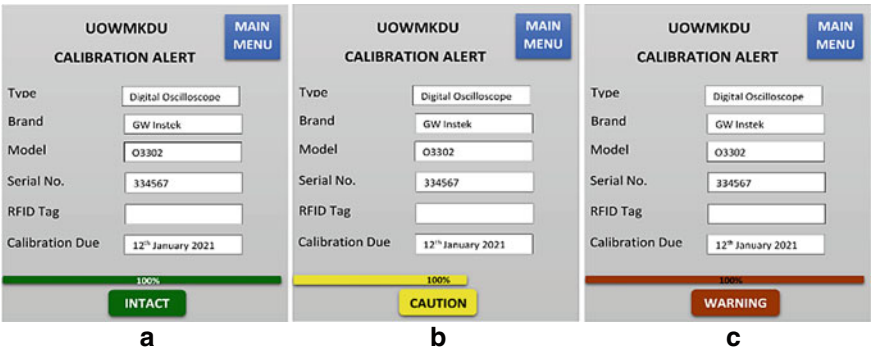

Fig. 5 Calibration alert page

In this setting, when the current date is within the due date, a green colour indicator is produced with a message "INTACT" is shown as illustrated in Fig. 5(a). In the event, the current date is approaching nearer to the due date, it will highlight yellow colour with a message "CAUTION" as illustrated in Fig. 5(b). Finally, when it is actually the due date or passed the due date, it will highlight red colour and shows "WARNING" message as illustrated in Fig. 5(c).

In addition, there will be a progress bar which will indicate of the time of expiry/due for the identified test and measurement equipment.

Under the maintenance alert page, maintenance and service schedules are crossed checked to ascertain and prompt these activities accordingly, Similarly, when the date sufficiently from due date, it will highlight green and display "INTACT" message as illustrated in Fig. 6(a). In the second scenario, when the date is approaching the due date, it will highlight yellow and show the message "CAUTION" as illustrated in Fig. 6(b) and when it is due date or pass due date, it will highlight red as and show the message "WARNING" illustrated in Fig. 6(c).

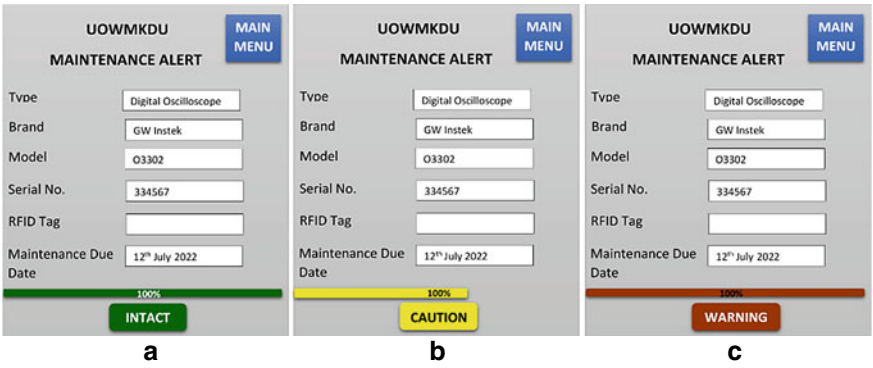

Fig. 6 Maintenance alert page

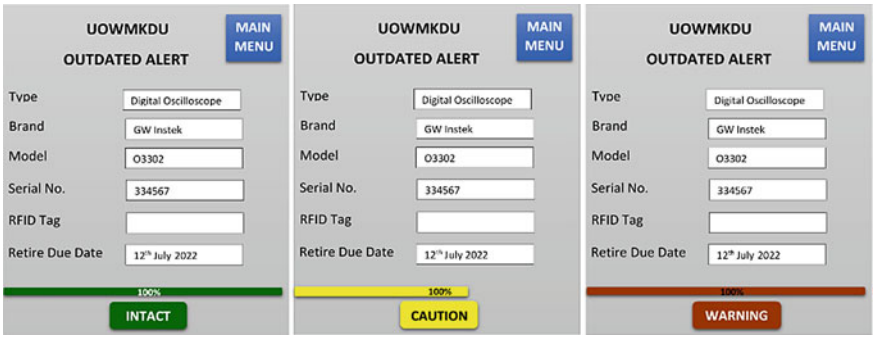

Fig. 7 Outdated alert page

In addition, there will be a progress bar which will indicate of the time of expiry/due for the identified test and measurement equipment.

In outdated alert page, the system will conduct a check on the purchase date to ascertain the life span of each test and measurement of the equipment. Base of the gathered data, notification will be prompted to highlight date of retirement has been reached and need to be removed from the workstation. As the equipment ages, the system will highlight the colour and message as illustrated in Fig. 7.

If the equipment is within the workable lifespan, the colour will be highlighted in green. In the second condition, if the lifespan is nearing expiry date, yellow colour is produced and over the lifespan reflects red colour. In addition, there will be a progress bar which will indicate of the time of expiry/due for the equipment.

As in any normal database system, it will store all the stock list and keep track of all available items at the lab. Besides that, it will keep track of all loaned items that have been loaned out to all staff and students. This will also show who is the person in charge who had released the items, whereby in such practice, the person will take responsible for any items that has been released out. If the item request is by an academic staff, therefore the responsibility can be set to that person and partly with the support person in charge of releasing the items.

4 Conclusion

- As an overall view, the system monitors critical status of various test and measurement equipment and update the lab support team on status which include due date of calibration, maintenance and service for individual equipment and machine as well as outdate equipment.
- This is to avoid any form of danger to occur as a safety precaution against the usage by the students and staffs.

- Besides that, this is also to monitor the location of the equipment or machine in order not to be misplaced or mixed up in another location.
- This system is developed with element of smart concept which would eventually triggers notification and generate different reports; thus ease the task of technical support team in sustaining quality compliance on record keeping and addressing issues on safety risk efficiently.
- As of the future development of the current system, an integration of smart application would be proposed for the mobile based application to link between the current system with the mobile application [14].

Acknowledgements The authors would like to thank Engineering Support Team, School Of Engineering for their kind support. We would like to acknowledge the equipment and technical knowledge support by University Of Wollongong Malaysia KDU, Glenmarie Campus.

References

1. Annisa N, Puteri F, Nurcahyo R (2018) Safety perceptions in university teaching laboratory
2. Meyer T (2012) How about safety and risk management in research and education? Procedia Eng 42:854–864. https://doi.org/10.1016/j.proeng.2012.07.478
3. Cho Nam, Ji Yong Gu (2016) Analysis of safety management condition & accident type in domestic and foreign laboratory. J Ergon Soc Korea 35:97–109. https://doi.org/10.5143/jesk.2016.35.2.97
4. Menard A Dana, Trant John (2019) A review and critique of academic lab safety research. Nat Chem 12:1–9. https://doi.org/10.1038/s41557-019-0375-x
5. Roy K (2016) Responding to laboratory accidents. Sci Scope 39(9)
6. Foderaro LW (2011) Yale student killed as hair gets caught in lathe. The New York Times
7. Bronstein S (2009) Multiple failures led to Iraq electrocution, pentagon says. CNN.com
8. Miller JD (2006) Ohio cites university in death. The Scientist Magazine®
9. Osang JE (2013) Evaluations of the effect of workshop/laboratory accidents and precautionary steps towards safety practice. IOSR J Electron Commun Eng 6(3):16–22
10. Khalidand M, Kadni T (n.d.) Safety enhancement through calibration and maintenance
11. Mohamad Z (2012) Laboratory quality management requirements of engineering at the polytechnics Ministry of Higher Education Malaysia
12. Hellström D, Wiberg M (2010) Improving inventory accuracy using RFID technology: a case study. Assembly Autom 30(4):345–351. https://doi.org/10.1108/01445151011075807
13. Chen ZN, Qing X (2010) Antennas for RFID applications. In: 2010 International workshop on antenna technology (iWAT). https://doi.org/10.1109/iwat.2010.5464865
14. Park S, Kim J, Kim J (2015) SLAN based user-customized cloud interface sharing for smart mobile devices. In: Kim K, Wattanapongsakorn N (eds) Mobile and wireless technology 2015. Lecture Notes in Electrical Engineering, vol 310. Springer, Berlin, Heidelberg

Optimization of PV Power Output Using Single-Axis Sun Light Tracker and MPPT Algorithm

Ryan Matthew Long, Ahmed. O. MohamedZain, H. S. Chua, J. Jamaludin, and K. M. Yap

Abstract The growth of global energy consumption and the depletion of the non-renewable recourses had caused many environment issues. These environmental issues and the demand of global energy had driven up the implementation of solar energy. The optimization of PV power output can be achieved using solar tracking and MPPT algorithm. Comparison of power output had been made with a system that does not have solar tracking to show the improvements made using a single axis solar tracking system. Power of 100 W solar tracker and two 50 W stationary panels connected in parallel. The values of the resistors of 4 and 8 Ω have been chosen based on the solar panels R characteristics. The system consists of three (3) important parts, software hardware, and electronic circuits. DC motor is used to rotate the solar PV panel (100 W) and Two (2) light dependent resistors (LDR) were used as light detectors. Solar tracker and stationary panels facing the East-West direction at University of Wollongon Malaysia KDU, Glenmarie Campus at the coordinates (3.092008, 101.559373). Two prototypes are built for data collection based on Arduino Mega 2560. An increase of 35–40% in power output compared to fixed rooftop installation.

Keywords Solar PV panel · Arduino mega controller · MPPT

1 Introduction

In this current era, there is an increasing need for energy, decrease in supply of fuel and more concerns about environmental issues when using non-renewable energy. This demand is shown in Fig. 1. It projects that the world energy consumption will

R. M. Long · H. S. Chua (✉) · J. Jamaludin
School of Engineering, University of Wollongon Malaysia KDU, Glenmarie Campus, Shah Alam, Malaysia
e-mail: hs.chua@kdu.edu.my

Ahmed.O. MohamedZain · K. M. Yap
HUMAC Research Centre School of Science and Technology, Sunway University, Bandar Sunway, Subang Jaya, Malaysia

Z. Zakaria and S. S. Emamian, *Advances in Electrical and Electronic Engineering and Computer Science*, Lecture Notes in Electrical Engineering 741,
https://doi.org/10.1007/978-981-33-6490-5_3

increase by 28% from 2015 to 2040 [1]. With high cost, limited sources of fossil fuels and worldwide primary energy consumption has grown by 1.8% in 2012 alongside with the need to reduce greenhouse gasses emission, renewable energy resources have become more attractive in the world's energy-based economics [2]. This has led researchers to find an alternative source of energy, which is renewable, and have less negative impacts on the environment such as photovoltaic/thermoelectric generator system (PV-TEG) [3]. In order to reduce the temperature of the PV cell, other researchers has investigated the effect of the temperature on the efficiency of the PV cell by conducting different types of methods [4]. Since the high temperature has a strong effect on the PV cell [5]. There are many renewable sources of energy such as Biomass energy, geothermal energy, Hydropower energy, Marine energy, solar energy and wind energy.

The Fig. 1 shows the ability of renewable energy sources to provide over 3000 times the current global energy needs and solar resource is the highest contributor with an amount of 2850 times the current global energy needs of 2014 [2]. This is because it is abundant across the Earth. The Photovoltaic cells also reduce the amount of carbon dioxide emissions. It is expected that by year 2030, the annual reduction rate of carbon dioxide due to PV cells may be around 1 Gton/year. This is the same amount of India's total carbon dioxide emission in 2004 or carbon dioxide emissions due to 300 coal plants. Many experts state that energy obtained from PV cells will be a very important renewable energy source until the year 2040 [6]. Solar energy is chosen as the energy to be optimized mainly because of its potentially infinite amount of energy supply, causing no air or water pollution.

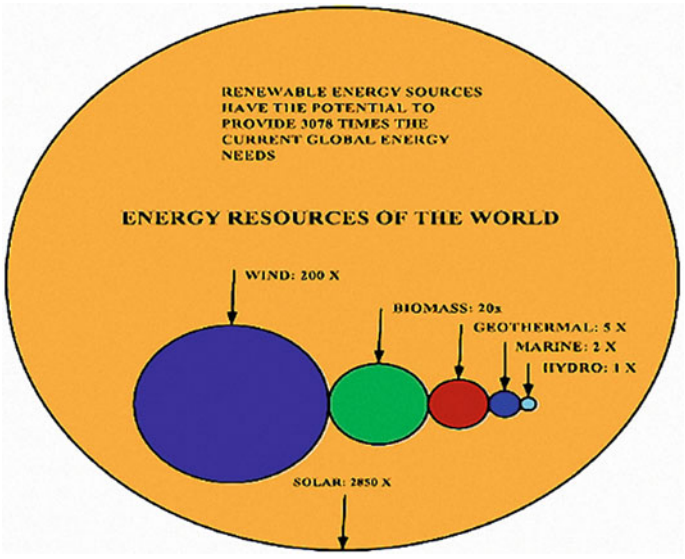

Fig. 1 Renewable energy resources of the world (Ellabban et al. [2])

2 Materials and Methods

An Arduino Atmega 2560 [7] is chosen to perform the functions as there are many pins on it and the experiment requires a lot of measuring and interfacing, it also has an ADC pin which is an analogue pin and can easily measure analogue data from the sensors required. A current sensor (ACS 712-20A) is used for this system. Its basic working principle is based on indirect sensing to determine the current passing through the wire. The voltage sensor is based on a simple voltage divider rule. The rating of the voltage sensor is any voltage below 25 V as the resistors used is to cater for this particular voltages. The Arduino Atmega 2560 is capable of changing is PWM frequencies to be up to 32 kHz easily with ease. This is another reason why the Arduino Atmega 2560 is chosen as the microcontroller used, so that the buck converter's MOSFET can be switched easily using the 5 V 32 kHz PWM pin. The complete system is shown in Fig. 2.

2.1 Solar Tracking Design

The solar 100 W PV panel was made to be imbalanced on the axle so that the auto gate motor can be the counter weight as shown in Fig. 3. The angle of the solar panel would be 45° to the horizontal axis to face either east or west with the 45° angle. The equipment used to move the structure of the solar tracker which is the Proton Wira power window motor which uses 12 V DC supply to control the turning of the solar panel based on the sensing of irradiance from the light dependent resistor circuit. The MD10C motor driver is used to control the motor. Pulse width modulation (PWM) is feed into the PWM pin of MD10C motor driver

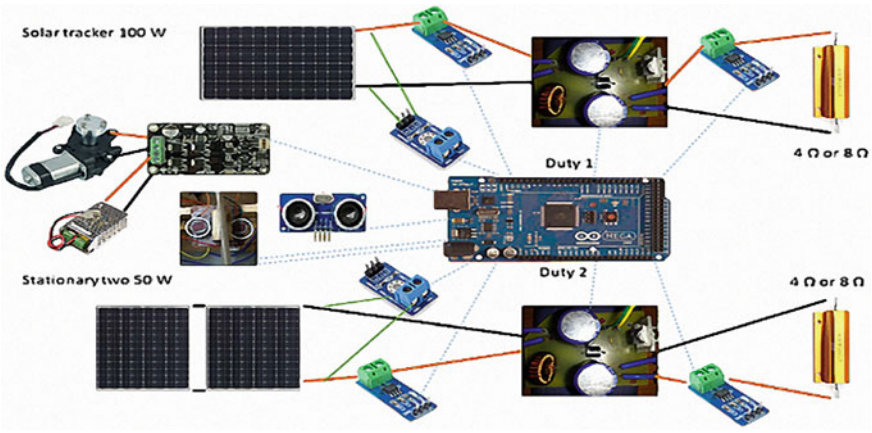

Fig. 2 Complete system of the diagram

to control the speed while DIR pin is used to control the direction and position of the solar panels. It is compared with a threshold and if it exceeds the threshold difference, it will move towards the direction of least resistance which means there is more irradiance.

2.2 Buck Converter Design

The buck converter [8] above works like a normal buck converter except the switching is controlled by the ground leg of the circuit whereby the output of the circuit is not grounded to the input of the circuit and is controlled by the IRF3205 MOSFET switch which is an n-type MOSFET which is required to switch the ground 'on' and 'off'. It is capable of turning 'off' and 'on' much higher currents than the gate pin of the MOSFET which is controlled by the Arduino Atmega 2560. The inductance value can be calculated as in Eq. (1):

$$L = \frac{D(Vs - Vo)R}{2f(Vo - Imin\ R)} \tag{1}$$

where D represents the duty cycle ratio of the PWM, Vs represents the voltage supply input, Vo represents the expected output voltage, R represents load resistance, f represents the switching frequency of the PWM and Imin represents the minimum current.

Based on the Eq. (1) above the assumptions are Vs = 19 V, Vo = 14 V, R = 8 or 4 Ω, f = 32 kHz, Minimum current = 0 A so that it will work in continuous mode. Even if minimum current increases, the inductance required will increase. Using the above assumptions the minimum inductance required is 44.64 µH. The inductance chosen is 100 µH that is capable of handling 5 A. The capacitance chosen at the input and output are the same which is 4700 µF. The input capacitor

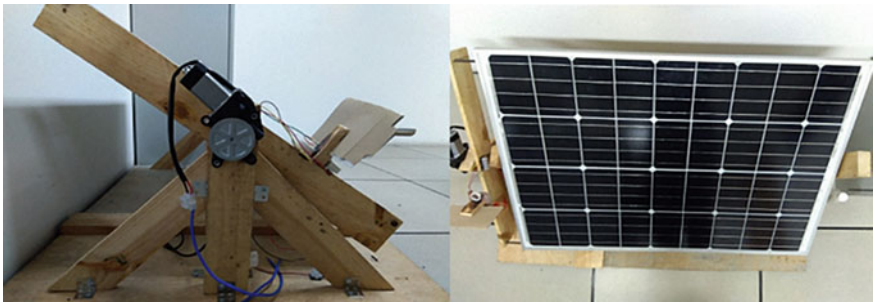

Fig. 3 Solar panel placed in the tracker

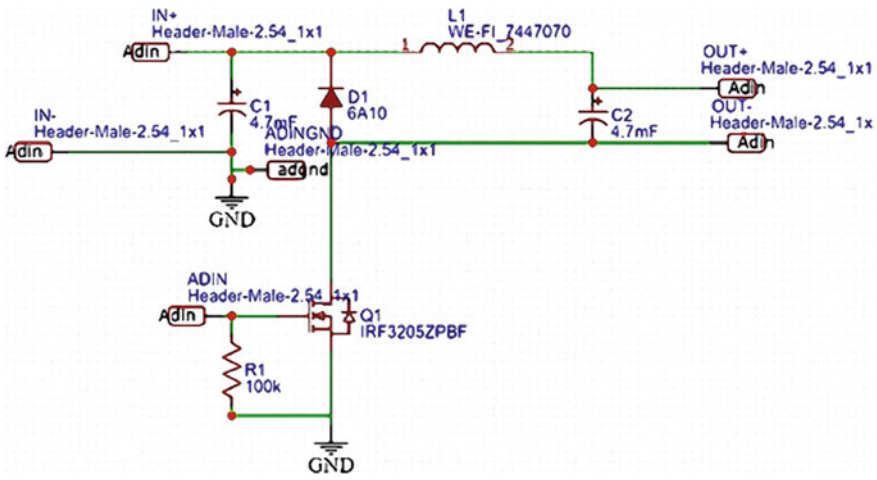

Fig. 4 Buck converter circuit design

is chosen to be so in order to reduce the amount of noise. It acts as a low pass filter such that high frequencies are reduced for a smoother waveform.

$$\text{Cout(min)} = \frac{\Delta \text{IL}}{8 \times \text{fs} \times \Delta \text{Vout}} \tag{2}$$

The input capacitor is chosen to be so in order Eq. (2) shows the rough value of output capacitance required. Whereby the estimated ripple current is determined by inductance shown in Eq. (3), switching frequency is 32 kHz and ripple output voltage is kept to a minimum so the value of output capacitance is increased. Thus, the value of the output capacitance is chosen to be 4700 µF. Equation (3) shows the rough value of inductor ripple current whereby Vinmax = 19 V, Vout = 14, fs = 32 kHz and L = 100 µH. This gives about 1.56(D) of ripple current depending on the duty cycle.

$$\Delta \text{IL} = \frac{(\text{Vinmax} - \text{Vout})\text{D}}{\text{fs} \times \text{L}} \tag{3}$$

2.3 *Maximum Power Point Tracking*

The Fig. 5 shows the flow chart of the MPPT being used. The flow chart is performed by the same Arduino Atmega that is being used to solar track the sun.

The perturb and observe method basically checks to its previous voltage and current(power) to determine whether duty cycle of the DC to DC converter has to change its operating voltage more to be more higher (shift up to right) or lesser duty

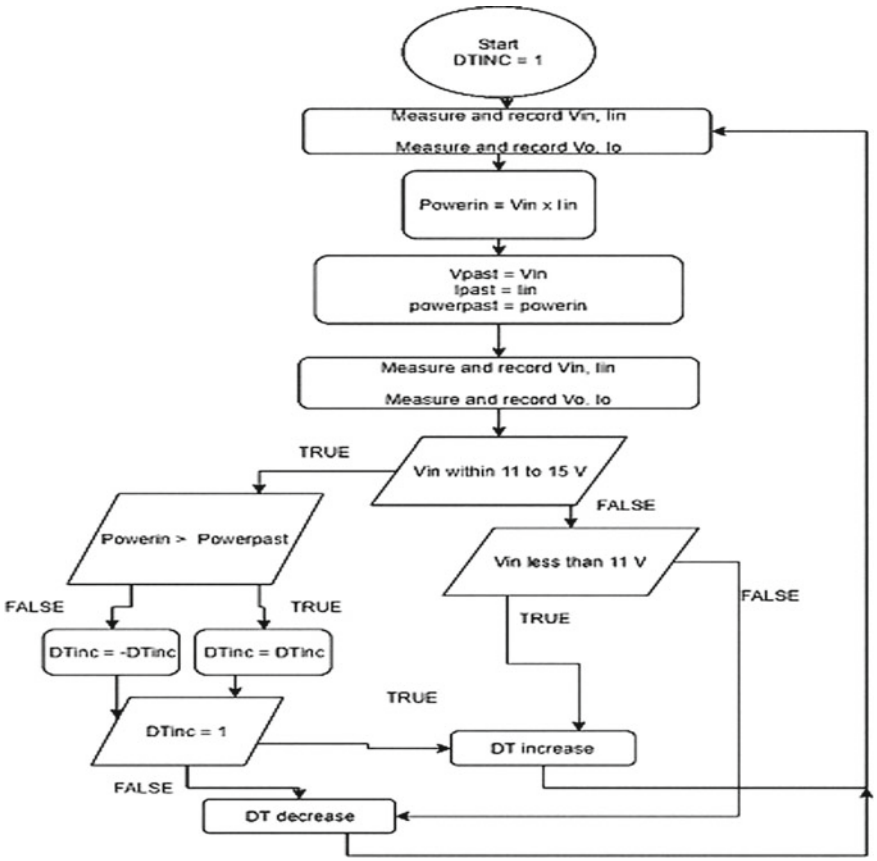

Fig. 5 Complete system of the diagram

cycle (shift down to left). It also checks the voltage output and makes sure that it is within the range of voltage it can be accepted. In this case between 10 and 15 V.

2.4 R Characteristic Load

The values of the resistors of 4 and 8 Ω has been chosen due to the solar panels R characteristics. This is defined by the maximum operating point of voltage and current of a specific solar panel. The R characteristic line is shown as Fig. 6. The experiment is repeated with the two different values of resistors to fit the two different R characteristics.

Using the equation to calculate the R characteristic, the R characteristic found for the 50 and 100 W panel are shown in Table 1.

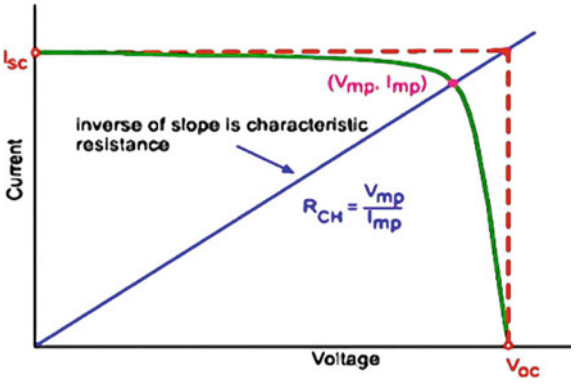

Fig. 6 R characteristic load

Table 1 R characteristic of 50 and 100 W

Solar PV (Watt)	Ohms
50	6.12
100	3.42

2.5 Data Saving Method and Implementation

All of the data that is being calculated and process will be recorded in Arduino's Serial port and will be kept to produce a graph for research. This is then saved into the computer used for the experiment by using an application call CooltermWin [9]. The application reads the Serial input from the Arduino microcontroller's port that is connected to the computer so that real time shown beside the data collected. The experiments of the stationary and solar tracking will be done together with the same value for the dummy load resistor which would be 4 Ω and 8 Ω respectively for two different experiments. The efficiency of the two systems will then be calculated and compared. The formula for efficiency will be determined by the power. Figure 7 shows the design to monitor a standard solar PV system in a residential household (pipe) for comparison with the single axis solar tracking system (wooden). The measured parameters that are most significant would be the output voltage and output current of the system. Since the irradiance is assumed to be the same since the experiments take place right beside each other, the temperature of the monocrystalline solar PV panels is assumed to be constant. The measurements that is to be recorded are the voltage and current of the solar panels before and after MPPT and with and without solar tracking.

The general program flow chart is shown below as Fig. 8. Noting that there is a 1 s delay reading of each set of input, output of solar tracker and stationary panels. This would allow rippling of the current and voltage to settle before the next reading, it is only an estimated safety measure so that the readings being read are correct.

Fig. 7 Solar tracker and stationary panels facing the East-West direction on left the location of the experiment is at UOW KDU University College at the coordinates (3.092008, 101.559373)

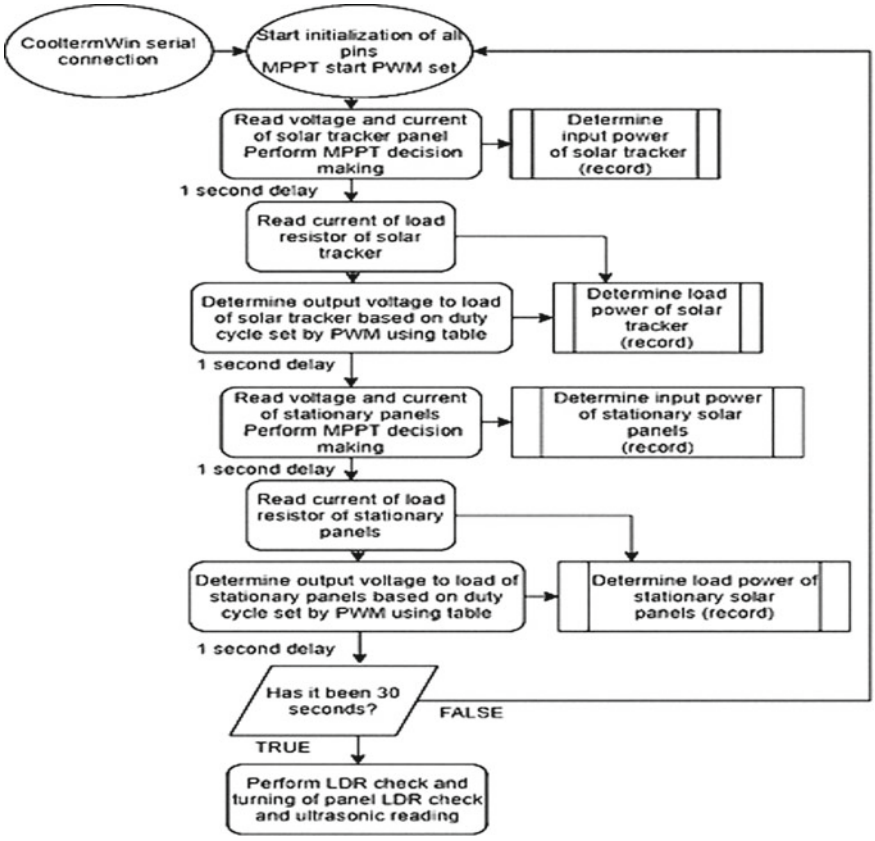

Fig. 8 General flow chart onto how both systems results and MPPT is determined

3 Results and Discussion

The overall design is made to monitor a standard solar PV system in a residential household (pipe) for comparison with the single axis solar tracking system (wooden). The measured parameters that are most significant would be the output voltage and output current of the system. Since the irradiance is assumed to be the same on each panel, since the experiments take place right beside each other, the temperature of the monocrystalline solar PV panels is assumed to be constant. The measurement that is to be recorded are the voltage and current of the solar panels before and after MPPT and with and without solar tracking. Irradiance represent one of the key factor that affect the Solar PV [3], which has been measured using solar meter (TES 1333R). As it has been shown in Fig. 9 the data was taken from 10 a.m. until 4 p.m. At 0 min irradiance was 1000 W/m^2 after 15 min it has drop to 75 W/m^2. Measurements of the power has been taken for the solar panels in the same time as shown in Figs. 10 and 11.

Time of experiment starts from 10:00 a.m. to 16:00 p.m. As shown in Fig. 10 star is solar tracker Ppanel. Circle is solar tracker Pload. Triangle is stationary panels in parallel Ppanel. Cross is stationary panels in parallel Pload.

It can be observed that the load power of the 100 W solar tracker is sometimes higher than the input power from the solar panel, this is due to tolerance of the current sensor, method of calculating output voltage and quick change in irradiance due to shading and dispersion. Since there is tolerance, the load power observed is very close to input power from the solar panel. It can also be seen that the two 50 W stationary solar trackers do not perform very efficiently after the buck converter when the load resistor used is 4 Ω. The actual R characteristic for a 50 W panel used in the experiment is about 6.12 Ω. Based on the results shown in Fig. 10 on the left, the power input from the solar tracker when compared to the stationary two 50 W panels is always higher. During noon, which is about 120 min in the graph shows that the power of the stationary panels is a little bit closer to the power of the solar tracker when compared to 10 a.m. or 0 min which is the very first few data's from the power input of the solar panels. It is observed from Fig. 12 on the left that the output power from the 100 W solar tracker is still higher than the two 50 W stationary panels output power.

As shown in Fig. 14 it can be clearly seen that although an 8 Ω, the load power of the 100 W solar tracker is still higher than the load power of the two 50 W stationary panels although the load resistor used is now closer to the R characteristics of the 50 W solar panel which is 6.12 Ω as shown in Fig. 13. It can be observed from Fig. 12 that is it harder to buck the voltage to be within voltage range set. Similarly, the system is also unable to keep the load voltage within the set range. The reason is also the same as there is an offset from the voltage sensor of −2 V which means that some of the higher voltages is within voltage range and the lower one is not within the range. Another cause would be the size of the output capacitor, which is 4700 μF, there is charging and discharging time of the capacitor

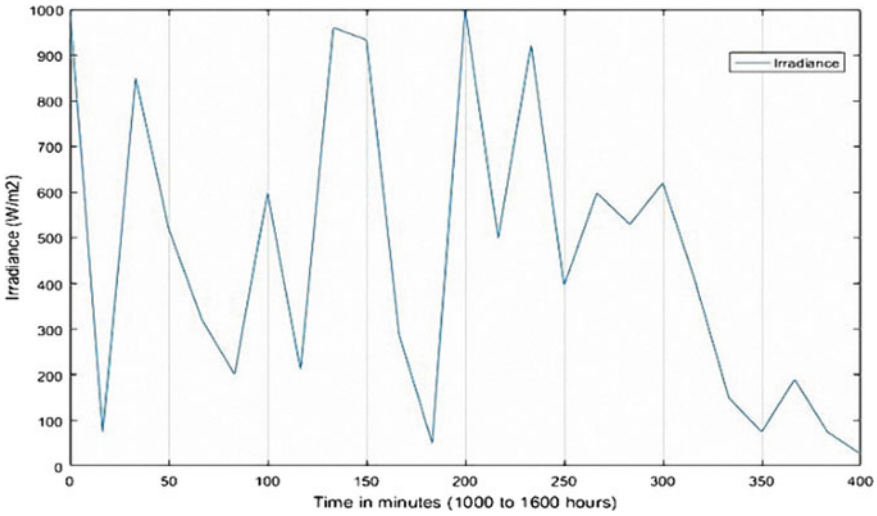

Fig. 9 Irradiance data

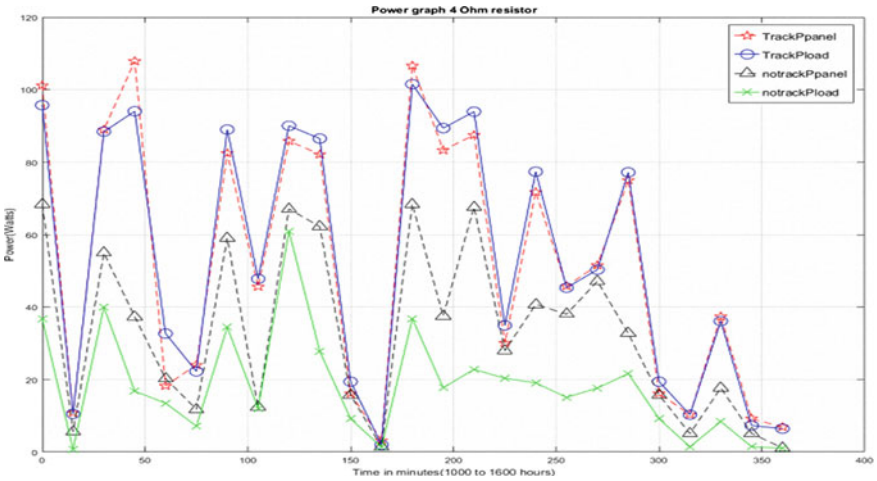

Fig. 10 Comparison of the output power of PV cell and load output power, of 100 W solar tracker and two 50 W stationary panels connected in parallel, using 4 ohms

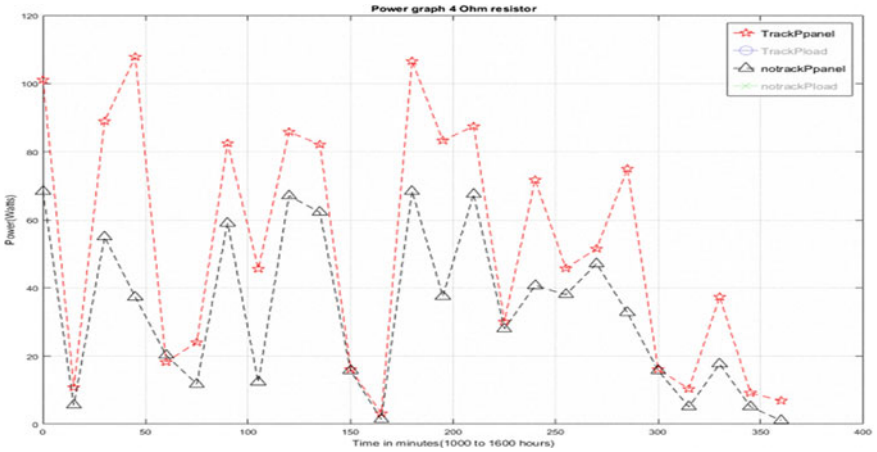

Fig. 11 Comparison of the output power with and without tracker, of 100 W solar tracker and two 50 W stationary panels connected in parallel, using 4 ohms

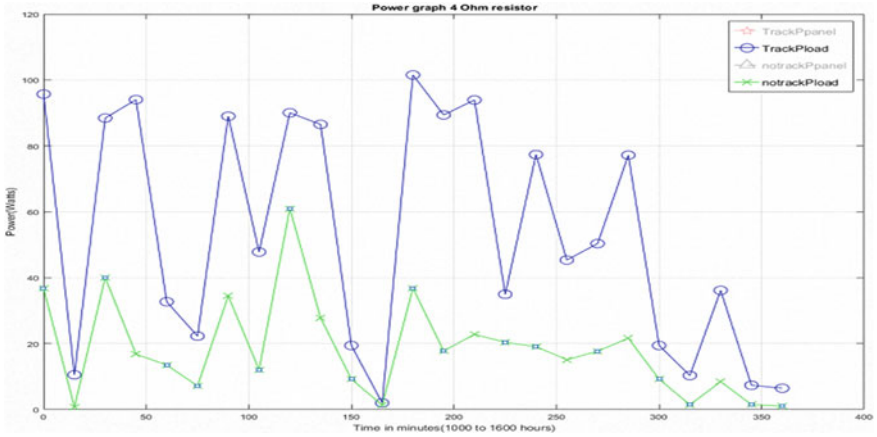

Fig. 12 Comparison of the load output power with and without tracker, of 100 W solar tracker and two 50 W stationary panels connected in parallel, using 4 ohms

which may affect the voltage data being collected whereby it takes longer time to change voltage with the buck converter. Since the output load resistance is very small, the discharge time is also reduced therefore not affecting the result very much. Another reason why the load voltage can stay within the voltage range set is because of the climate in Malaysia whereby it is the monsoon season during November.

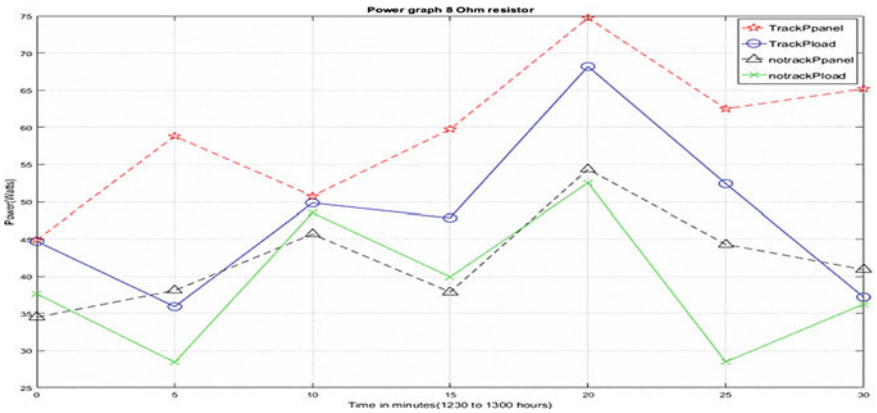

Fig. 13 Comparison of the output power of PV cell and load output power, of 100 W solar tracker and two 50 W stationary panels connected in parallel, using 8 ohms

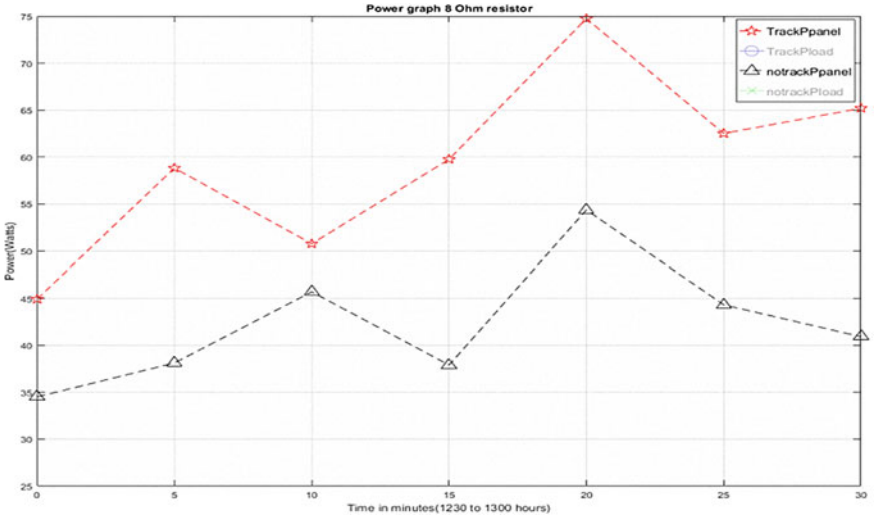

Fig. 14 Comparison of the output power with and without tracker, of 100 W solar tracker and two 50 W stationary panels connected in parallel, using 8 ohms

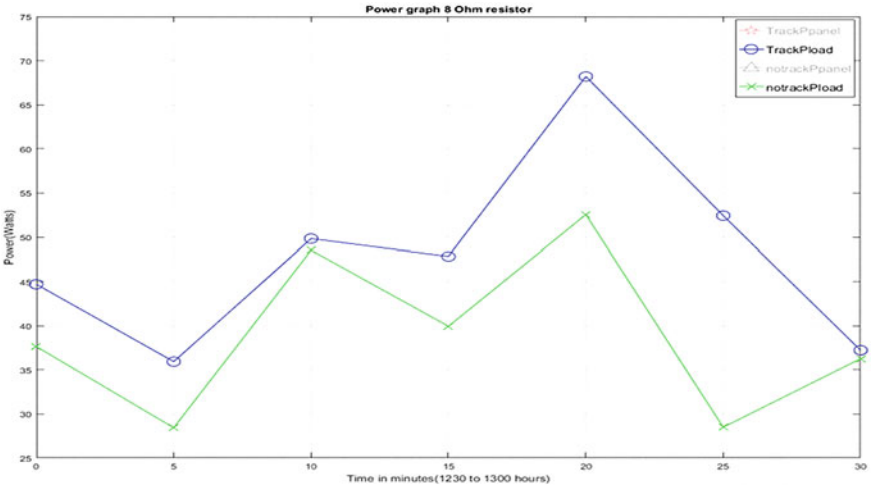

Fig. 15 Comparison of the load output power with and without tracker, of 100 W solar tracker and two 50 W stationary panels connected in parallel, using 8 ohms

4 Conclusions

The experiment was carried out at the same location and same time using two different load resistors and the results show that solar tracking has better performance than no solar tracking even with different load resistors for the 50 W solar panel and 100 W solar panel. The results show that the solar tracking system with MPPT can further optimize the output power to the load by further taking into consideration the R characteristic of a solar panel. By using energy efficient components such as the worm motor that doesn't use any power to keep the solar panel in place and further improvements by using gearing, the systems efficiency is further increased.

References

1. Doman L (2017) EIA projects 28% increase in world energy use by 2040, 14 Sept 2017. Available https://www.eia.gov/todayinenergy/detail.php?id=32912
2. Ellabban O, Abu-Rub H, Blaabjerg F (2014) Renewable energy resources, current status, future prospects and their enabling technology. In: Renewable and sustainable energy reviews, vol 39, Nov 2014, pp 748–764
3. MohamedZain AO, Chua HS, Yap KM, Al-Talib AAM (2020) Outdoor experimental comparison between PV cell and combined system PV-TEG. Sci Int (Lahore) 32(3):279–283
4. Mohamedzain OA, Govinda S, Chua HS, Al-Talib AAM (2020) Experimental investigations of the effect of temperature on power in a combined photovoltaic cell and thermo-electric. Lecture notes electrical engineering, vol 619, Nov, pp 199–210

5. Albert FYC, Mason CHS, Kiing CKJ, Ee KS, Chan KW (2014) Remotely operated solar-powered mobile metal detector robot. Procedia Comput Sci 42:232–239
6. Kotrov OI, Smulsky JJ (2014) New computing algorithm of the earth's insolation. Appl Phys Res 6(4):56–82
7. Gusa RF, Sunanda W, Dinata I, Handayani TP (2018) Monitoring system for solar panel using smartphone based on microcontroller. In: Proceedings—2018 2nd international conference on green energy and applications ICGEA 2018, pp 79–82
8. Baharudin N, Mansur T, Nizar TM, Hamid F, Ali R, Irwanto M (2018) Performance analysis of DC–DC buck converter for renewable energy application. J Phys: Conf Ser 1019:012020
9. Mason CHS, William Y, Albert FYC (2014) Design and implementation of sub-GHz wireless light switch with integrated Wi-Fi. In: 2014 IEEE international conference on communication networks and satellite, pp 34–38. IEEE

Dielectric Properties Measurement of Agarwood Using Vector Network Analyzer for Frequency 200 MHz Until 1 GHz

Nurfarahin Ishak, Chua King Lee, and Siti Zarina Mohd Muji

Abstract Non-destructive technique has potential to be used in agricultural for example to inspect the formation of agarwood. However, to build a system using the non-destructive technique need to know the dielectric properties itself. The aim of this paper is to measure the dielectric properties of agarwood by using Vector Network Analyzer (VNA). Measurement was conducted at frequency 200 MHz until 1 GHz with open-ended coaxial probe method. Both relative permittivity and conductivity were affected by frequency, moisture, and temperature. The most significant influence of dielectric properties was observed between these ranges of frequencies. The relative permittivity decreases with increasing the frequency and conductivity showed maximum and minimum values under various conditions.

Keywords VNA · Relative permittivity · Conductivity

1 Introduction

Aquilaria Malaccensis also called (agarwood) is a species of plant that can be found in Malaysia. Agarwood is commonly known as Gaharu which produced fragrant resinous wood. The formation of resin occurs as a response to fungus infection in the stem of the trees. Generally, the resin raises the mass and density of the infected wood and shifts the colour of the bark to black. [1]. Agarwood is high valued wood for extensive uses such as perfumes, incense, and medicine. China is famous produced agarwood products such as carminative, anti-emetic effects and sedative

N. Ishak · C. K. Lee (✉) · S. Z. M. Muji
Faculty of Electrical and Electronic Engineering, Universiti Tun Hussein Onn Malaysia, Parit Raja, Malaysia
e-mail: chua@uthm.edu.my

N. Ishak
e-mail: farah.ishak25@gmail.com

S. Z. M. Muji
e-mail: szarina@uthm.edu.my

Z. Zakaria and S. S. Emamian, *Advances in Electrical and Electronic Engineering and Computer Science*, Lecture Notes in Electrical Engineering 741,
https://doi.org/10.1007/978-981-33-6490-5_4

medication [1]. The natural forming of high-quality agarwood takes several years or might be decades until the tree is affected by any extrinsic causes, such as lightning strikes, animal weeding, insect attacks or microbial invasions [2]. Due to the economic value, the agarwood has been exposed to the exploitation by the agarwood hunter. The agarwood farmer uses the inoculants which act as a booster and inject into the tree to expedite the agarwood formation. Compare to the traditional wounding methodologies, the chemical inducers seem to be able to rapid the agarwood formation. The inoculants are containing active compounds made from the microorganism or chemical concoctions.

Regarding understanding the electrical properties of wood, instrumental and industrial use, wood's dielectric properties are beneficial. Several researchers have recently been investigating the use high-frequency and microwave approaches to increase reliability of energy and end-product quality. The interaction between the alternating electromagnetic field and wood allows different properties of this substance to be elucidated. There are two components in the electromagnetic field: electrical and electromagnetic fields. Such different compounds' effect on wood. The magnetic field effect on wood is insignificant, however the impact of the electrical field in wood may occur since the interference with the magnetic field findings in the development of electrical currents in the material [3].

For this experiment, coaxial probe open-ended was chosen because do not need sample machining, and quick preparation of the sample. After measurement, a wide number of samples of dielectric properties may be calculated regularly over a limited period of time. The measure can then be carried out in a temperature-controlled environment.

2 Definition and Principles

The measurement of dielectric properties includes of the materials' relative permittivity (εr), relative permeability (μr) measurement and conductivity (σ). The permittivity properties consist of a real section and an imaginary section. Permittivity, also called as dielectric constant, is the calculation of the sum of energy from the exterior electric energy contained in the material. For lossless materials, the imaginary element is zero which is often regarded as the loss factor. It is a representation of the level of energy degradation of the substance owing to an external electrical field. The term tan δ is named loss tangent and reflects the connection between the hypothetical component and the real element of the permittivity. Terms such as tangent loss, dissipation factor, or loss factor also apply to the loss tangent [3]. The permeability is the measure of the resistance of a material against the formation of a magnetic field. The conductivity is the measure of the ease at which an electric charge or heat can pass through a material.

The dielectric parameters of wood can be influenced by several factors. Several studies have been published on the relationships between dielectric wood parameters and relevant material properties such as porosity rate, pore scale, pore

allocation, moisture levels and density [4]. It is also correlated with the microstructure of wood, the interaction mechanisms between the wood and water, and the behavior of wood under a high-frequency electromagnetic field [5]. It has been observed that the dielectric properties can be affected by the frequency [4–6]. With increasing frequency and loss coefficient increases, relative permittivity decreases with increasing frequency for all species of wood and fiber orientation [4]. As dielectric properties studies became more complex, many factors such as temperature, structural direction, and density are considered with the findings showed the other factors do had something significant effect wood's dielectric behavior [7].

3 Experiment Setups

3.1 Test Sample Preparation

A cylindrical of agarwood samples were chosen for experiment. Then, it cut into three samples with the length 15 and 59 cm in diameter. Each of the samples has different size agarwood formation inside because it is formed scattered. The measurement reading is taking until nine (9) points in horizontal condition for precise and accuracy. The points were taken surrounding the samples. However, the structure of the test samples is not flat and it was an obstacle to get an accurate reading because the air gap has occurred and only reflection measurement is available.

There are several steps has been taken to prevent reading error and overcome the solution for air gap:

- Take the air reading before starting the experiment. Dielectric constant value at room temperature (25 °C, or 77 °F) is 1.00059. This value is compared to the reading value and make sure the reading place have no air gap.
- Take a few times reading at one point.
- Find the best point which has a flat area to place a probe.

The reaction of relative permittivity and conductivity toward frequency, temperature and moisture content are recorded.

3.2 Apparatus Setups

Calibrations are necessary before experimenting. The purpose of the calibration operation is to establish a relationship between the measured complex reflection coefficient and the predicted one. This method enables all post-calibration measurement information to be fixed. If carried out properly, a good calibration procedure results in reliable readings. Figure 1 below shows the experiment setup equipments.

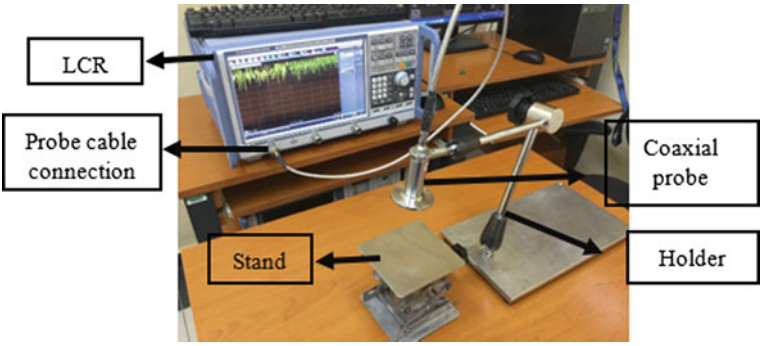

Fig. 1 The experiment setup

The copper is well known as good conductivity. During calibration and the conductivity of copper used in the validation step equally—indeed, the same types of reference can be used either for calibration or validation as in Fig. 2.

The temperature of the load fluid must be preserved and controlled during the calibration phase, as the dielectric parameters are temperature-dependent. Liquid permittivity varies by up to 2.2% per degree Celsius. Measurement of deionized water or any normal liquid as a load of calibration may be conducted at room temperature or any set temperature. If the temperature of the liquid differs from the temperature of the probe, it is suggested to wait for the temperature to stabilize before continuing with the measurement as in Fig. 3.

3.3 Testing Open-Ended Coaxial Probe

The coaxial probe technique is ideal for liquid and semi-solid (powder) materials. The method is simple, reliable, non-destructive with one measurement. In this mode, the sample is pushed contrary a specimen or dissolved in the solvent and the coefficient of reflection is measured and used to determine dielectric properties. Dielectric constant, loss tangent and conductivity data were taken by Rohde & Schwarz Vector Network Analyzer (VNA). The frequency range is used from 200 MHz to 1 GHz. The system composed of an open-ended coaxial probe DAK 3.5 with 3.5 mm diameter and fully computer interfaced as in Fig. 4. The data from open and short response of coefficient was measured by the VNA system.

Next, the probe device is calibrated in such a way that the reflection coefficient measurement is apply to the aperture plane of the probe. This can be achieved by using reference liquids at the open end of the sample for precise calibration. The specified fluid is used as a comparison norm and must be a fluid with proven dielectric properties as in Fig. 3.

Fig. 2 Calibration with copper plate

Fig. 3 Calibration with water

While testing the specimens the coaxial probe must have a strong contact with the specimens. Any air gap between specimen and probe would affect the readings [8]. As microwaves are applied to a substance, some of the energy is being obscured, some of it transferred via the surface and some of the part is consumed by the latter level. The proportions of energy in these three classes were described as dielectric

Fig. 4 DAK 3.5 coaxial probe

properties [9]. The basic electrical properties from which the encounters take place are represented is the relative permittivity of the material ε* [9, 10]. The mathematical expressed as:

$$\varepsilon^* = \varepsilon' - j\varepsilon'' \tag{1}$$

where

ε′ = dielectric constant, and
ε″ = dielectric loss factor.

The dielectric loss factor is a function of conductivity and frequency:

$$\varepsilon'' = \sigma/2\Pi f \tag{2}$$

$$\varepsilon = \varepsilon' - j\sigma/\omega \tag{3}$$

where

ω = 2∏f
σ = conductivity.

4 Dependence of Dielectric Properties

4.1 Frequency Dependence

Polarization as a consequence of the alignment with the applied electrical molecule field with persistent dipole moments is a significant factor responding to the reliance on frequency of certain dielectric properties of materials [7, 11]. Different kinds of the dipole would have different times of relaxation. Therefore, as the frequency rises, the permittivity declines in phases and the dielectric loss peaks.

Dipolar water molecules are lined up in the field at low frequencies and the relative permittivity received approximately 80. The permittivity decreases in a phase at higher frequencies, and the power factor has a limit [12]. Previously reported was the effect of the measurement conditions such as temperature, frequency, and orientation of the electrical field concerning the wood structure [4].

4.2 Temperature Dependence

Relative permittivity can increase with rising temperatures in a dispersion area, while the loss factor can change depending on whether the frequency of operation is different from frequency of relaxation [11].

4.3 Density and Moisture Dependence

In the surrounding water, the undefinable regions are more permeable as the amount of moisture rises. It is reasonable to presume that ions will move through the amorphous regions under the influence of the external electrical field and concentrate at the edges of the crystals until the inner field of separated ion charges is equivalent to the applied field, or until the external field is inverted. [7].

5 Result and Discussion

This experiment was tested at the three *Aquilaria* samples with agarwood formation. Each sample was labeled as A, B and C as in Fig. 5. Nine points readings were taken for each sample. The data has precise by using the standard deviation and mean calculation. From the statistic graph value shows the patterns movement in increment of frequencies. The size and location of agarwood inside the samples are different. This is because of the formation of agarwood are scattered. Therefore, size agarwood formation is influenced by the reading of the dielectric. The different size formation of agarwood inside the sample giving a different measurement reading. Sample A have a least formation gave high reading while sample C have large formation gave low reading of permittivity.

The relative permittivity indicates the molecule's tendency to polarize within the electrical field and the loss coefficient indicates the material ability to convert electromagnetic energy to heat at a specific frequency and temperature. At higher frequencies, relative permittivity is found to decrease further effects are attributed to the involvement of electrical polarization. Many additions are negligible and even decline as polarization will not arise instantaneously owing to the strength of the electrical field [12]. All forms of polarization apply at low frequencies. As

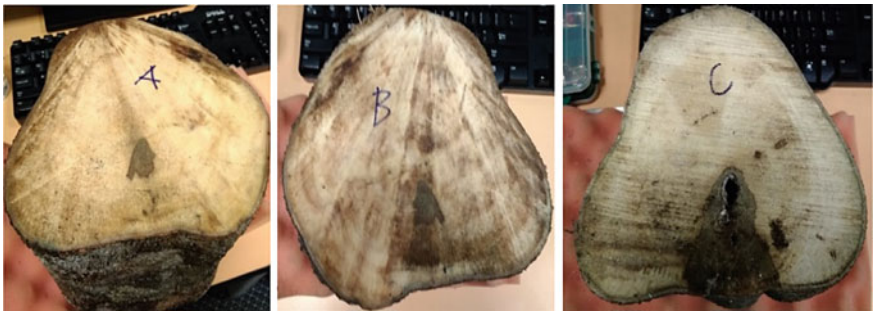

Fig. 5 The fresh *Aquilaria* sample with agarwood

frequency increases, those with long time of relaxation times cease to react, and thus the relative permittivity decreased [5, 6].

The relative permittivity and conductivity of Aquilaria samples have been measured by using VNA with a frequency range from 200 MHz to 1 GHz. High values of the relative permittivity (ε') and conductivity (σ) found due to moisture content. Observation was found that temperature and frequency indicating the conduction mechanism, where the thermal conductivity of wood comparatively poor owing to the porosity of timber as wood is a very complex material with low permeability and thermal conductivity. Thermal conductivity increases as the wood density increases. The higher the amount of moisture was, the greater the frequency impact on the factor of loss.

The graph in Figs. 6 and 7 below shows the linear regression of relative permittivity and conductivity for samples A, B, and C. These graphs are the correlation between average relative permittivity and conductivity versus frequency. The previous researcher showed the example approach to determine their result whether to be reliable by the interpreting by correlation coefficient as in Table 1 [13]. Linear regression (R) is a common technique for statistical data analysis. It is used to determine the extent to which a consistent relationship exists between a dependent variable and one or more independent variables. By referring to the Table 1 correlation coefficient shows that the value regression of relative permittivity in the graph is moderate correlation where sample A, $R2 = 0.5704$ while sampling B, $R2 = 0.5474$ and sample C, $R2 = 0.1939$. The R2 value for sample C is low because of the sample condition where has a hole inside and the agarwood formation is not solid. The accuracy reading distracted by the air gap. Then, for the regression of conductivity result shows that near to strong correlation. For sample A, $R2 = 0.9019$, sample B, $R2 = 0.5031$ and sample C, $R2 = 0.7981$. This correlation results, depending on the initial results of the measurement. As in the discussion, many factors are influencing the readings such as moisture, temperature, and frequency. However, to achieve a strong correlation need to minimize the factors that interfere during the measurement reading.

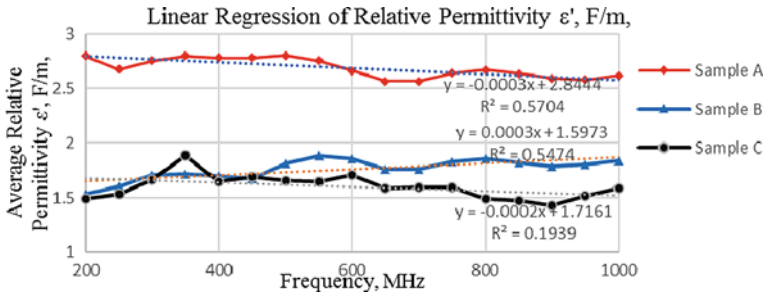

Fig. 6 The linear regression of relative permittivity

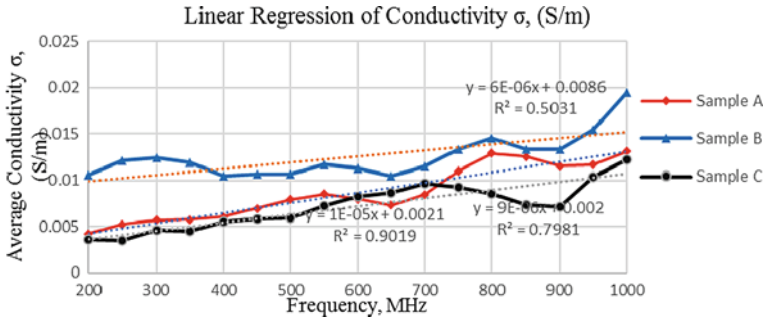

Fig. 7 The linear regression of conductivity

Table 1 Correlation coefficient interpreting table [13]

Correlation coefficient	Interpretation
0.00–0.001	Negligible correlation
0.10–0.39	Weak correlation
0.40–0.69	Moderate correlation
0.70–0.89	Strong correlation
0.90–1.00	Very strong correlation

6 Conclusion

The measurement dielectric properties of agarwood with used the open-ended coaxial probe method shows that the relative permittivity data slightly decreasing while the frequency is increased opposite to the conductivity, the measurements data is increasing while the frequency is increased. The measurement data are massively inclined by frequency, temperature, and amount of moisture. However, fatal error such as air gap during measurement processed have also given effect on dielectric reading.

The relative permittivity measurement at frequency 650 MHz until 700 MHz for all samples shows the flatted readings because of relaxation times cease to react. The dielectric properties data of agarwood provided would fulfill all of the needs for potential high-frequency research.

Acknowledgements This research was supported by Fundamental Research GRANT Scheme (FRGS) research Vote K087 (Ref: FRGS/1/2018/TK04/UTHM/02/28). Thank you Ministry of Education (MOE) and Research Management Centre (RMC) of Universiti Tun Hussein Onn Malaysia for the financial support to achieve the research goal.

References

1. Chen X et al (2018) Trunk surface agarwood-inducing technique with *Rigidoporus vinctus*: an efficient novel method for agarwood production. PLoS ONE 13(6):1–13
2. Chen X et al (2017) Agarwood formation induced by fermentation liquid of *Lasiodiplodia theobromae*, the dominating fungus in wounded wood of *Aquilaria sinensis*. Curr Microbiol 74(4):460–468
3. Torgovnikov GI (1993) Dielectric properties of wood and wood-based materials. Springer-Verlag
4. Pento K, Łuczycka D, Wysoczanski T (2017) Dielectric properties of selected wood species in Poland. Wood Res 62(5):727–736
5. He X et al (2017) Study on dielectric properties of poplar wood over an ultra-wide frequency range. BioResources 12(3):5984–5995
6. Varada Rajulu KC, Mohanty BN (2016) Dielectric and conductivity properties of some wood composites. Int J Eng Technol 8:51–60
7. James WL (1975) Dielectric properties of wood and hardboard variation with temperature, frequency, moisture content, and grain orientation
8. Riminesi C, Olmi R, Bini M, Ignesti A (2000) Dielectric of properties of wood from 2 to 3 GHz. J Microw Power Electromagn Energy 35(3)
9. Venkatesh MS, Raghavan GS (2005) An overview of dielectric properties measuring techniques. Can Biosyst Eng 47
10. Norimoto M (1976) Dielectric properties of wood
11. Nelson SO, Kraszewski AW (1990) Dielectric properties of materials and measurement techniques. Dry Technol 8(5):1123–1142
12. Morton WE, Hearle JWS (2008) Dielectric properties. In: Physical properties of textile fibres, pp 625–642
13. Schober P, Schwarte LA (2018) Correlation coefficients: appropriate use and interpretation. Anesth Analg 126(5):1763–1768

Energy Consumption and Cost Estimation Considering Renewable Energy Sources in Integrated Next-Generation Wireless Access Network

Arnidza Ramli, Abubakar Abdulkadir, Nadiatulhuda Zulkifli, and Adam Wong Yoon Khang

Abstract Energy consumption in telecommunication industries is a major challenge for the network providers where most of the power consumed equipments are from the wireless access network and the optical network transmission. The non-renewable energy are the main sources of electricity such as diesel, burning fossil fuel and only a small percentage of energy comes from clean renewable energy source such as solar, wind, biomass and tidal power. Therefore, this research work is aimed to estimate the precise power consumption of an integrated optical-wireless access networks by characterizing the most power demanding equipment and providing an alternative source of a clean renewable energy to power them. The main advantage of this technique is the simplicity in which the power consumption can simply be modelled by using Matlab and to mitigates the GHG emissions of the system by hybridizing renewable energy which are solar and wind into existing energy sources and simulated using Homer Pro. The obtained results were based on Skudai-Malaysia location where 77% reduction of carbon emissions through renewable integration and 56% operational cost were achieved.

Keywords Next-Generation-Passive optical network · Operational cost · Power consumption · Renewable energy · Wireless access network

A. Ramli (✉) · A. Abdulkadir · N. Zulkifli
Lightwave Communication Research Group, Faculty of Engineering, Universiti Teknologi Malaysia UTM, 81310 Johor Bahru, Malaysia
e-mail: arnidza@fke.utm.my

A. W. Y. Khang
Broadband & Networking Research Group (BBNET), Center for Telecommunication Research and Innovation, Fakulti Teknologi Kejuruteraan Elektrik Dan Elektronik (FTKEE), UTEM, Hang Tuah Jaya, Melaka, Malaysia

Z. Zakaria and S. S. Emamian, *Advances in Electrical and Electronic Engineering and Computer Science*, Lecture Notes in Electrical Engineering 741,
https://doi.org/10.1007/978-981-33-6490-5_5

1 Introduction

The power consumption in mobile communication industries are the major concern. The integration of next generation-passive optical network (NG-PON) and Wireless Access Network (WAN) provides high speed broadband network, but energy consumption increases due to network overloads by additional number of computers connected to the base stations (eNBs) network [1]. The integrated NG-PON-WAN systems is powered by diesel generators which produces green-house gases (GHG) emission (environmental impact) [2]. The diesel generator releases polluted air in forms of Carbon dioxide, carbon monoxide, ammonia, nitrous oxides, sulfur dioxide, chlorofluorocarbon and methane are the major contributors of global warming causes genetic change, depletion of ozone layer, cancer and acid rain [3]. Therefore, this paper proposed a method to estimate the energy consumption as well as cost by integrating renewable energy source to power all the major hungry components for the entire architecture.

2 Related Works

Almost a decade, significant achievement has been made by hybridizing renewable and conventional energy sources into a smart grid to succeed in supplying electricity to the base station (BS) sites. In [4], the authors presented an analytical model and evaluated the power consumption based on the integration of PON-Wireless networks. However, the valuation of energy consumed by the components for such networks have been realized significantly. The analytical model used for measuring the energy consumption of the network elements was derived from the datasheets reported in [1, 4]. Therefore, the overall power consumption model for the integrated networks was expressed as:

$$P_{IOB} = \sum_{i=1}^{M} P_i^{OLT} \times \sum_{i=1}^{N} \left(P_i^{ONU} + P_i^{FBS}\right) \tag{1}$$

where M and N are the number of an optical line terminal, OLT and the power integrated optical-base station, P_{IOB}, the P_i^{OLT}, P_i^{ONU}, and P_i^{FBS} are the power consumed by the OLT, optical network unit (ONU), and Femto-Base Stations (FBS) respectively. The individual power consumption models for different network components was reported in [4]. The power consumption mostly depends on the traffic load and distance (or site factors). However, the power consumption of the end-user equipment's was not accounted such as laptops and smartphones.

Authors in [5], proposed the feasibility study and simulation of an integrated Solar Photovoltaic with battery storage to power some selected mobile BSs within the Soshanguve in Pretoria, South Africa. The proposed study was aimed at the

possibility of implementing a hybrid power system (HPS) for cellular BSs and analyzes the economic and environmental impact of the study against the diesel generator set as the main source of electricity to BSs. The total selected BSs power was modelled [5] as:

$$P = \sum_{n=1}^{N} P_n \cdot \frac{T_n}{24\,\mathrm{h}} \tag{2}$$

where P represents the total DC load power, P_n and T_n are the components power consumption is the run time (n = 1, 2, 3, …). However, the proposed technique used to consider the solar PVs architecture for a period of 10 years only while the result obtained was able to achieve reduction in GHG emission and operational cost as compared to the diesel genset, but still for 10 years project, the total net present cost (NPC) was at $255,812.00.

3 Methodology

3.1 Optical-Wireless Access Network Architecture

Figure 1 shows the integrated NG-PON-WAN architecture considered in this paper. The architecture can be divided into four parts, three of which are considered as power hungry components and the units are, the OLT, ONU, eNBs and another one part passive splitter node. The maximum fiber distance between OLT and ONU are typically 40 km, but is capable to reach up to 60 km, depends on the bandwidth capacity and service requirements. The ONU is connected to OLT through the passive splitter with splitting ratio up to 1:256 considered in this work. The eNBs are located at customer premises equipment (CPE) and they are long term evolution (LTE) base stations connected to ONUs that offers internet access to the mobile users.

3.2 Network Power Consumption Model

The power consumption (PC) model of an integrated NG-PON-WAN architecture shown in Fig. 1 can be expressed as [6]:

$$P_{overall} = \frac{3}{2}(P_{SN} + P_{EN}) + P_{CPE} \tag{3}$$

where $P_{overall}$, P_{SN}, P_{EN} and P_{CPE} are the overall PC of an integrated NGPON-WAN, the power consumed at the splitting ratio SN (typically is zero),

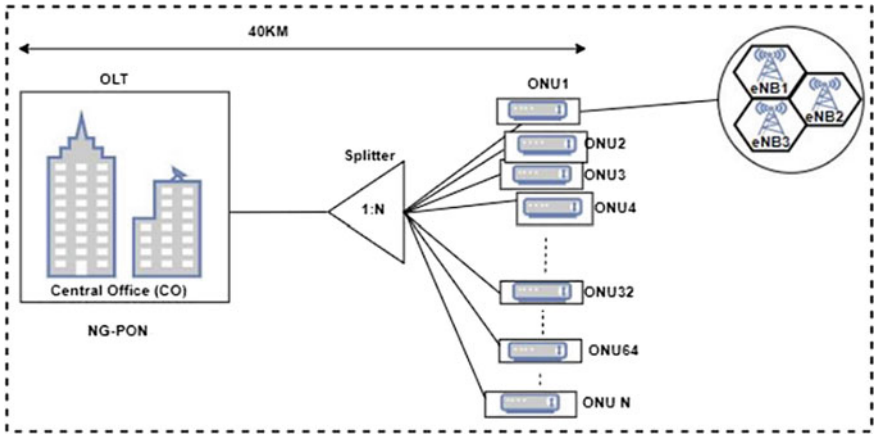

Fig. 1 NG-PON-WAN architecture

because it's a passive component, the power at edge node EN and plus the power consumed at the CPE node. The constant fraction number, $\frac{3}{2}$ is a multiplier power factor usage for the effective cooling and the uninterrupted power system (UPS), located at the network site.

The NG-PON described as an OLT equipment located in central office is referring to as the PC at the P_{EN} and can be modelled as [6]:

$$P_{EN} = P_{ONU} = P_{idle} + \left(\frac{P_{idle} + P_{\max}}{C_{\max}}\right) \times C \tag{4}$$

where P_{ONU} is the PC at ONU, $P_{idle}, P_{\max}$, are the energy consumed at maximum peak load and at no-load measured in watts (W), while $C_{\max}$ and C are the maximum traffic load and the data rate, all are measured in bit per second (bps). The parameters for both the OLT and the ONU equipments used in this work was based on "Cisco ME4600 series" and the simulation parameters selected from its datasheet [7, 8].

The International Telecommunication Union-Telecommunication (ITU-T G.989.1) recommendations of the NG-PON provided the symmetric peak data-rate, C for downlink and uplink as 10 Gbps/10 Gbps. Therefore, both the OLT and ONU equipments (Cisco ME4600 series) satisfied the requirements of the maximum load traffic at 5 Gbps and the data rate, C at 3 Gbps was selected because only remote or less populated are considered in this work. The $P_{\max}$ of both the OLT and the ONU (ME4624-ONT-RGW) are <545 W and 15 W accumulated energy consumption reported in datasheet [7, 8]. In an idle situation, the power consumed at less traffic (no-load) is 90% of the $P_{\max}$ as reported in [7]. The PC of an OLT and ONU are summarized on Table 1.

Table 1 Power consumption parameters [7, 8]

	P_{EN} ($ME46XX{-}OLT$)	P_{ONU} ($ME4624{-}ONT$)
$P_{\max}$	540 W	15 W
P_{idle}	486 W	13.5 W
$C_{\max}$	5 Gbps	5 Gbps
C	3 Gbps	3 Gbps

The LTE-eNB described as the major power-hungry equipment that contains the power amplifier (PA) known as radio-remote head (RRH), radio frequency (RF) unit, the baseband (BB) unit, the air-conditions (ACs) used for cooling system, security lighting (SL). The above mentioned component's PC was calculated and reported [9, 10]. The LTE-eNB power model can be expressed as [11]:

$$P_{eNB} = \frac{P_{PA} + P_{BB} + P_{RF}}{((\sigma_{cool}) \times (\sigma_{ms}) \times (\sigma_{dc}))} \times N_{sector} \tag{5}$$

The LTE-eNB PC of the following components; the RRH, the integrated RF and BB devices considered in this work are summarized in Table 2:

The P_{eNB} refer to PC of an LTE-eNBs, P_{PA}, P_{BB}, P_{RF} are the PC for power amplifier, baseband and radio frequency units measured in watts. Other symbols of the denominator in Eq. (5) are losses due the cooling system (σ_{cool}), the main-supply (σ_{ms}) and dc-to-dc (σ_{dc}) conversion losses [11]. The N_{sector} denotes to the number of base station sectors used as depicted on Fig. 1. The PC at the CPE node refers to as the summation of single ONU and the eNBs. Therefore, mathematically, P_{CPE} expressed as [4]:

$$P_{CPE} = P_{eNB} + P_{ONU} \tag{6}$$

The entire energy consumed by an P_{CPE} was calculated as 6589 W, that is including the two pieces of 2-horse power AC's each per sector used for network equipment cooling, two security light of 200 W each used for exposing a trespasser within the base station.

Table 2 LTE-eNB PC parameters [11]

Components	Values
P_{PA}	185 W
$P_{RF} + P_{BB}$	55 W
σ_{cool}	9%
σ_{ms}	7%
σ_{dc}	6%
N_{sector}	3

Table 3 Required bandwidth for FTTH services

Applications/Services	Required Bandwidth (Mbps)
Additional TV channels	16
Internet downloads	10
High-definition TV	8
Standard definition television	3
Music on demand	2
Multimedia	2
Online gaming	1
Voice over IP (VoIP)	1
Video conferencing	1
Total	44

3.3 FTTH Scenario

Based on the recommendations from the ITU-T G.989.1 (March 2013), the central office where an OLT is located, is therefore linked to numerous ONUs over a passive splitter to the fiber to the home (FTTH). The FTTH applications, services and the required bandwidth associated with those services are summarized in Table 3.

Table 3 shows the required bandwidth per service or application to work without any hitches and the total required data per single ONU is 44 Mbps. The splitting ratio considered in this research work was 1:256 and the $C_{\max}$ used for FTTH uplink and downlink are 156 Mbps and 78 Mbps as calculated. Therefore, the integrated NG-PON-WAN with a maximum SR 1:256 different ONUs satisfied the requirements efficiently compared with 78 Mbps. The $C_{\max}$ model can be expressed as [12]:

$$C_{\max} = \frac{1}{SR} \times (R_{ul} + R_{dl}) \tag{7}$$

where SR denote as the split ratio, while the R_{ul} and R_{dl} are the uplink and downlink data rates of the integrated network. The summation of R_{ul} and R_{dl} considering an NG-PON symmetrical data rate of (10/10 Gbps) that is the total amount of data can be conveyed from an OLT to 256 different ONU within the network via an SR over a time.

4 Results and Discussion

In this work, we used Matlab and Homer Pro simulation software tools. The Matlab simulation tool was used to model the PC at an EN, CPE and the overall PC with splitting ratio up to 1:256. The hybrid optimization of multiple electric renewables

Fig. 2 Skudai-Johor, Malaysia location

(HOMER) Pro was used to estimate the designed cost for both renewable and non-renewable energy sources. The eNBs are considered the main source of PC in cellular networks which are usually located at remote areas. We consider Skudai-Johor, Malaysia as our remote location (Fig. 2).

4.1 Power Consumption Analysis

The PC of an integrated NG-PON-WAN with distribution of different split ratio (SR) which leads to a dissimilar energy consumption of the same loads was considered. This shows the variation of PC is due to the fact that the lower number of SR, the less energy consumed. The SR of 1:32 has the lower number of network devices connected to an OLT equipment through the passive device, can save power consumption of about 97.5% compared to the highest number of 1:256 SR as depicted on Fig. 3.

Figure 3 shows the simulation results for the entire nodes considered in this work. We observed the energy consumed with 1:32 SR at 2 Gbps was around 7415 W and at the same data rate with 1:256 SR, the consumption increased to around 7455 W as shown in Fig. 3. On the same figure, at 8 Gbps data rate with 32, 64, 128 and 256 different SR has the following PC of 7425, 7445, 7485 and 7565 W. Therefore, the highest SR has more PC due to number of connected devices in the network system.

At idle power and zero load, the energy consumption is as much as 90% of the total device PC and that gives 7400 W. Accordingly, from the result we analyze that considering different SR causes a linear increase in energy consumption. However, the increase in PC is caused by the daily increment for the number of

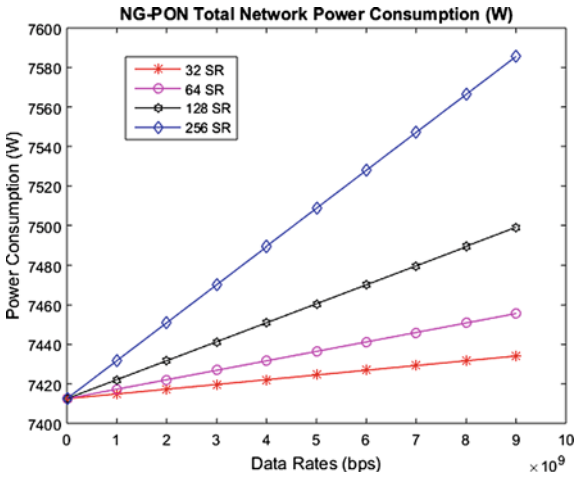

Fig. 3 NG-PON-WAN power consumption

mobile devices connected to the CPE nodes. Hence, the operational cost of the cellular companies will be increase when fossil fuel is used to power their network equipment's with a diesel generator at the remote locations.

4.2 Renewable Energy and GHG Emission Analysis

The renewable energy and GHG analysis have been conducted using Homer Pro software. Figure 4 shows the design diagram of the implemented for both renewables (solar-PV and wind-EO10) and non-renewable (Gen) energy resources coupled to the electrical loads (eNB1, eNB2 and eNB3) with an overall energy consumption of 186.47 kWh/day and a peak power of 15.92 kW.

In these analyses, the project life time was designed for 25 years and the load profile was generated based on the calculated PC and the sensitivity list of the components used over the period per hour. The solar PV has limitation due to sun

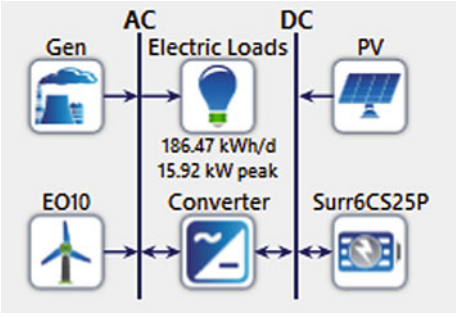

Fig. 4 Renewable and conventional energy sources schematic

availability during day time and at night the battery bank (Surr6c25P) supplies the power to the loads through converter for a period of the battery capacity. The wind (EO10) provides energy to the loads when solar PV and the battery are not accessible. The generator (Gen) system was used in the design simply to complements system's design, when other sources are under maintenance and therefore Gen can be used as a backup for maximum efficiency of the system.

The loads profile was made based on the operating hours by the CPE node. A single eNB comprises of PA, RF, BB and ONU located at an CPE node which operated 24 h per week. In this case, each eNB has some components that operated 24 h and others work for 12 h (from 18 to 6 h) only during the night when the temperature decreases and less traffic (off-peak).

Figure 5 shows the GHG emission produced per month from January to December considering the combination of solar, wind and genset architecture. The month of February (3.43%) and April (2.72%) has the less emissions compared to with July (11.27%), August (14.24%) and September (13.02%) indicating that the amount of solar radiation is higher in the first quarter compared to the third quarter of the year. The use of fossil fuel for GenSet in the third quarter of year is significant which increases the volume GHG emissions as shown in Fig. 5. However, the overall emissions released for the integrated NG-PON-WAN have been reduced by 77% within the project life time compared in [5].

4.3 Operational Cost Analysis

The system and the operational cost for an integrated NG-PON-WAN are presented on the bar chart diagram below. Figure 6 presented system cost which comprises the initial cost, operation and Maintenance (O&M) cost, replacement and fuel cost are accumulated in each component shown in Fig. 6a. The solar PV has highest cost, while the Autogenset recorded as the second highest cost. The solar PV will be the cheapest when selected for the period of 25 years of the project life time. On the

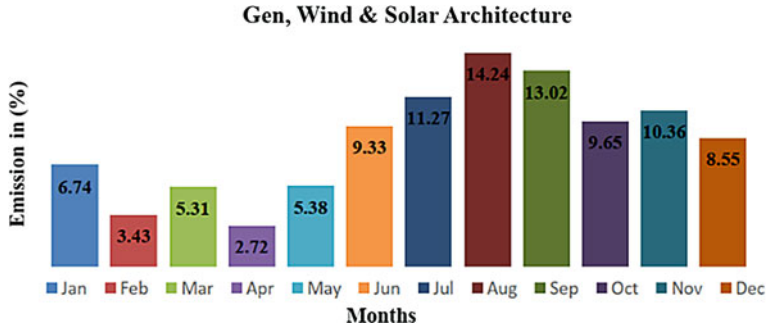

Fig. 5 Percentage of GHG emission considering solar, wind and genset architecture

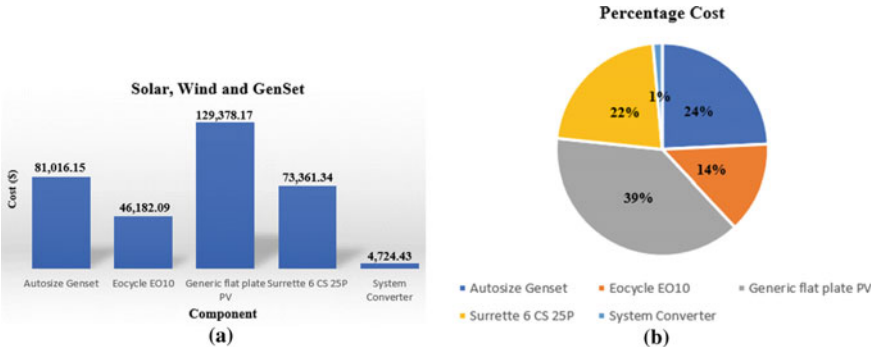

Fig. 6 Solar, wind and genset, **a** system cost and **b** percentage cost

other hand, Fig. 6b shows the percentage cost of the entire system and the highest indicated solar have 39% cost, an autogenset 24, 22% for batteries, wind turbines 14 and 1% for the system converter.

5 Conclusions

In conclusion, we presented the NG-PON-WAN system, which was modelled and simulated using Matlab software. The simulation was done in phases; the EN in the OLT location and the combined ONU-WAN at the CPE node. The Homer Pro software was used in simulating the CPE system's load with and without renewable energy sources. The renewable energy sources considered was based on the Skudai, Malaysia location and the obtained results were compared based on operational cost and CO_2 emission. A significant reduction of 77% GHG emission were achieved and 56% cost were saved for the project life time of 25 years.

Acknowledgements The authors would like to thank the Ministry of Higher Education of Malaysia and the administration of Universiti Teknologi Malaysia (UTM) for the financial assistance through Transdisciplinary Research Grant fund vote number 05G80.

References

1. Ricciardi S, Palmieri F, Fiore U, Castiglione A, Santos-Boada G (2013) Modeling energy consumption in next-generation wireless access-over-WDM networks with hybrid power sources. Math Comput Model 58(5–6):1389–1404. https://doi.org/10.1016/j.mcm.2012.12.004
2. Zhu M, Zeng X, Lin Y, Sun X (2017) Modeling and analysis of watchful sleep mode with different sleep period variation patterns in PON power management. J Opt Commun. Netw. https://doi.org/10.1364/jocn.9.000803

3. Alsharif MH, Nordin R, Ismail M (2015) Energy optimisation of hybrid off-grid system for remote telecommunication base station deployment in Malaysia. Eurasip J Wirel Commun Netw 2015(1):1–15. https://doi.org/10.1186/s13638-015-0284-7
4. Ramli A, Zulkifli N, Idrus SM (2017) Power consumption modeling and analysis of integrated optical-wireless access network. Int J Electr Comput Eng 7(6):3475–3483. https://doi.org/10.11591/ijece.v7i6
5. Aderemi BA, Daniel Chowdhury SP, Olwal TO, Abu-Mahfouz AM (2018) Techno-economic feasibility of hybrid solar photovoltaic and battery energy storage power system for a mobile cellular base station in Soshanguve, South Africa. Energies 11(6). https://doi.org/10.3390/en11061572
6. Al-Shammari HQ, Lawey A, El-Gorashi T, Elmirghani JMH (2019) Energy efficient service embedding in IoT over PON. In: International conference transparent optical networks, vol 2019-July, no April. https://doi.org/10.1109/icton.2019.8840429
7. OLT Cisco ME 4600 series optical line terminal, pp 1–8
8. Cisco (2013) Cisco ME 4600 series optical network terminal data sheet, pp 1–8
9. Kumagai Y, Funyu Y, Maeda H (2012) High-efficiency power amplifier for LTE/ W-CDMA system
10. Watanabe K, Machida M (2012) Outdoor LTE infrastructure equipment (eNodeB). Fujitsu Sci Tech J 48(1):27–32
11. Arnold O, Richter F, Fettweis G, Blume O (2010) Power consumption modeling of different base station types in heterogeneous cellular networks. In: 2010 Future Network & Mobile Summit, pp 1–8
12. Luo Y, Zhou X, Effenberger F, Yan X, Peng G, Qian Y, Ma Y (2013) Time-and wavelength-division multiplexed passive optical network (TWDM-PON) for next-generation PON stage 2 (NG-PON2). J Lightwave Technol 31(4):587–953

Integrated Circuit Characterisation Using Low-Cost Coaxial Probe Measurement

Lik Suong Ding and Xavier Ngu

Abstract This paper presents a method to characterise integrated circuit (IC) using a low cost coaxial probe. The characteristic impedance of the IC can be used in both time and frequency domain, where it significantly improves the behavioral model of a printed circuit board (PCB) circuitry which is currently being used with limited functionality. S-parameter results obtained from the measurement using the coaxial probe was combined in the simulation model of the PCB which was simulated using three-dimensional (3D) full wave simulation. A comparison between the measurement and simulation results was made and it shows that the measured IC characteristic impedance through the devised low cost probe method produces good correlation up to 1,000 MHz. This study concludes that the feasibility of using the proposed technique for impedance characterisation of IC to be included into the PCB circuitry would provide a better understanding of signal and power integrity, and electromagnetic compatibility (EMC).

Keywords Electromagnetic compatibility · Impedance · Integrated circuit · Printed circuit board · S-Parameter · Probe · Low cost

L. S. Ding · X. Ngu (✉)
Faculty of Electrical and Electronic Engineering, University Tun Hussein Onn Malaysia, 86400 Batu Pahat, Johor, Malaysia
e-mail: xavier@uthm.edu.my

L. S. Ding · X. Ngu
Center for Applied Electromagnetic, University Tun Hussein Onn Malaysia, 86400 Batu Pahat, Johor, Malaysia

L. S. Ding
RF Station Sdn. Bhd, A-2-7, Glomac Damansara, Jalan Damansara, 60000 Kuala Lumpur, Malaysia

Z. Zakaria and S. S. Emamian, *Advances in Electrical and Electronic Engineering and Computer Science*, Lecture Notes in Electrical Engineering 741,
https://doi.org/10.1007/978-981-33-6490-5_6

1 Introduction

Characterisation of IC is extremely important. Without good understanding of the IC, engineers are unable to correctly utilise the full potential of the IC. This is because each IC normally has typical, minimum and maximum performance. Engineers need to use the IC with correct characteristic in their simulation model to simulate the rise time and fall time along with their parasitic effect in order to maximize the value of each IC produces. Characteristic impedance is relevant to signal integrity analysis. However, Input/Output Buffer Information Specification (IBIS) models that are provided by most IC suppliers are inadequate due to the lacking of characteristic impedance information. IBIS model only provides the rise time and fall time of certain input/output (I/O) pins, but the characteristic impedance of the pins are not available. The input/output buffer information that is provided by the IBIS model is only useful for engineers to evaluate the signal integrity and the quality of the signals. The characteristic impedance is important for frequency domain analysis of the transmission line on the printed circuit board (PCB). Study done by Pucili et al. [1] has shown that IBIS has certain limitation, which includes lacking information of power supply rail stabilization, as compared to a SPICE model which is the actual or lumped components of the complete IC.

Automotive Electronics Council highlights the importance of the characterisation of the IC through a guideline [2] that recommends all automotive components suppliers to follow in order to comply to different standards worldwide. This will facilitate a standardized model for simulation in order to reduce the product development cycle, where each prototype will take months to complete and verify. When the crucial characteristic impedance information of an IC is not available, the prototype will be either over or under-designed. This wastes a lot of time, efforts and cost to the original equipment manufacturer (OEM).

Characterisation of an IC begins by obtaining the equivalent circuit of a transistor gate, by representing a transistor with an Equivalent-Tee circuits [3]. However, representing a complex IC into many Equivalent-Tee manually is a complicated task and would waste a lot of time and cost. Many researchers [4] have shown many complex measurement methods to extract data of an IC, in which correct termination and shorting the internal connections to accurately capture the resistance, capacitance and inductance of each pins are required. This method is not feasible for application engineers, who only have access to the commercialize ICs.

A recent research paper [5] summarises the existing methodologies available to characterise ICs and interconnects. IC characterisation is crucial because it improves the efficiency of the design and development stage. Proposals to use frequency domain and time domain were also introduced in the summary shown in [5].

Recently Jeong [6] performed a study on electrical characterisation of a ball grid array (BGA) using S-parameter method, and compared it with other traditional methods like the impedance measurement and the Time Domain Reflectometry (TDR) methods. The results show that by using one-port S-Parameter method the measurement time is a lot faster and the accuracy can be kept within 0.3% for

frequency up to 500 MHz. However, this method requires expensive probe station and it neglects the coupling between the pins. Another study [7] on BGA was done using a microprobe station to study the coupling effect between tracks. It was found that the frequency domain method is more accurate when used with the correct de-embedding method to remove the effect of the cable losses, fixture effect and parasitic effect. The disadvantage of this method is the need to prepare a customised BGA board to measure the open, short, load, and thru. This is not feasible in many applications where limited resources are available and also engineers are normally required to characterise more than one IC. To characterise all ICs in their applications, the job is simply too overwhelming.

While it is important to characterise an IC, it is also equally important to characterise the used test board. Wang et al. [8] demonstrated a noble way to characterise all components on a low-dropout (LDO) voltage regulator test board. After characterising all the components on the test board, an accurate model of the LDO IC can be obtained up to 2,000 MHz. The non-linear impedance of the IC and test board are captured reasonably well and translated into equivalent circuits of individual RLC components. However, the completed equivalent circuits are still unable to fully correlate with the characteristic of the LDO's immunity at high frequency. This can be improved by representing the equivalent circuits with higher order equivalent circuits.

Another way of characterising the IC is by using RF micro-probes [9]. High precision RF micro-probes can be used to measure the IC impedance up to 110 GHz [10]. However, RF micro-probes are very expensive and must be used delicately to ensure correct probing of the IC. They must be handled with care and often only dedicated experts are allowed to operate the machines. Calibration techniques of the RF micro-probes are also very crucial in order to measure the characteristic of the IC correctly.

Another challenge when measuring the IC impedance is that the calibration technique requires the IC to be shorted or loaded internally. This is impossible for engineers because only the manufacturers has access to the internal circuits of the IC only. The manufacturers can customise the IC to the desired conditions for calibration purposes. Their engineers can then calibrate their probes or boards using these ICs for Open-Short-Load calibration before actually measuring the final IC impedance. This allows the engineers to obtain more accurate data up to 3 GHz [11]. However, this is not possible for user other than the manufacturers themselves where they only have access to off-the-shelf IC that is commercially available.

2 IC Impedance Measurement Using Low-Cost Coaxial Probe

2.1 Low-Cost Coaxial Probe Fabrication

For the measurement of the IC impedance in this study, a customised probe was produced. A 50 Ω RG402 semi rigid cable was used to create the probe. Semi rigid

cable was used because of its stable performance and ability to connect to the 50 Ω cables with different connectors. The cable was connected to a female 3.5 mm coaxial connector on one end, A-Side, and the other end was left open, B-Side, as shown in Fig. 1. The B-Side was prepared to connect and disconnect from a male 3.5 mm coaxial connector acting as a connection to the calibration kit. When the B-side's coaxial is disconnected, it will be used as the probe to measure the chip impedance. During the calibration, the B-Side will be connected to the male 3.5 mm coaxial connector securely to ensure the ground of the semi rigid cable is connected properly. For the calibration, Rohde & Schwarz R&S®ZV-Z135 Calibration Kits was used because of its performance up to 15 GHz. This method is more accurate as compared to customised Thru-Reflect-Line (TRL) calibration board due to the broadband requirement.

In the first design of the probe, a spring loaded pogo pin is connected to the outer shell of the coaxial cable as shown in Fig. 1. The pogo pin provides a good contact during the measurement because of the spring inside the pogo pin, but it lacks flexibility in terms of the gap between the center conductor and the pogo pin. This is problematic if different sizes of ICs are required to be measured. Hence, a revised probe was designed using a copper wire, which can be bent to accommodate contact at different distances. The revised probe is shown in Fig. 2.

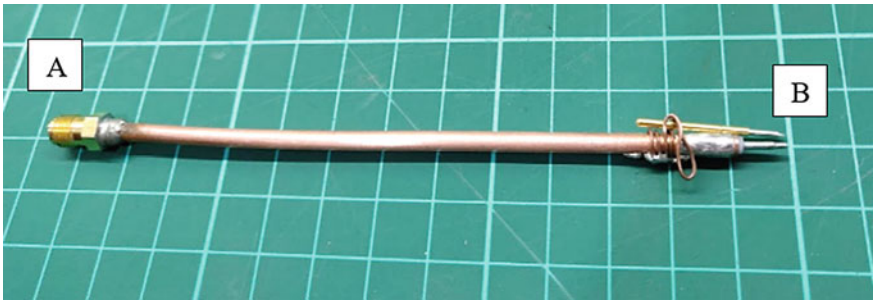

Fig. 1 Customised probe with pogo pin

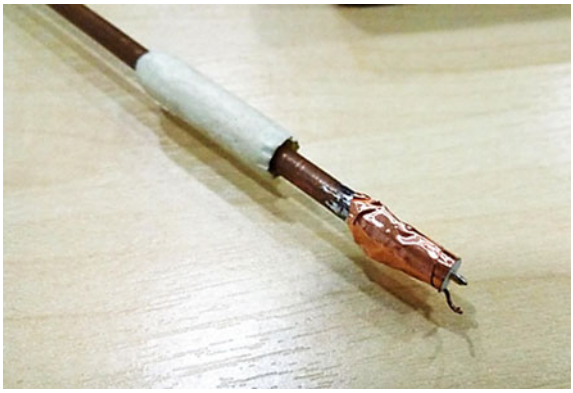

Fig. 2 Revised probe with copper wire, Teflon insert and copper tape

To reduce stray parasitic inductance and capacitance caused by the wire, the Teflon insert from the coax connector was also left at the tip of the probe to shorten the length of the center conductor. Copper tape is then used to wrap the wire, coaxial cable and the Teflon insert to maintain a constant 50 Ω as much as possible. This final setup is more similar to the physical setup of the coax connector when it is connected to the 3.5 mm SMA calibration kit.

2.2 Test Board for IC Characterisation

IC used in this study is an Electromagnetic Interference (EMI) filter at line termination for USB upstream ports from STMicroelectronics. Model of this IC is USBUF [12]. This IC was chosen because it is one of the most popular device used in modern devices due to its small footprint and its cost effectiveness. This IC not only filters the EMI from the PCB but also used to withstand Electrostatic Discharge (ESD) up to 15 kV air discharge. In this study, the challenge is to handle this device due to its size, the dimension is merely 2 mm (length) by 1.25 mm (height). Each pin's width is only 0.3 mm. The functional diagram and dimension of the IC are shown in Fig. 3.

To measure the S-Parameter of the IC, a customised FR4 PCB test board was fabricated to hold the IC (test board A) as shown in Fig. 4. The IC's ground pin and the 3.3 V voltage input pin were shorted to the PCB ground through vias with the bottom ground. Other pads are then connected to 50 Ω surface-mount device (SMD) resistors to perfectly matched probe's impedance. First, test board A was set up by leaving pin 1 and 6 open, pin 2 and 5 shorted to ground, and pin 3 and 4 soldered to 50 Ω resistors. The test board was held in place by a fixture to prevent movement during the probing measurement. The probes were held stable by a rotary arm to prevent accidental movement while capturing the data obtained from a

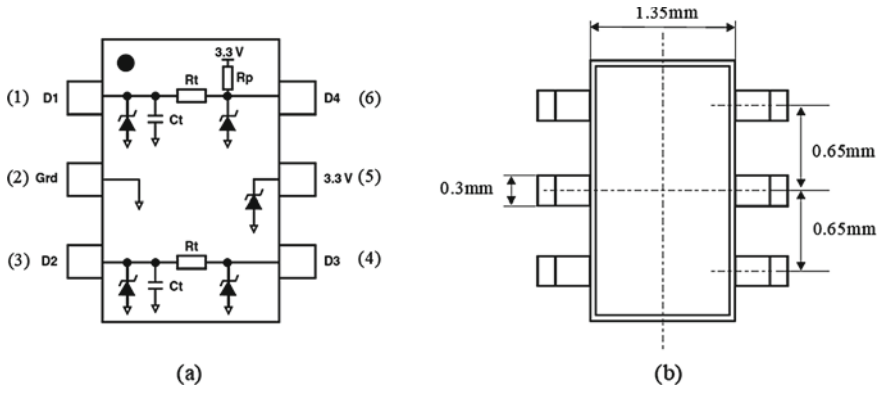

Fig. 3 **a** Functional diagram of the IC, and **b** package dimension of the IC

Vector Network Analyzer (VNA) from R&S® model ZVB8. Pin 1 and pin 6 were measured with port 1 and port 2 respectively. Ferrite cores were installed along the length of the cable to prevent emission due to the unbalanced current at the outer layer of the coaxial cable. The measurement setup is shown in Fig. 5.

After measuring pin 1 and 6, the obtained S-Parameters of the IC are stored as touchstone file, namely s2p to be used later in test board B simulation. The S-Parameter results are shown in Fig. 6. A slight resonant can be observed at around 1,700 MHz for both S1,1 and S2,2 which is due to the parasitic effect of the copper wire. When both probes are near to each other, coupling between them becomes stronger and they act as a miniature antennas. This coupling is difficult to prevent because the ground wire is needed to maintain flexibility and at the same time measures the S-Parameters of the IC at various locations.

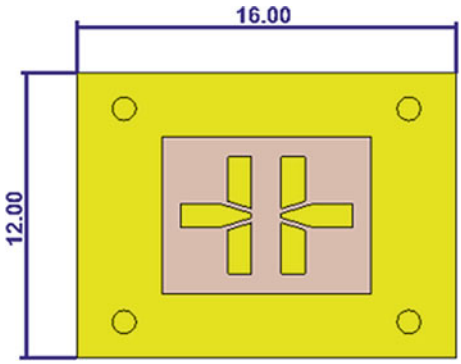

Fig. 4 Test board A to measure IC impedance

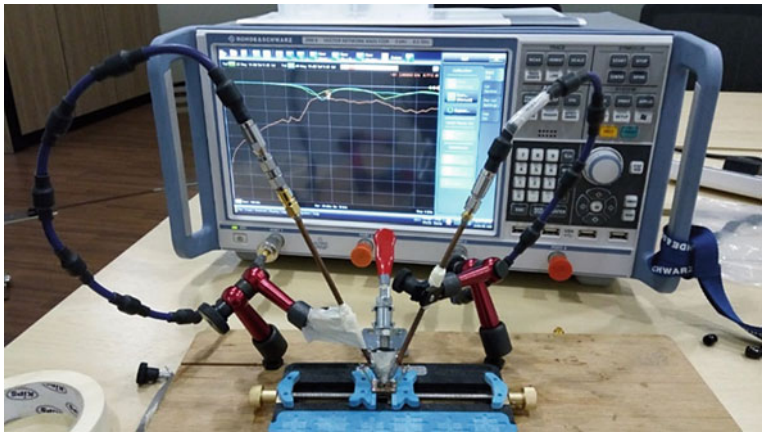

Fig. 5 Measurement setup of test board A with probes being held by a fixture

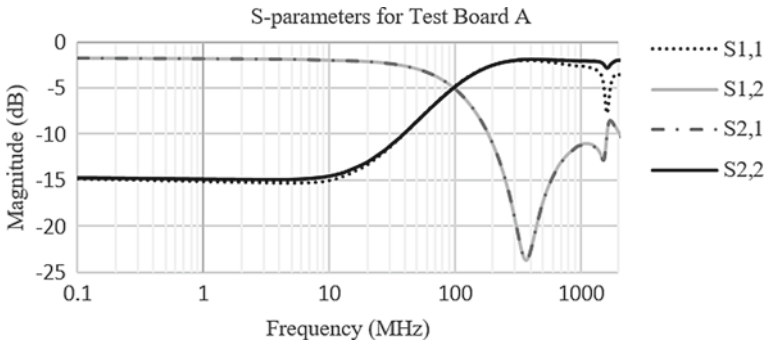

Fig. 6 Measured S-parameters on test board A

3 IC Characteristic Impedance Implementation

3.1 Combining the S-Parameters of Simulated Test Board with Measured IC Characteristic Impedance

Another test board (test board B) was fabricated to verify the IC characteristic impedance measured in test board A. Test board B as shown in Fig. 7 (a) was fabricated based on the datasheet from STMicroelectronics as shown in Fig. 7 (b). Since test board B has less discontinuity i.e. close to 50 Ω characteristic impedance transmission line and connected to a 50 Ω SMA connector, test board B shall yield better result. The aim here is to compare the results between test board A and B. To maintain a 50 Ω transmission line from the coaxial connector, coplanar waveguide with ground (CPWG) transmission line was used in test board B. In order to achieve 50 Ω on the CPWG transmission line with a 1.6 mm FR4 PCB, the track width is 2.5 mm with ground clearance of 1 mm. The width of the transmission line is very different as compared to the datasheet because the manufacturer did not mention the material used for the PCB as well as the transmission line physical properties. Hence, FR4 is used for the test board B due to this limited resources. For this test setup, the ground pin (pin 2) of the IC was shorted to the voltage input pin (pin 5), while pin 3 and pin 4 are left open, as documented in the datasheet model.

Test board B is then modeled in 3D within Computer Simulation Technology (CST) software. CST is a full wave 3D electromagnetic (EM) simulation software that can accurately simulate the behavior of the EM wave across 3D structure based

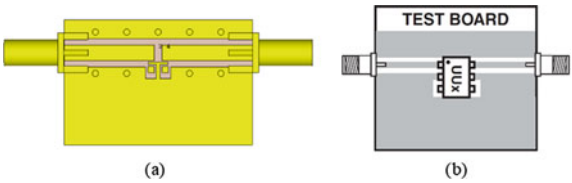

Fig. 7 **a** Fabricated test board B based on datasheet, and **b** test board model from datasheet

on Maxwell Equation [13]. In the simulation model, the SMA connectors were also included to improve the realism of the transmission line. The vias location are also similar to the actual fabricated PCB.

In the 3D simulation of test board B, ports are defined to capture the S-Parameters. Port 1 is defined on the SMA connector on the left, port 2 is defined at pin 1, port 3 is defined on the SMA connector on the right, and lastly port 4 is defined at pin 6. Simulated 4-ports S-Parameters of the 3D model can then be renormalised in Design Studio which is the circuit simulator of the CST.

Within the Design Studio as shown in Fig. 8, the block with four pins represents the simulated four-port S-Parameters. Each pin represents the simulated ports from the 3D model. Pin 1 and pin 3 are connected to the excitation Port 1 and Port 2 respectively, while pin 2 and pin 4 are connected to the measured touchstone file acquired from test board A. This touchstone file is the s2p of the IC's S-Parameters acquired from the probe. In the Design Studio, new S-Parameter results are simulated in which the 3D results are renormalised by including the IC characteristic impedance.

Test board B is also fabricated based on the exact dimension in the simulation model as shown in Fig. 9. Test board A has the practicality to be implemented in existing PCB, but the accuracy of this method must be proven by comparing results obtained from test board B which are more accurate due to the continuity of the 50 Ω characteristic impedance on the CPWG transmission line.

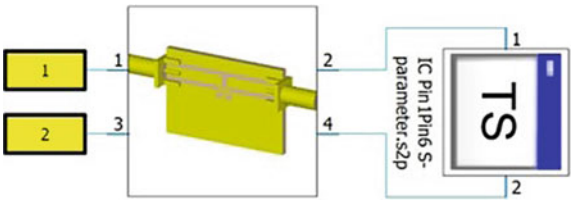

Fig. 8 Test board B 3D model configuration inside CST design studio using measured touchstone file from the measurements

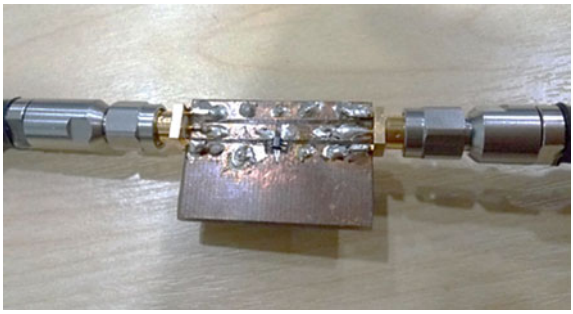

Fig. 9 Test board B measurement of pin 1 and pin 6 through CPWG transmission line with SMA connectors

3.2 Characteristic Impedance Verification with Test Board

Figure 10 shows the comparison between results obtained from Test board B measurement and the simulated 3D model. Both measured and simulated results have identical S1,1 and S2,2, due to the symmetry transmission line. Hence the graph is simplified to improve visibility of the comparison. It is observed that both the return loss (S1,1) and the transmission (S1,2) correlate reasonably well up to 1,000 MHz. A resonant in S2,1 at 400 MHz can be noticed in both the results. Transmission is also good from 0.1 MHz to 100 MHz at around −2 dB to −5 dB. There is a mismatch in S2,1 between 1,000 MHz and 2,000 MHz which could be caused by the said imperfection of the copper wire from the probe. It is already known from above chapter, that there is resonant from the copper wire at high frequency, therefore only up to 1 GHz result should be focused on. The simulated results is also identical to the probe results from test board A (Fig. 6), which means that the transmission line from the test board B has minimum impact to the characteristic impedance of the IC.

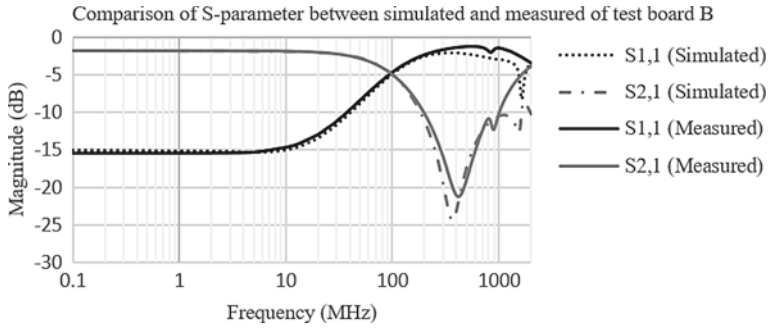

Fig. 10 Comparing S-Parameter results obtained from (simulated) with the (measured) test board B

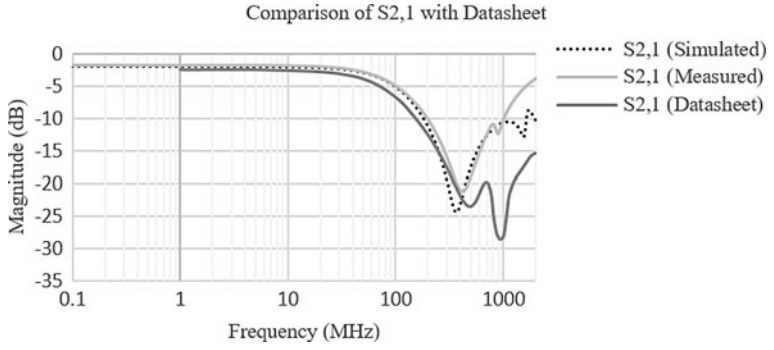

Fig. 11 Comparison of S2,1 between simulated and measured test board B, and the manufacturer's datasheet

Comparison was also made between the declared S2,1 from the datasheet of the IC manufacturer, fabricated test board B and the simulated results as shown in Fig. 11. First resonant is present on all of the results at around 500 MHz but the second resonant at 1,000 MHz is not available in both measured test board B and simulated results. This may be due to the difference on the test boards. The manufacturer does not disclose the PCB design specification and the track width of the test board, which is obviously much narrower as compared to the fabricated test board B. The effect captured in the datasheet is not the IC characteristic alone but also included the effect of tracks and pads on the PCB.

4 Conclusion and Future Work

The paper has shown that the method of using a low cost coaxial cable is able to characterise the impedance of the IC pins. This method was used on the test board A and later included the characteristic impedance of the IC in the simulation model of test board B. The results are then compared with fabricated test board B, which technically should produce better result. Both results correlates reasonably well. This verifies the method of using low cost coaxial cable in obtaining characteristic impedance of an IC.

Future work is to further improve on the probe and to perform similar approach on a more complicated 64 pins quad flat package (QFP) IC.

References

1. Pulici P et al (2008) A modified IBIS model aimed at signal integrity analysis of systems in package. IEEE Trans Circuits Syst I Regul Pap 55(7):1921–1928
2. Sullivan MO et al (2013) Guideline for characterization of
3. Pritchard RL (1998) Transistor equivalent circuits. Proc IEEE 86(1):150–162
4. Caggiano MF, Ou J, Bulumulla S, Lischner D (2001) RF electrical measurements of fine pitch BGA packages. IEEE Trans Compon Packag Technol 24(2):233–239
5. McGibney E, Barrett J (2006) An overview of electrical characterization techniques and theory for IC packages and interconnects. IEEE Trans Adv Packag 29(1):131–139
6. Jeong J (1999) Electrical characterization of ball grid array packages from S-parameter measurements below 500 MHz. IEEE Trans Adv Packag 22(3):343–347
7. Horng TS, Tseng A, Huang HH, Wu SM, Lee JJ (1998) Comparison of advanced measurement and modeling techniques for electrical characterization of ball grid array packages. Proc Electron Compon Technol Conf F1334:1464–1471
8. Wang Z, Zhou C, Member S, Liu T, Zhao S, Liang Z (2016) Nonlinear behavior immunity modeling of an LDO voltage regulator under conducted EMI, pp 1–9
9. Bullard B, McNamar R, McNally S (2018) RF probing of custom ASIC's. In: 2005 66th ARFTG microwave measurement conference: digital communication system metrics, ARFTG 2005, pp 1–7

10. Sattler SW, Gadringer ME, Gentili F, Alterkawi ABA, Bösch W (2017) PCB RF probe landing pads for multiline deembedding. In: PRIME 2017—13th conference on PhD research in microelectronics and electronics, proceedings, vol 1, pp 209–212
11. Boyer A, Sicard E, Fer M, Courau L (2008) Electrical characterization of a 64 ball grid array package. In: IEEE international symposium on electromagnetic compatibility, vol 1
12. STMicroelectronics. USBUF—2-line EMI filter and ESD protection with R pull-up, for USB interfaces. Available: https://www.st.com/en/emi-filtering-and-signal-conditioning/usbuf.html . Accessed on 26 Mar 2020
13. Vandenbosch GAE, Vasylchenko A (2012) A practical guide to 3D electromagnetic software tools. Microstrip Antennas 1:23–38

A More Efficient and Accurate Approach to Characterise an IC into Macro Model

Lik Suong Ding and Xavier Ngu

Abstract Traditional workflow to obtain macro model of an Integrated Circuit (IC) requires expensive probing measurement system as well as complex in-house program. In this paper, a more practical method to create an accurate macro model of an IC is introduced. IC's characteristic impedance has to be measured using a special probe be-cause most of the circuitry are proprietary and inaccessible to engineers. After acquiring all the combinations of the IC's characteristic impedance, the complete sets of the measured results are compiled by using a software specifically written for this purpose. The compiled results are then converted into a macro model where passivity and causality are then enforced. The macro model has to be passive to correctly represent the actual behavior of the IC. Passivity and causality of the model are enforced by using a commercially available tool and is further simulated using Computer Simulation Technology (CST) software.

Keywords Electomagnetic compatibility · Characteristic impedance · Integrated circuit · Printed circuit board · S-Parameter · Macro modeling · Passivity · Causality · SPICE

L. S. Ding · X. Ngu (✉)
Faculty of Electrical and Electronic Engineering, University Tun Hussein Onn Malaysia, 86400 Batu Pahat, Johor, Malaysia
e-mail: xavier@uthm.edu.my

L. S. Ding · X. Ngu
Center for Applied Electromagnetic, University Tun Hussein Onn Malaysia, 86400 Batu Pahat, Johor, Malaysia

L. S. Ding
RF Station Sdn. Bhd, A-2-7, Glomac Damansara, Jalan Damansara, 60000 Kuala Lumpur, Malaysia

Z. Zakaria and S. S. Emamian, *Advances in Electrical and Electronic Engineering and Computer Science*, Lecture Notes in Electrical Engineering 741,
https://doi.org/10.1007/978-981-33-6490-5_7

1 Introduction

In this paper, an Integrated Circuit (IC) called Digital Transmitter from an Advanced Driver Assistance System (ADAS) evaluation board was chosen as the Device Under Test (DUT) where the IC internal impedance are known only to the chip manufacturer. To characterise the IC correctly for all simulation purposes, a novel method is required to acquire the characteristic impedance quickly and accurately. This work will ensure that future simulations no longer assume an IC as a black box. A black box is a condition where there is no coupling between the pins internally. As a results, this simulation produces less accurate results. The workflow of this work is shown in Fig. 1.

There are many methods to characterise multi-ports device using only two (2) ports vector network analyzer (VNA), such as the work done by Tippet and Speciale [1], where a method to renormalise the measured Scattering Parameter (S-parameter) by a known impedance was introduced. In a S-Parameter measurement, each port will be terminated with a known load, which is normally 50 Ω. However, the mismatched load will introduce parasitic effects into the measured S-Parameter results. To counter this shortfall, Kam [2] performed a conversion with an error-correction method to renormalise the measured results with a known termination.

However, this method requires extensive understanding of the mathematics behind the conversion in order to perform this calculation accurately. Furthermore, it is only logical to perform this conversion by using a software because the ICs used in commercial are normally more than four pins.

There is also a limitation where the calculation requires a correctly determined termination [3] in order to solve the unknown in the calculation. This unknown normally comes from the tracks which are connected to the IC pins. Without accurate measurement of the termination, it will produce errors in the mathematical

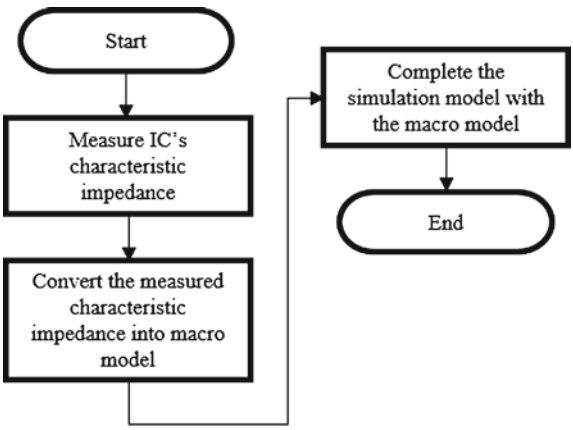

Fig. 1 Project workflow

calculation matrices. Without a clear understanding of the probes, the DUT is almost impossible to be correctly characterised.

In this paper, a method is introduced by terminating the IC with 50 Ω resistor networks. In this work, the IC is characterised up to 1,000 MHz only due to the limitation of the equipments. The characteristic impedance of the IC is measured in terms of S-Parameter, which is normally used in frequency domain analysis.

After characterising the IC, the S-Parameters of the IC are converted into a macro model [4], namely the SPICE model. SPICE model is a representation of a component in terms of equivalent circuits, which consist of resistor-inductor-capacitor (RLC) lumped components. A SPICE circuit is more practical in real cases because it can be used in both time and frequency domains. On the other hand, a touchstone file which contains only the frequency response data has two noticeable limitations. Firstly, the data beyond the measured frequency will not be known e.g. frequency response at 2,000 MHz could not be obtained or estimated from a S-Parameter result of 0–1,000 MHz. Secondly, to obtain the time domain response, vector fitting has to be performed in each of the simulations to estimate the time domain response based on the frequency data. This increases the simulation time significantly. In addition, there is also a limitation due to the vector fitting algorithm used in the simulation software.

The SPICE model on the other hand is generated based on a certain level of order of vector fittings by using RLC lumped components in order to synthesise the frequency domain responses [5]. There is no need to perform further vector fitting in the simulations because the accuracy is reasonably acceptable from direct current (DC) up to the provided frequency range. Higher frequency results can also be simulated and measured, but it is necessary to maintain the accuracy of the SPICE model because at higher frequency, higher order resonants will also be present. Without characterising these higher order resonants in the SPICE model, the model beyond its frequency range should not be used.

After converting the characteristic impedance of the IC into a SPICE model, the causality and passivity enforcements will be performed on the model. This is because most of the measurement will contain certain level of parasitic effects, for example a small resonant or a spike where it is normally difficult to notice. RLC lumped components are always passive, where the energy output will never be higher than the energy input. A causal system means that the response of an output signal will never be earlier than the input signal [6, 7, 8]. Both causality and passivity enforcements will further improve the accuracy of the SPICE model which is normally introduced by human error and/or measurement devices.

2 IC Characterisation Using a Two-Port VNA

To successfully characterise the IC, measurements on all relevant pins are performed using a two-port vector network analyser (VNA), to obtain the S-Parameters of the pins i.e. S1,1, S1,2, S2,1 and S2,2. In this work, Texas Instrument's

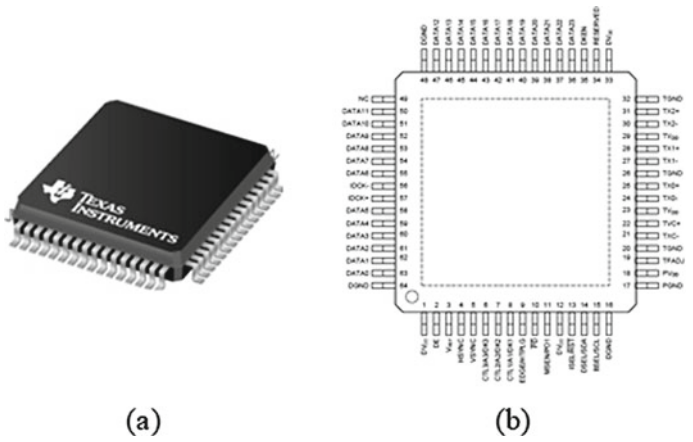

Fig. 2 **a** TI PanelBus digital transmitter and **b** pins configuration [9]

TFP410 TI PanelBus™ Digital Transmitter was chosen because it is commonly used in many ADAS system to interface with display panel such as the HDMI interface. This IC is housed in a 64 pins Thin Quad Flat Package (TQFP) with different combinations of input/output (I/O) pins, differential pins, as well as power and ground pins. The physical structure and pin configuration are shown in Fig. 2.

In the S-Parameter measurement, all the pins except power and ground pins will be characterised. The reason of the exclusion is because both the power and ground pins are designed to have low internal resistance and they are connected directly to the power planes and ground planes. The power and ground pins need to have low impedance in order to ensure smooth power delivery, which will not be explained in details in this work. During the characterisation, the power pins and ground pins are shorted to ground. Out of the 64 pins, only 48 pins are required to be characterised, because the remaining pins are power and ground pins.

Prior to the measurement, the IC is soldered onto a breakout board. The power pins and ground pins are shorted to a 150 mm by 150 mm ground plane, while the remaining 48 pins are terminated with 50 Ω series resistors networks. The breakout board is shown in Fig. 3, where the breakout board is slightly elevated with a 3D printed support, to prevent the exposed soldered connections of the series resistors from shorting to the ground plane.

In another work, a low cost coaxial probe was designed using a pogo pin as a solid connection to the ground. The pogo pin is soldered to the ground of the coaxial to restrict the pogo pins from movement during the probe measurement. The probe is shown in Fig. 4. The coaxial probe is connected to the VNA so that S-Parameter measurement can be performed on the IC pins.

The measurement flowchart is shown in Fig. 5. All possible combination of the pin pairs are selected by using the combination equation in (1) which is also known as "*n* choose *r*" where it shows the number of ways to choose from *r* elements from a total number of *n* objects. The equation states that for a 48 pins configuration,

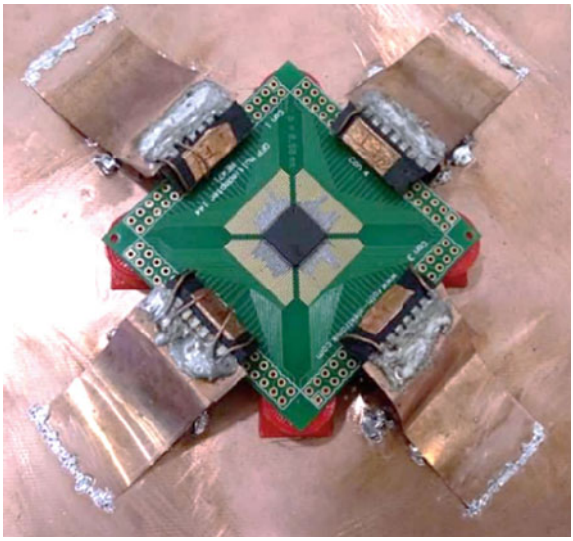

Fig. 3 The IC soldered onto a breakout board with series resistor networks for termination

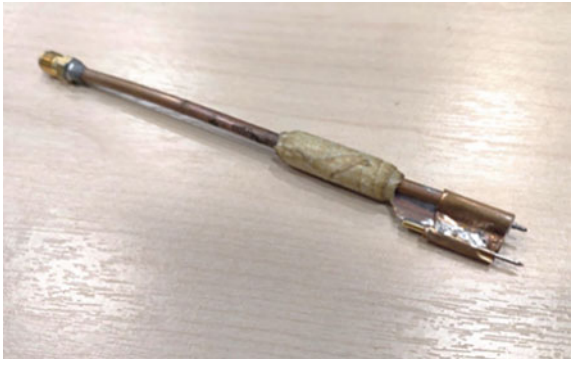

Fig. 4 A low cost coaxial probe with a pogo pin soldered to the ground

without repeating the same combination, there will be a total of 1,128 combinations, e.g. *S1*,*2*, *S1*,*3*, *S1*,*4*, …, *S47*,*48*, etc.

$$\frac{N}{2} = \frac{N!}{2!(N-2)!} = \frac{N \cdot (N-1)}{2} \tag{1}$$

To ease the probing process, additional grounds are connected at the corners and also at the top of the IC as shown in Fig. 6. This is to ensure that the common grounding is accessible to the probe during the measurement due to the limited distance between the inner conductor of the probe and the pogo pins (ground). The final breakout board with the probe is shown in Fig. 6 where it can be seen that the probe has to be precisely probing the intended track without touching the neighbouring track.

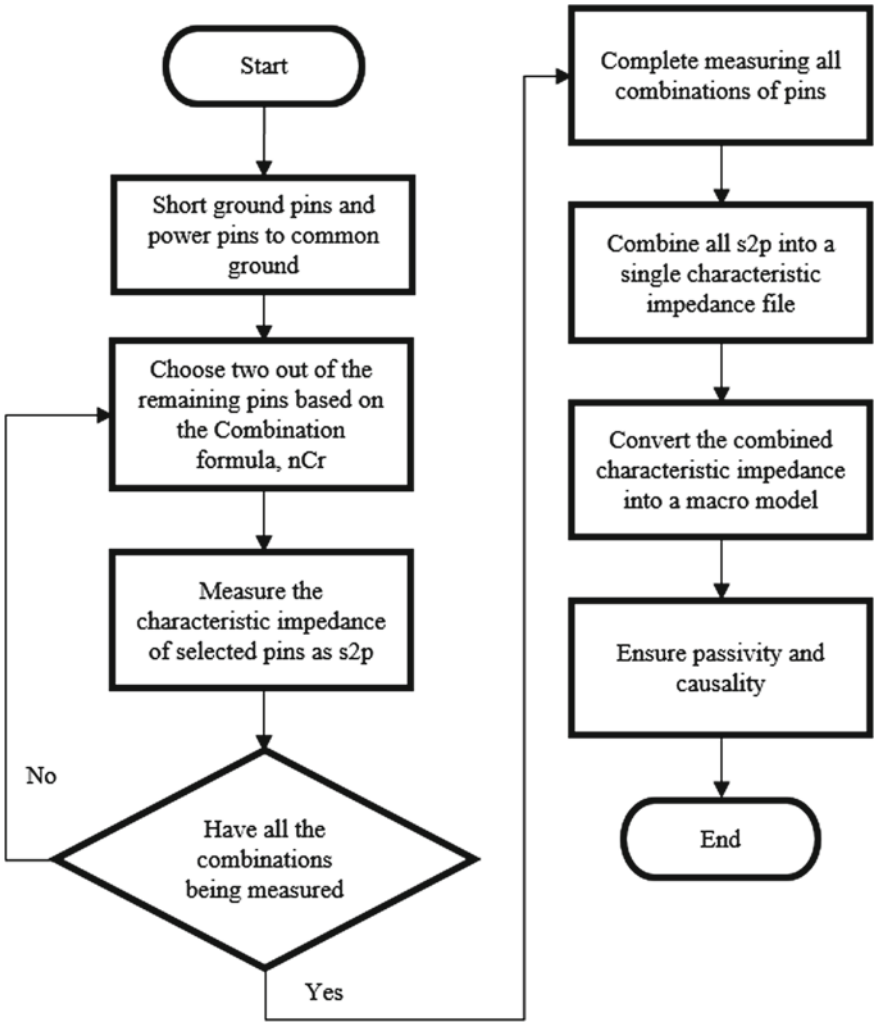

Fig. 5 The measurement process flowchart

During the measurement, the tracks have to be sliced to create an open circuit. Otherwise, they will be terminated with the 50 Ω resistors. For example, in order to obtain *S1*,*2*, pin 1 and pin 2 have to be disconnected from the resistor during the measurement. Next, to obtain *S1*,*3*, the track on pin 2 has to be reconnected by soldering it with thin wire, while the track on pin 3 has to be sliced. Due to the enormous effort and the possibility of damaging the tracks permanently if all 48 tracks have to be sliced and reconnected through the 1,128 combinations, only 10 pins are measured as to prove this concept. The pins chosen are based on their different functions, i.e. general I/O pins, differential pins and clock pins. There are

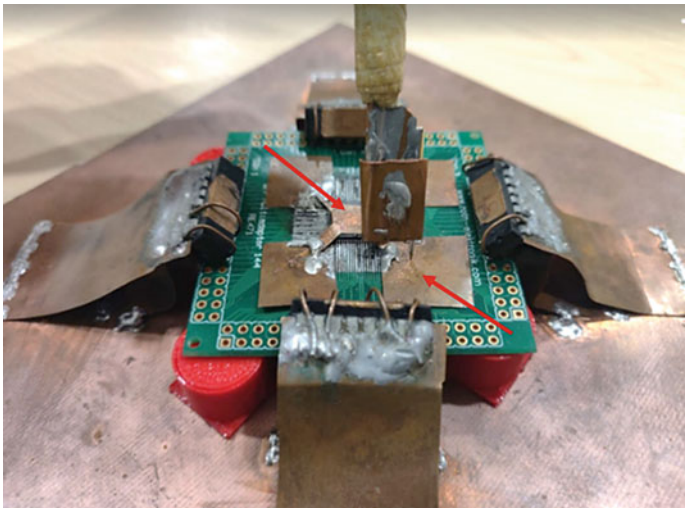

Fig. 6 Final breakout board with probe (arrows show additional ground plane)

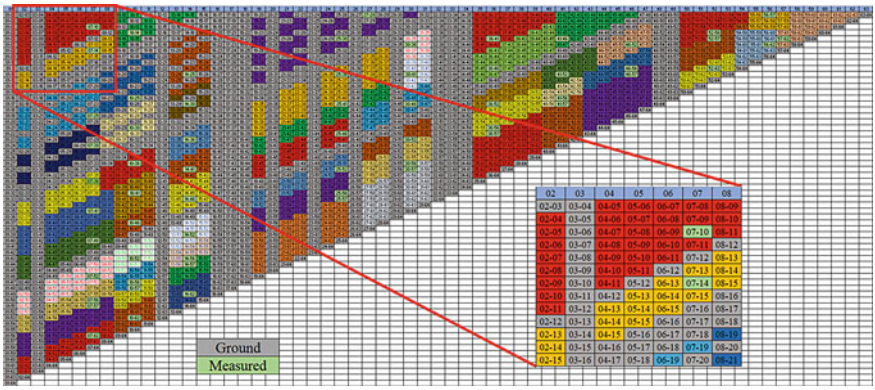

Fig. 7 Final measured pin combinations, and colour coded according to the neighbouring pins. Zoom in view for better visualisation for pin 54 to pin 63

also selected based on their location at different quadrants of the IC, in order to obtain variation information on all four quadrants. By selecting only 10 pins, the total number of measurement reduced to 55 combinations. The final measured data is shown in Fig. 7. Grey columns represent ground, while light green columns represent the measured combinations. Assuming that the neighbouring pairs will have similar coupling responses, the measured pin combinations are then applied to these neighbouring pins. They are colour coded to groups based on the measured data. Referring to Fig. 7's zoom in view, the top row represents the pin number, while 07–10 means the pair combination of pin 7 and 10. The light green color of

07–10 means that it is measured, while the red color cells around it are duplicated based on the measured results from 07 to 10. This is repeated for all combinations.

The measured data is captured in touchstone format, namely the s2p format which is the frequency response of a two-port S-Parameters. They are *S1*,*1*, *S1*,*2*, *S2*,*1* and *S2*,*2*. The combinations of s2p are replicated on pins that are not measured based on the color coded groups shown in Fig. 7. After acquiring all the s2p of 1,128 combinations out of the 48 pins, they are combined into s48p. These measured data are then combined using a self-written software where all the relevant data will be restructured from a 4 × 4 matrix to $N^2 \times N^2$ matrix, where N is the number of pins. Each s2p contains the real and imaginary part of each S-parameter i.e. *S1*,*1*, *S1*,*2*, *S2*,*1* and *S2*,*2*, therefore giving us the 4 × 4 matrix. Therefore, the s48p is a $48^2 \times 48^2$ matrix.

To perform the combination, it is more practical to use a self-written software. The software was written in JAVA due to the simplicity of utilizing the built in libraries e.g. array list library, file chooser library, file writing library and etc. After combining all the 1,128 combinations of the results, a final touchstone file is produced in a single output file which represents the s48p. Part of the touchstone file is shown in Fig. 8. A touchstone file is defined to start with the frequency point, following by real and imaginary of each data sample separated by a common space.

The s48p touchstone file is then validated in Computer Simulation Technology (CST) circuit simulator to ensure the usability. The s48p touchstone file is successfully simulated with 48 ports, and the S-Parameters of a 48-port system is obtained. Part of the simulated S-Parameters is shown in Fig. 9 where it can be noticed that the return loss (*S1*,*1*) is near to 0 dB at low frequency and starts to couple to neighbouring tracks at high frequency. This confirms the capacitive behaviour of an IC where during DC the signal is unable to couple to neighbouring tracks within the IC itself. The different coupling behaviour between different pins also confirms that one could never assume that the IC as a black box because at different frequencies, the coupling for *SN*,*1* (with $N = 2, \ldots, 48$) exists in different magnitudes between the neighbouring tracks, as well as the opposite tracks.

Fig. 8 s48p touchstone file

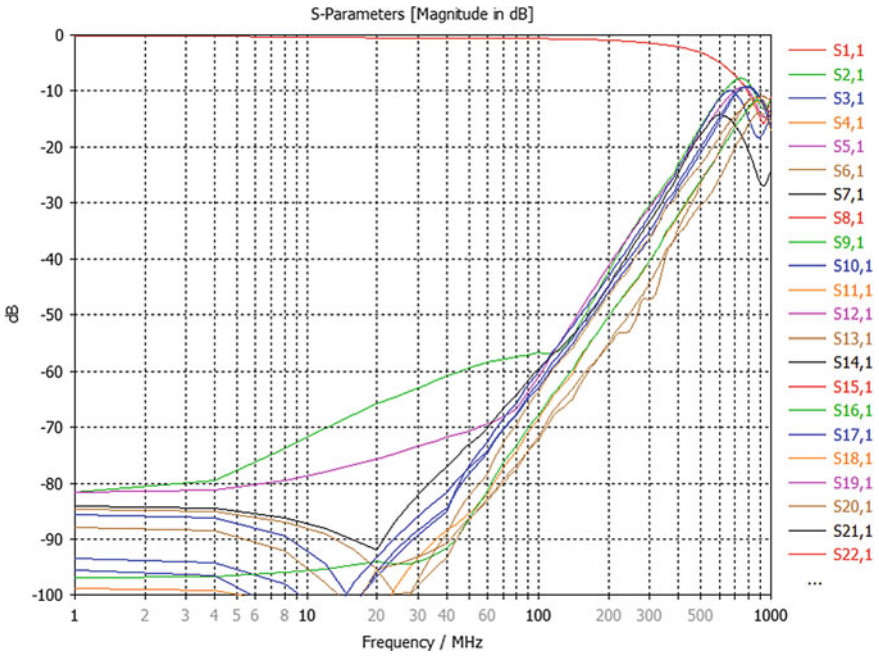

Fig. 9 Simulated sNp touchstone output file, for N = 1, 2, 3, …, 48. Showing only SN,1 where S1,1 is the return loss and SN,1 is the coupling with other tracks

It is also interesting to note that for differential pair tracks, the coupling behaves similarly to the non-differential pair tracks. Although the IC is packaged in a very small dimension, the coupling for *SN,1* (with $N = 3,\ldots, 48$) falls below—80 dB even though they are just two to three tracks away. Similar behaviours applies to the opposite tracks. Only the neighbouring track *(S2,1)* shows higher coupling.

3 Macro Modeling Using IdEM

Finally, the s48p touchstone file is imported into macro modelling tool, IdEM [10] to generate a SPICE model, which is shown in Fig. 10. IdEM utilises state of the art vector fitting algorithm to convert the frequency response data into RLC lumped components equivalent circuits. The color within the IdEM panel is representing the dataset, where yellow color has the highest error. The error can be causality error or passivity error. Each cube in the dataset represents the behaviour of *SN,N* (where $N = 1,\ldots, 48$)

Within IdEM, different level of orders can be used to perform the macro modeling using vector fitting. Higher order would allow vector fitting of higher accuracy, where small resonant within the results can be included in the macro model as

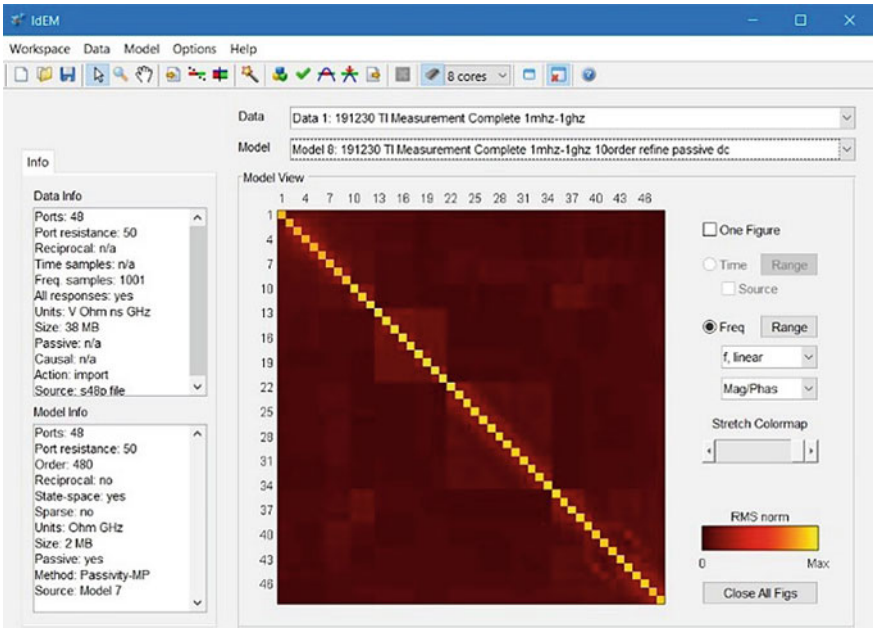

Fig. 10 IdEM macro modelling tool interface

well. But in this work, 10 orders lumped components is selected for the measured results. There is no major difference in choosing higher order except the increase of the simulation time. Hence, it is recommended to choose an acceptable accuracy within the capability of the available workstation. The targeted accuracy for this vector fitting is 10 e^{-3} and the highest error achieved is less than 0.1 in linear form. However, the accuracy of the macro model is reasonably acceptable as there is also measurement uncertainties introduced during the measurement using the probe.

From the touchstone file, the lowest measured frequency is 9 kHz due to the limitation of the VNA. This can be overcome in IdEM, where the DC point can be included during the creation of macro model, which will ensure the usability of the SPICE model for DC simulation.

The next step is to ensure passivity and causality of the macro model which is performed by utilizing Hamiltonian solver [6]. The passivity enforcement can be performed from DC to infinite frequency, but in this work it is only performed up to 1,000 MHz. The Hamiltonian algorithm will eliminate the frequency band where violations occur based on the eigenspectrum matrices. The output results are shown in singular values of the eigenvalues where more than one represent non-passive behaviour. After performing the passivity enforcement, causality enforcement is also performed. Causality enforcement is based on generalised Hilbert transform algorithm [11], where it minimises the numerical error and also it removes the truncation error which also caused the system to be non-passive.

After the passivity and causality enforcement, the output file is exported as a SPICE model with a common ground. This common ground is used as a ground reference for all the pins. This is similar to the actual IC where the pins are referenced to the ground pins available throughout the IC package. The SPICE model was then simulated in CST circuit simulator to obtain the final S-Parameters. It is shown that the coupling behaviour is now different from the measured results (shown in Fig. 9) where the coupling for *SN,1* (with $N = 2, \ldots, 48$) are spread from −48 to −85 dB, as shown in Fig. 11. In the first SPICE model, the passivity and causality checks show that the SPICE model is not passive. This could be caused by the measurement error from soldering and de-soldering of the tracks. Passivity and causality was then enforced on the SPICE model. The result is shown in Fig. 11. This means that the 48-pins equivalent circuits in the SPICE model is now causal and passive.

The time responses are also shown in Fig. 12. In this simulation, port 1 is excited with a 1,000 MHz Gaussian pulse while all other ports of port *N* ($N = 2, \ldots,48$) are terminated with 50 Ω load. In Fig. 12 (a), touchstone file is used while in Fig. 12 (b), the converted SPICE model is used. Both results show similar responses despite some differences in coupling behaviour seen from the S-Parameters. The SPICE model can be used in both frequency and time domains and can be simulated with relatively faster speed. The time response from the

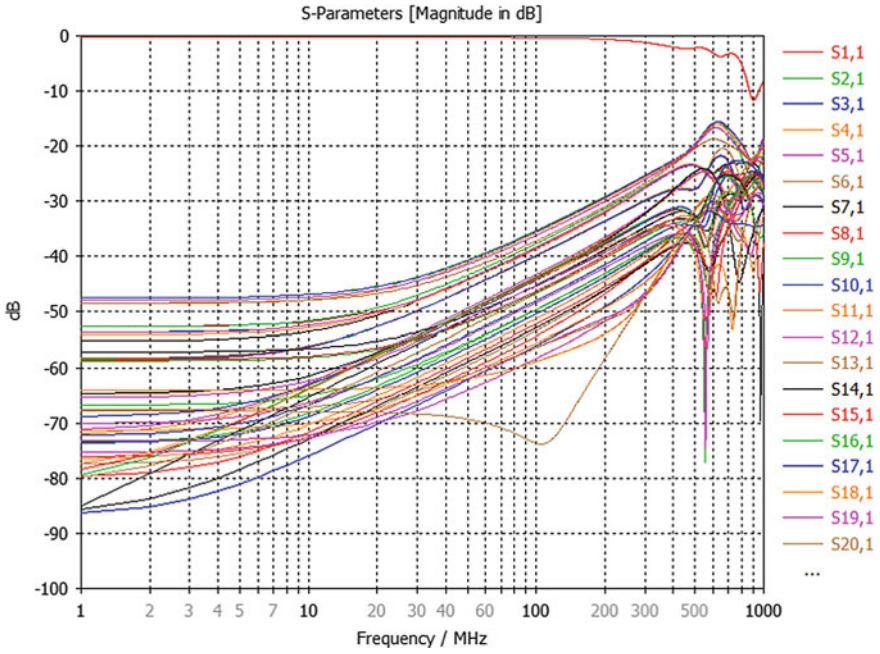

Fig. 11 Simulated *SN,1* of the SPICE model, for $N = 1, \ldots, 48$

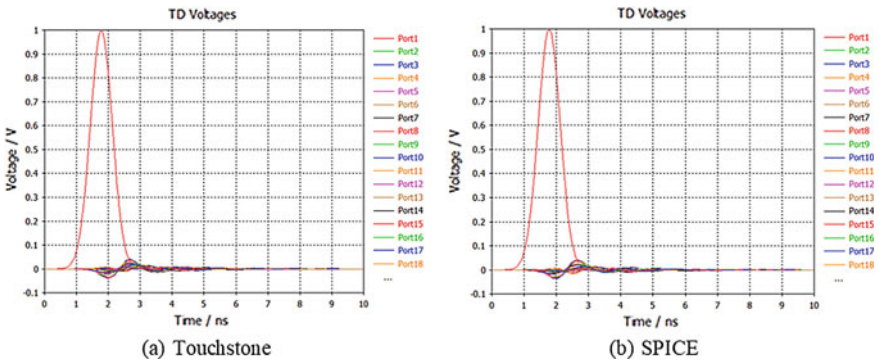

Fig. 12 Time responses of the **a** touchstone file and **b** SPICE model, where Port 1 is excited with a 1,000 MHz Gaussian pulse and Port N (N = 2, …, 48) are terminated with 50 Ω load

SPICE model also shows that the causality and passivity requirements are met. If a model is not passive, the output signal will have ringing behaviour after the first ripple where the ringing increases over time. In worst case scenario, the ringing will continue infinitely.

4 Conclusion and Future Work

From the comparison between measured touchstone results and SPICE model results, it can be concluded that the measurement introduced errors which was then corrected automatically by the macro modelling tool. The measurement errors can be noticed from the comparison of the dataset, where higher order of vector fitting would not be able to reduce the difference between measured S-Parameters with the equivalent circuit's S-Parameters. Although the measured results does not contain passivity violation, the passivity violation will appear at higher frequency after the vector fitting. The measurement errors could be introduced during the probing measurement, where soldering and de-soldering the tracks could have damage the transmission lines.

This new methodology where combination of low cost coaxial probe as well as market available macro modelling tool is revolutionary as it greatly simplifies the IC characterisation. With this, the SPICE model of the IC can be included in the 3D simulation model and the final result will be greatly enhanced and achieve more accurate results.

Future work is to implement the SPICE model of the IC onto a 6 layers ADAS development board where the digital transmitter component will be mounted on. This work is to verify the usability and accuracy of the proposed methodology.

References

1. Tippet JC, Speciale RA (1985) A rigorous technique for measuring the scattering matrix of a multiport device with a two-port network analyzer (comments). IEEE Trans Microw Theory Tech 33(3):286–287
2. Kam DG, Kim J (2007) Multiport measurement method using a two-port network analyzer with remaining ports unterminated. IEEE Microw Wirel Compon Lett 17(9):694–696
3. Rolfes I, Schick B (2005) Multiport method for the measurement of the scattering parameters of N-ports. IEEE Trans Microw Theory Tech 53(6 II):1990–1996
4. Schutt-Ainé JE et al (2011) Comparative study of convolution and order reduction techniques for blackbox macromodeling using scattering parameters. IEEE Trans Compon Packag Manuf Technol 1(10):1642–1650
5. Deschrijver D, Gustavsen B, Dhaene T (2008) Computer code for fast macromodeling of large multiport systems. Electr Perform Electron Packaging, EPEP, pp 299–302
6. Grivet-Talocia S, Ubolli A (2007) Passivity enforcement with relative error control. IEEE Trans Microw Theory Tech 55(11):2374–2382
7. Gustavsen B, Semlyen A (2008) Fast passivity assessment for S-parameter rational models via a half-size test matrix. IEEE Trans Microw Theory Tech 56(12):2701–2708
8. Odabasioglu A, Celik M, Pileggi LT (1998) PRIMA: Passive reduced-order interconnect macromodeling algorithm. IEEE Trans Comput Aided Des Integr Circuits Syst 17(8): 645–654
9. TFP410 TI PanelBus™ Digital Transmitter (2001)
10. Grivet-Talocia S, Ubolli A (2006) On the generation of large passive macromodels for complex interconnect structures. IEEE Trans Adv Packag 29(1):39–54
11. Triverio P, Grivet-Talocia S (2008) Robust causality characterization via generalized dispersion relations. IEEE Trans Adv Packag 31(3):579–593

Contactless Attendance Method with Face Recognition, Body Temperature Measurement and GPS System Using Blockchain Technology

Afiqah Mohammad Azahari, Arniyati Ahmad, and Syarifah Bahiyah Rahayu

Abstract Most workplace is recording their employee's attendance via attendance system. The existing attendance systems include traditional method, punch card, QR Code, RFID and biometric. However, these methods require an employee's physical interaction directly with the system. Due to COVID-19 pandemic, any direct physical contact with the system should be avoided. Moreover, the existing attendance system platforms lack the security foundations upon which vulnerable to cyber threat, such as forge by irresponsible employees and unauthorized users. This paper aims to develop a contactless attendance system. The system is using face recognition and GPS location to record attendance with body temperature on blockchain technology.

Keywords Contactless · Attendance system · Face recognition · Location detection · Blockchain

1 Introduction

Workplace attendance is fundamental importance to economy of the industry. Primarily, this appears most directly to affect those in industry as a cost of production, yet lost productivity also affects the whole economy and society directly and indirectly.

There are various methods to record employee attendance. Most organizations are recording the employee using an attendance system. The attendance system, usually, are recording employee timestamp for attending and leaving workplace.

When COVID-19 pandemic outburst, the business environment has changed to the extent that health and well-being of employees comes first. Nevertheless, employee attendance at work, their productivity and performance also become

A. Mohammad Azahari (✉) · A. Ahmad · S. B. Rahayu
Cyber Security Centre, National Defense University of Malaysia,
57000 Kuala Lumpur, Malaysia
e-mail: afiqah.azahari@upnm.edu.my

Z. Zakaria and S. S. Emamian, *Advances in Electrical and Electronic Engineering and Computer Science*, Lecture Notes in Electrical Engineering 741,
https://doi.org/10.1007/978-981-33-6490-5_8

critical component that obviously affect the performance of the business. COVID-19 pandemic changes the method of recording attendance of the employee to the workplace. Attendance system is the first point of contact for employee. The future of work and office hygiene would require the termination of physical direct contact with attendance system. Employees would be scared and unwilling to touch the biometric machines due un-hygiene spot that would spread virus. Biometric attendance system such as fingerprint method heighten security and add convenience, but this method is now being looked at as an epicenter for germs in the workplace that could include the coronavirus. This has become a potential health risk to the employees.

A new approach of contactless attendance system is expected to overcome issue of current attendance method. A contactless attendance system provides interaction between human and system without physical or direct contact with the device. The new attendance system will be able to record employee's attendance using contactless method with secured data recording. Further, this will help employers to implement fast and practical contactless attendance recording and management system, thus helping preserve a safe society.

Hence, the paper proposes contactless attendance is using face recognition algorithm, body temperature measurement and GPS location system on blockchain technology. The proposed approach is expected to overcome current issues (i.e. health and cybersecurity) and preserve a healthy workspace on top of secured technology.

2 Related Works

There are multiple methods developed for attendance recording and management system. Suitable attendance recording and management system has become important, as attendance is one of the work ethics valued by most employers. In open literature, there are multiple methods implemented using information technology for recording and managing attendance. Some methods introduced are using QR Code for scanning attendance information [1–3]. However, this method is easily manipulated by irresponsible employees. After they take a picture of displayed QR Code for scanning, they might share it with the absences. Then, the absences could scan back the QR Code and the system will record the data of absences to the attendance system. To overcome this issue, there are also methods introduce of using QR Code with Global Positioning System (GPS) [4, 5]. GPS used to authenticate location of employees when they are scanning the QR Code. However, most researchers that introduced this method did not discussed about the issue of cyber security. Not using GPS, Rahni et al. [6] introduce method of collecting students' attendances information in classes. By generating QR Code on the student's device, lecturers will scan the generated QR code from each student. This method is cumbersome, time consuming and requires lecturer's intervention. On the other hand, there are also biometrics with artificial intelligence method

introduce for recording and managing attendance system. This includes fingerprint scanner and face recognition technology.

The biometric system used in attendance management system has encouraged adherence to workplace rules, all at once eliminates employee theft, 'buddy punching' and other problem and loophole caused by outdated attendance system [7–9]. However, in this current situation, method of recording attendance by using fingerprint scanner with RFID is not applicable because the devices are unsanitary and a potential source of germs, which could cause illness. Furthermore, as the novel coronavirus that causes COVID-19 could survive for 16 h on the surface, there are needs of contactless attendance system. Although, there are also contactless biometric system introduce by researchers, which is using face recognition. This method allows employees to scan their face to the special camera installed at the premises or by using CCTV and scanning the employee's face "in the wild", meaning the person does not have to pose to the scanner [10–13]. Although this method could solve the needs of contactless attendance issue, however this method required large data storage and high processing units as it need to store, recognize, and train the data of faces. Furthermore, all face recognition methods used for attendance recording and management system does not elaborate on the implementation of security for securing their stored data. Another popular biometric method is using fingerprint scanner to authenticate, identity the population and record attendance [14–16]. However, with the emerging of novel virus at the end of year 2019, fingerprint scanner as attendance recording system is impractical as the virus could transmitted via human touch. To researcher knowledge, RamcoGEEK is the only attendance system embedded with temperature recording. The system is using biometric method and thermal scanner to records employees' attendance and temperature. However, the system is still in the software testing stage.

According to Marsico et al., mobile security protocol must be heightened to preserve data confidentiality, integrity, and availability from unauthorized access. Therefore, for enhancing data security, blockchain technology will be introduced. Blockchain will be applied for securing record of employee's attendance data. Data stored in the blockchain will be transparent and immutability. Known as decentralized and distributed ledger, data stored in the blockchain cannot be modified at ease and tempered with. This is because the stored attendance data will be in a form of blocks and all the blocks are connected to each other ultimately forming a chain of records. Any changes on the block will notify other blocks for approval. This technology will prevent modification of data from third party members or from the organization itself [17].

3 Proposed Main System Components

This study is proposing a contactless attendance recording and management system. This system allows employee to record their attendance and temperature at the same time. Employees will use the system via mobile device. There are four main components of the proposed contactless attendance system as follows:

3.1 Face Recognition

Four important processes involved to recognize the employee's face. First the image for each employee will be captured and converted into greyscale. The image then stored with the ID in the database. During face detection process, a face detection algorithm will be used to identify local features of the face by dividing the image into pixels. While during feature extraction process, the Region of Interest (ROI) are parts of the face from where features are extracted and information about the gradients in the face is captured. After the completion of detecting and processing the face, the face present will be compared with data in the employee's database. When a face is detected by the camera it checks the corresponding values of the current visible face with values stored in the database. If the values are a match, then the face is recognized.

3.2 GPS Locator

There are two major process of location locator and attendance registration. The location locator will use GPS coordinates to instantly determine the employee's workplace location, based on the coordinates received. The GPS will obtain both x- and y-coordinates using ground and space satellites. The employee workplace location based on coordinates will be saved into the employee's database. The attendance system will be developed to automatically updates attendance in the database for any faces that recognized and registered. Including the x-coordinate, y-coordinate that matched the employee workplace, the employee's data and timestamp.

3.3 Temperature Measurement

The system will use a digital thermometer application from the employee's smartphone to measure their body temperature. Employee temperature will be recorded and check to ensure that the employee's body temperature is normal and able to work. Daily temperature data will be saved into the database. If the body temperature is over 37.5 °C, a notification will be sent to the organization's health department or human resource department for further action.

3.4 Blockchain Implementation

Blockchain in the attendance system will store employee records in form of blocks and validate employee certificates. Each record is treated as a block in the

blockchain. The block structure consists of block header and employee data. The block header consists of hash code of the previous block, current hash value, time stamp and nonce. Each employee record is treated as a block in the blockchain. Once the block is created, a block address is created. The block is sent to the network for storage. Once the block is stored successfully, data owner will receive an acknowledgement. The certificate can be validated anytime in a future.

4 System Architecture

This contactless attendance system will introduce a new contactless attendance recording and management system with block chain technology for securing attendance data. A new mobile application will be developed, functioning for face scanning, measuring body temperature, and locating location of the employee. This research will integrate existing face detection algorithm, body temperature measurement and GPS method.

Figure 1 shows a flowchart for employee registration to the contactless attendance system. During registration, employee must bring their mobile device to be

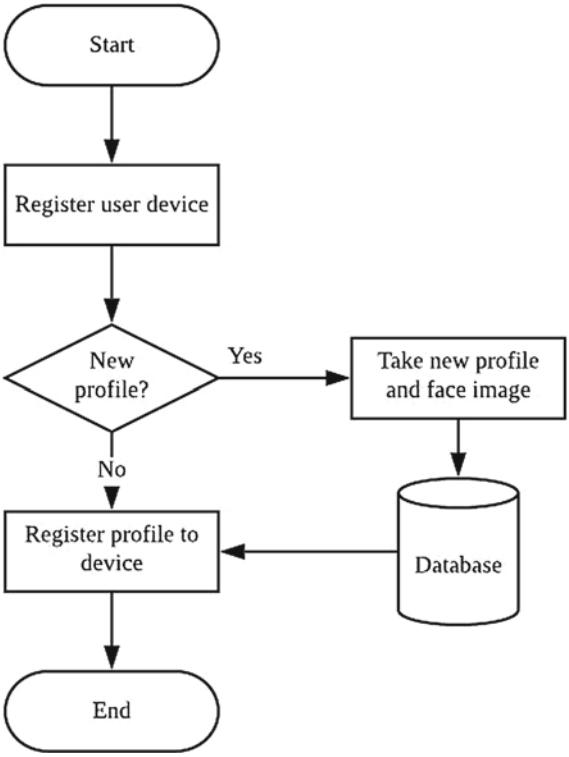

Fig. 1 Registration flowchart

registered. A new profile will be created. Administrator will take picture of employee face. Then, the new profile and face image will be stored into a database. Then, the system will register employee profile on the mobile device. If the employee already has stored his/her profile and face image, then the system will only register employee profile to a mobile device.

Figure 2 shows the flowchart for recording employee's attendance. Employee will login to the contactless attendance system using face recognition. If it is valid, then the GPS location will be located. The GPS will be compared with the coordinates of workplace. After the GPS location and face recognition are validated, the contactless attendance system will measure employee body temperature. If the reading body temperature is above 37.5 °C, the application will send a notification to Health Department/Human Resource Department for further action. Next, information such as employee identification, clock-in, date and location of employees will be sent and stored in the distributed database. The same process will be run when employee's clock-out.

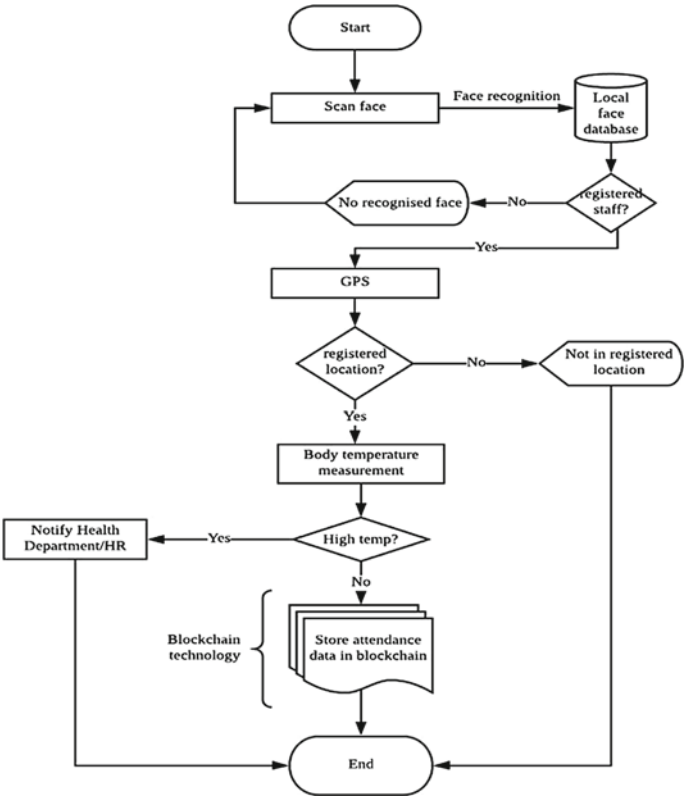

Fig. 2 Attendance flowchart

5 Conclusions

This contactless attendance system is secured and applicable for all sectors such as educations, industries, governments, tourisms etc. to record of employee attending and leaving their workplace. At the same time, this system measures employee temperature in real time when they clock-in, which stated in Malaysia Ministry of Health (MOH) and Ministry of International Trade and Industry (MITI) Standard Operation Procedures for all organizations in Malaysia. Moreover, this new approach will eliminate the probability to get infected of COVID-19. Employee may get infected if using attendance system with shareable scanner. For example, attendance system with fingerprint scanner might spread COVID-19 left by a positive carrier. Next employee will catch the virus after touching the contaminated fingerprint scanner and then touching their eyes, nose, or mouth.

Blockchain technology will be able to secure the attendance data, thus improve the integrity of the stored data. In addition, this method will be easy to implement, as no additional devices are required. On the employee side, they need to install the developed mobile application on their smart phone. The mobile application will be used to authenticate their attendance to the workplace. While employers are required a computer storage for storing all employees' data. Therefore, the proposed contactless attendance system using face recognition, body temperature measurement and GPS on blockchain technology will overcome current issues, thus helping in preserve a healthy workplace on top of secured technology.

Acknowledgements The authors would like to express sincere gratitude to National University of Malaysia for supporting this research.

References

1. Al Sheikh R et al. (2008) Developing and implementing a barcode based student attendance system. Int Res J Eng Technol 497:1–12. Available: www.irjet.net
2. Navin K, Shanthini A, Mukesh Krishnan MB (2018) A mobile based smart attendance system framework for tracking field personals using a novel QR code based technique. Proc 2017 Int Conf Smart Technol Smart Nation SmartTechCon 2017, 1540–1543. https://doi.org/10.1109/smarttechcon.2017.8358623
3. Deugo D (2015) Using QR-codes for attendance tracking. Int Conf Front Educ CS CE, 267–273. Available: http://worldcomp-proceedings.com/proc/p2015/FEC2508.pdf
4. Elbehiery H (2019) Enhancement of QR code student's attendance management system using GPS, 21(4):18–30. https://doi.org/10.9790/0661-2104011830
5. Ayop Z, Lin CY, Anawar S, Hamid E, Azhar MS (2018) Location-aware event attendance system using QR code and GPS technology. Int J Adv Comput Sci Appl 9(9):466–473. https://doi.org/10.14569/ijacsa.2018.090959
6. Abd. Rahni AA, Zainal N, Adna MF, Othman NE, Bukhori M (2015) Development of the online student attendance monitoring system (SAMS^{TM}) based on QR-codes and mobile devices, 10:28–40
7. Kamaraju M, Kumar P (2015) Wireless fingerprint attendance management system

8. Yadav D (2015) Fingerprint based attendance system using microcontroller and labview. Int J Adv Res Electr Electron Instrum Eng 04:5111–5121. https://doi.org/10.15662/ijareeie.2015.0406029
9. Zainal NI, Sidek KA, Gunawan TS, Manser H, Kartiwi M (2014) Design and development of portable classroom attendance system based on Arduino and fingerprint biometric. In: The 5th international conference on information and communication technology for the muslim world (ICT4M), pp 1–4. https://doi.org/10.1109/ict4m.2014.7020601
10. Bhattacharya S, Nainala G, Das P, Routray A (2018) Smart attendance monitoring system (SAMS): a face recognition based attendance system for classroom environment
11. Sawhney S, Kacker K, Jain S, Singh SN, Garg R (2019) Real-time smart attendance system using face recognition techniques. In: 2019 9th international conference on cloud computing, data science and engineering (confluence), pp 522–525. https://doi.org/10.1109/confluence.2019.8776934
12. KPN Reddy, Alekhya T, Sushma Manjula T, Krishnappa R (2020) AI-Based attendance monitoring system 9
13. Fell S (2019) AI to mark attendance. Telegraph. https://www.telegraphindia.com/technology/ai-to-mark-attendance/cid/1688348. Accessed 20 Apr 2020
14. Ho CC, Eswaran C (2011) Consodilation of fingerprint databases: a Malaysian case study. Proc 2011 11th Int Conf Hybrid Intell Syst HIS 2011, pp 455–462. https://doi.org/10.1109/his.2011.6122148
15. Bitzionis T (2020) Malaysian government to implement national biometric registration system. Find Biometrics. https://findbiometrics.com/biometrics-news-malaysian-government-seeks-implement-national-biometric-registration-system-021102/. Accessed 20 Apr 2020
16. Sajadi AM (2017) Call for biometric system to screen students. The Star. https://www.thestar.com.my/news/education/2017/01/08/call-for-biometric-system-to-screen-students/. Accessed 20 Apr 2020
17. Kumar SMKVP, Kumar KK, Krishna RS, Sri PSGA (2019) Incorporation of blockchain in student management system. Int J Innov Technol Explor Eng 8(6):664–668

Identification and Detection of RTN in Short-Channel MOS Devices of Communication Power Supply

Xinxin Fan, Hongmei Yan, Xin Xu, and Hui Yao

Abstract Random Telegraph Noise(RTN) is an important parameter to characterize the short channel MOS device reliability of communication power supplies, in order to identify and detect the RTN, we adopt the noise scattering plot(NSP), combined with k order median filter to identify the noise and we propose an improved variable step size LMS algorithm for the detection. The experimental results show that the new method can effectively identify the RTN component and its related parameters, especial in smaller time constant and the same precision, the error of the parameter extraction decreased 40% than traditional methods.

Keywords RTN · NSP · LMS algorithm · Short channel MOS devices · Communication power supply

1 Introduction

At room temperature, the relative amplitude of the RTN over 60% in short-channel MOS devices of Communication power supply [1, 2]. It is the existence of noise that not only reduces the sensitivity of low frequency electronic circuit system but also coupled with phase noise, influence the high frequency digital logic device application [3, 4], which directly results in the decrease of device reliability. Thus the study of the RTN is a significant important.

The first step is to identify the RTN and then detect it, However, at present we can only identify bi-level RTN by observing the RTS time series, but for Multi-Level RTN, we can not judge through direct observation, because of the complex waveform and the interference of background noise, even cannot detect whether it has the RTN in short-channel MOS devices [5].

X. Fan (✉) · X. Xu · H. Yao
State Grid Tongling Electric Power Supply Company Tongling, Tongling, China
e-mail: Fanxxok@126.com

H. Yan
State Grid Zongyang County Electric Power Supply Company, Zongyang, China

Z. Zakaria and S. S. Emamian, *Advances in Electrical and Electronic Engineering and Computer Science*, Lecture Notes in Electrical Engineering 741,
https://doi.org/10.1007/978-981-33-6490-5_9

In this paper, we adopt the combination of NSP and median filter method to identify RTN. We propose an improved detection algorithm based on adaptive digital filter for detection.

2 Identification Method of RTN

In short-channel MOS devices, the component of Gaussian noise includes a low thermal noise, flicker noise, etc. If RTN still exists, its influence is more important than other Gaussian noise components [6]. So it is important to the recognition of the RTN. NSP method can identify RTN component in low frequency noise signal, its algorithm process is as follows (Fig. 1):

First, measure the low frequency noise signal $x(t)$, get the time series (1) through the AD conversion.

$$\{x(n)\} = \{x(1), x(2), \cdots x(2N)\} \tag{1}$$

Second, establish the relation between the matrix **X** and **Y**, classify the sequence $\{x(n)\}$ as follows:

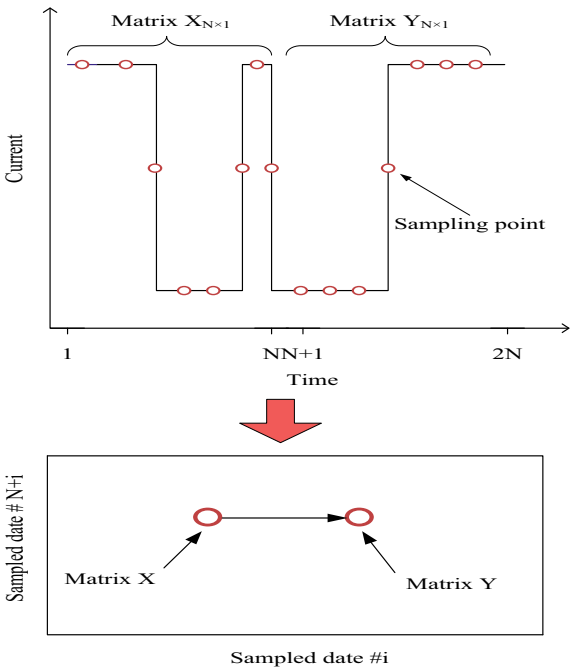

Fig. 1 The process of RTN identification

$$\mathbf{X} = \begin{bmatrix} x(1) \\ x(2) \\ \vdots \\ x(N) \end{bmatrix}, \quad \mathbf{Y} = \begin{bmatrix} x(N+1) \\ x(N+2) \\ \vdots \\ x(2N) \end{bmatrix} \tag{2}$$

Finally, draw a scatter plot of X on Y by using MATLAB or Origin.

Because the low frequency noise signal of short channel MOS devices often contains Non-Gaussian RTN, Gaussian background flicker noise and thermal noise, etc. In view of these two types of noise, to facilitate the analysis of noise components, we can divide it into three cases for discussion.

2.1 *Only Non-gaussian RTN Components Exist*

If the low frequency noise signal contains only the RTN. First, we assume that the low frequency noise signal contains only two level RTN, get Fig. 2 by NSP method, we can see the RTN in the scatter plot which has four similar to oval respectively around the center coordinate of (−X, −X), (−X, X), (X, −X), (X, X). In the same way, if the noise signal contains three RTN levels, the NSP diagram should be in center of eight around their approximate elliptic distribution pattern. If there are more than N value levels of the RTN, we can get the total of N2 the NSP figure which is similar to ellipse shape pattern [7].

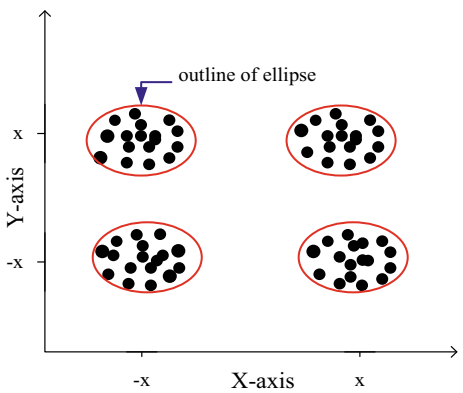

Fig. 2 RTN scatter plot

2.2 *Only Gaussian Noise Composition Exist*

If the low frequency noise signal contains Gaussian components of flicker noise and thermal noise, etc. the NSP graphics as shown in Fig. 3, we can only see that its scatter distribution is similar to that of ellipse.

2.3 *Mixture of Gaussian Noise and Non-gaussian Noise*

As shown in Fig. 4, this is a scatter diagram with Gaussian and Non-Gaussian mixed low-frequency noise. By comparing Fig. 2 with Fig. 3, it can be seen the mixed low-frequency noise that contains background noise points which resulting in mixed the intersection of scattered points in the boundary of adjacent ellipses. To eliminate the influence of these cross isolated noise points, we use K-order median filter, get sequence (3) after the data is framed.

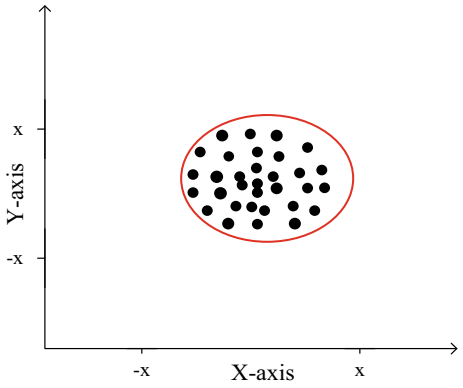

Fig. 3 1/f noise scatter plot

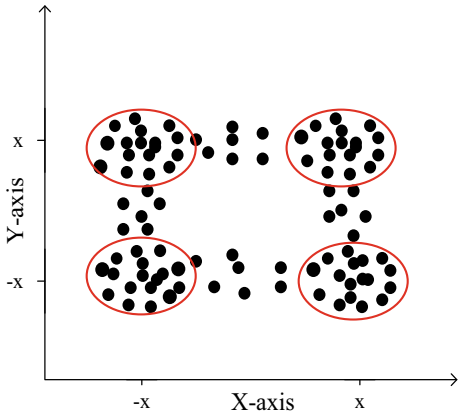

Fig. 4 Mixed noise scatter plot

$$m\{x(n)\}_k = med\{x(n-k), x(n-k), \cdots x(n+k)\}, n = k+1, 2, \ldots, 2N-k \quad (3)$$

3 Detection Method of RTN

The detection method of RTN is extraction the noise amplitude ∇ID and extraction time constant of the RTN such as trap capture ζc and emission time ζe.

3.1 Extraction of the Time Constant

The traditional time constant extraction method is to calculate the average value of rising edge, falling edge, rising edge and RTN [8, 9] ,because of the limitation of sampling points and superposition in high and low level of noise signal interference, the precision of extraction time constant is greatly restricted. To extract the adjacent two points of time series, there was related literature proposed recurrence relation [10], its concrete structure difference equations:

$$y_n = \begin{cases} x_{n+1} - x_{n-1}, & (x_{n+1} - x_{n-1})(x_n - x_{n-1}) > 0; \\ x_n - x_{n-1}, & (x_{n+1} - x_{n-1})(x_n - x_{n-1}) < 0; \end{cases} \quad (4)$$

where y_n is time series after the successive difference, x_{n+1} is sampled points at $n + 1$ moment, x_n is Sampled points at n moment, x_{n-1} is Sampled points at n − 1 moment.

Because the RTN signal from the actual test often contains three parts, including low frequency interference from thermal noise, high frequency disturbance of flicker noise and RTN components. But the accuracy of extraction has been curbed. Therefore, in this paper, the LMS algorithm is improved, and a variable step LMS algorithm is proposed. Its design idea is as follows:

According to the expression of the adaptive filter [11]:

$$\mathbf{W}(n+1) = \mathbf{w}(n) + \mu \mathbf{u}(n)\, e(n) \quad (5)$$

$$e(n) = d(n) - \mathrm{w}^H(n)\, \mathbf{u}(n) \quad (6)$$

where $\mathbf{W}(n)$ is the weighted coefficient of filter, $\mathbf{u}(n)$ is the differential input signal, $e(n)$ is the relative value error, μ is to control the disturbance of the step length.

The traditional LMS algorithm cannot optimize convergence speed and stability at the same time, due to the error signal RTN have the strong correlation and weak cross correlation caused by the traditional LMS algorithm which is sensitive to noise. To solve the problem of traditional LMS algorithm, the correlation between

step function and error expression is established to reduce the sensitivity of LMS algorithm to noise. The specific process is as follows:

According to the discrete expressions of correlation function (7), It is concluded that the correlation function (8), we know the index has the nature of explosive growth, to make $R_e(k)$ minimum, power exponential function $\exp|e(n)e(\mathrm{n}-1)|^{\mathrm{k}}$ can be introduced as denominator of expression, at the same time, we should consider the convergence speed of step length, so a variable α is introduced, the power exponential function is complemented to speed up the convergence speed. Final, build function expressions such as (9)

$$R_e(1) = E\{e(n)e(n-1)\} \tag{7}$$

$$R_e(k) = E\{e(n)e(n-k)\} \tag{8}$$

$$\mu(n) = \left(a - \frac{1}{\exp|e(n)e(n-1)|^b}\right) \tag{9}$$

where $R_g(1)$ is the cross-correlation function of sampling interval at 1, $R_g(k)$ is the cross-correlation function of sampling interval at k, $E\{.\}$is expectation, $e(n-k)$ is the relative value error at $n-k$, a is a constant definition and b is need to measure the optimal constant.

The specific ideas of the algorithm are:

In the beginning of convergence, to accelerate the convergence speed, we take the big step length. As the error is reduced gradually, take the small step length, to achieve small steady state low-offset noise. The introduction of factor $e(n)(n-1)$ can eliminate the error signal of weak cross correlation and strong correlation between each other, thus inhibiting the phenomenon which traditional LMS algorithm is sensitive to noise, from Fig. 5 shows that when the equation of b = 1, in the initial stage of Fig. 5, step down quickly, when the error close to zero, step length is still obvious change, do not have slowly changing characteristics. When the equation of b = 2, it improves the convergence rate of $\mu(n)$ at the condition of b = 3, and overcomes the disadvantage of a big step change at the condition of b = 1. Therefore makes the algorithm has small steady state low-offset noise, thus to achieve the best filtering performance.

3.2 *Extraction of the Amplitude Parameter*

Traditional method of amplitude parameter extraction [12–14] is to measures the relative magnitude of the RTN $\nabla I_D/I_D$. But under the same bias, we need to measure the absolute amplitude of the RTN ∇I_D and channel current I_D, there is a problem that under the same bias circuit condition it is hard to measure direct current and alternating current at the same time, this will brings great inconvenience and error at the extraction of the amplitude.

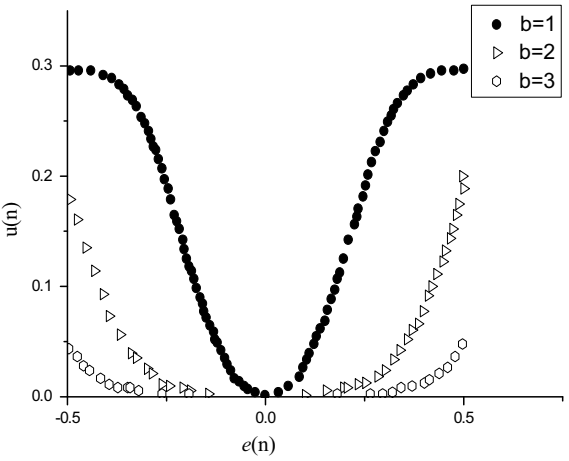

Fig. 5 Dependence of k and $\mu(n)$ also $e(n)$

Therefore, the positive and negative to measure absolute magnitude is adopted, using the transfer characteristic curve Under the condition of the same gate bias, Finally, we establish ∇I_D about I_D the graph, and then extract the amplitude parameter.

4 Experiment and Result Analysis

The samples of the experiment are SMIC 90 nm feature sizes CMOS devices, using the technology of LDD and Silicide technology, etc. The threshold voltage VT = 0.2 V, junction depth is 0.02 μm, the injection depth of LDD is 30 nm, the effective thickness of gate dielectric is 1.6 nm, the channel size NMOS single pipe is 0.18 × 0.16 μm.

4.1 Identification Verification and the Result

As shown in Fig. 6, this is the experiment used in the system of measuring short-channel MOS device, the type of Semiconductor Device Analyzer is Agilent 1,500A, WGFMU is waveform generator and fast measurement unit and RSU is remote sensing and switch unit to deliver our noise data, the DUT is our samples of short channel MOS. NSP method is used to draw the sample point for 10,000 points, the results is shown in Fig. 7 (b), after a median filter, we can get Fig. 7 (c). It can be seen the filter can eliminate noise isolated point and the influence of background noise from the RTN.

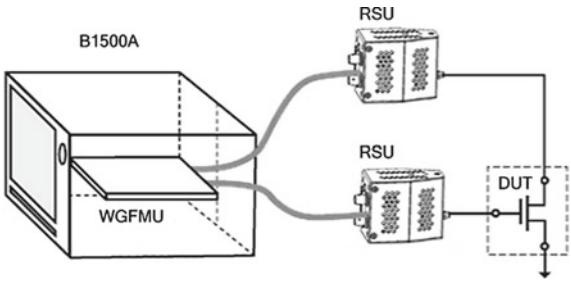

Fig. 6 The RTN measurement system

According to the analysis of the above conclusion, combined with Fig. 7 (c), we can not only identify the RTN from the sample, but also determine the level of RTN, it is consistent with the Fig. 7 (a), we can draw the basic information of the RTN, and the points around the nine center is in non-uniform distribution.

There are nine central coordinates of RTN have uneven density, we can preliminary judgment ζc is not equal with the ζe, the specific reason may about the different trap position or level in the sample inside.

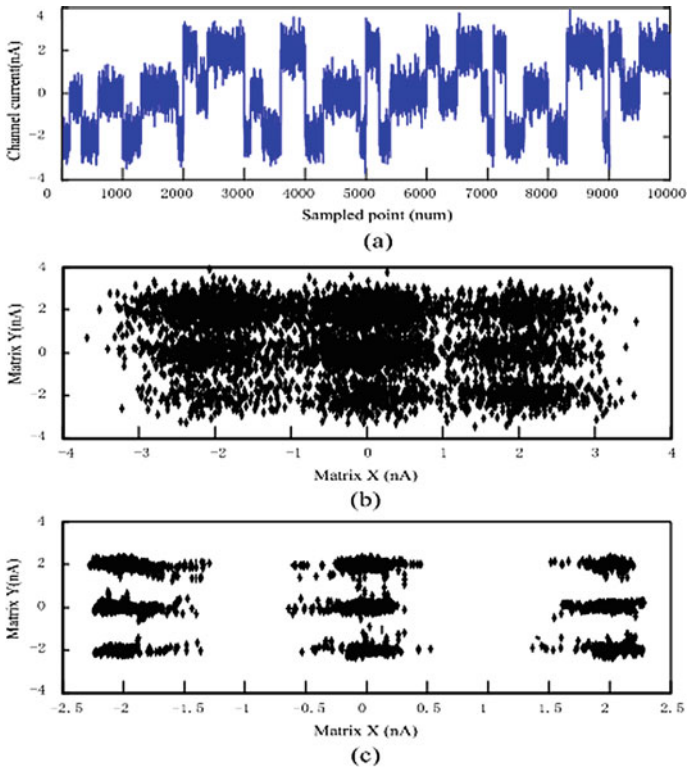

Fig. 7 The RTN sampling sequence and NSP figure and scatter plot after filtering

4.2 The Extraction of RTN Time Parameter

To extract the time parameters, first we design variable step LMS digital filter, define a = 1, and take b = 2, set up the drain voltage is 320 mv, grid voltage range from 400 to 800 mv, Sampling rate selected for 100 Kps, Sampling accuracy for 14 bit, Continuous sampling for each grid bias at point 30 s. We can get trap capture time and emission time respectively, the relationship between the gate voltages as shown Fig. 8, this is consistent with the results of literature research and satisfied with the exponential distribution. At the same time, monte carlo method and difference equation method are used to simulate the traditional extraction and literature method respectively, the detailed simulation result as shown Fig. 9, from the figure we can see the new method of error performance is superior to the traditional method and the difference equations method, compared with the traditional average algorithm, under the same precision, sampling point averages about 1/10 of the traditional method. When the time constant of trap capture and emission is relatively small, the advantage of the new method is more prominent, the error can be reduced by 40% within the number of sampling 10 points, can significantly improve the precision of parameter extraction. Compared with the modified LMS algorithm and the relevant literature proposed using finite difference equation method [2], the result follows the same trend. While in the small time constant, the modified LMS algorithm is better than difference equation method, it can increase 10% error precision. When the time constant is higher, it can increase 5% error precision.

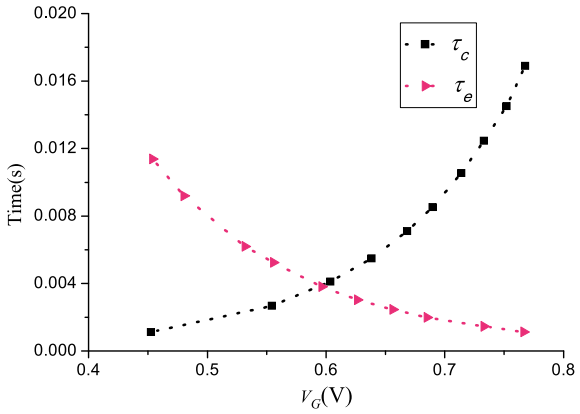

Fig. 8 Dependence of RTS time constant and gate bias

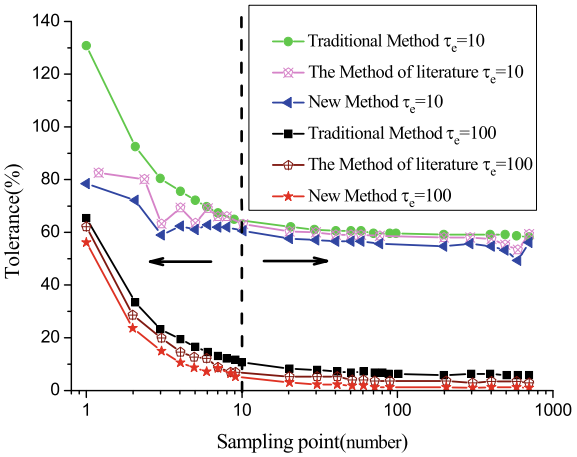

Fig. 9 The monte carlo simulation

4.3 The Extraction of RTS Amplitude Parameter

To extract the amplitude parameter, changing the gate voltage range from 0 to 280 mV, continuous sampling for each grid bias at point 200 s, Fig. 11 is RTN amplitude curves under positive and negative bias conditions, combined with the transfer characteristic curves as shown Fig. 11, according to the value of any point of $V_{G,}$ between Figs. 10 and 11, we can determine the relationship between I_D and $\nabla I_{D.}$ Meanwhile compare with mathematical model from the literature [12], we can clearly a draw conclusion that the new way to measure the margin of RTN is identical with the calculation results of the literature. Because of the expression (10) which is derived in the premise of exponential distribution, so we can infer that the new method to get the margin of RTN also accords with exponential distribution.

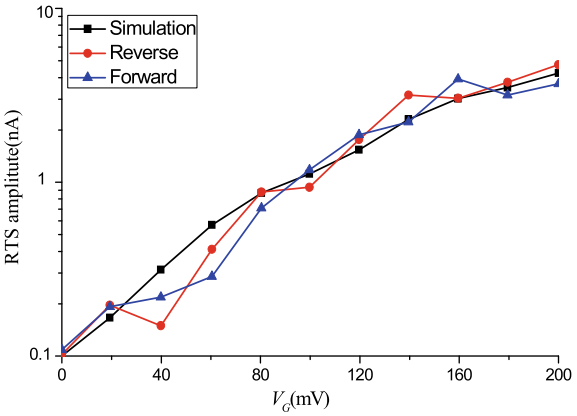

Fig. 10 Dependence of RTS amplitude and gate bias

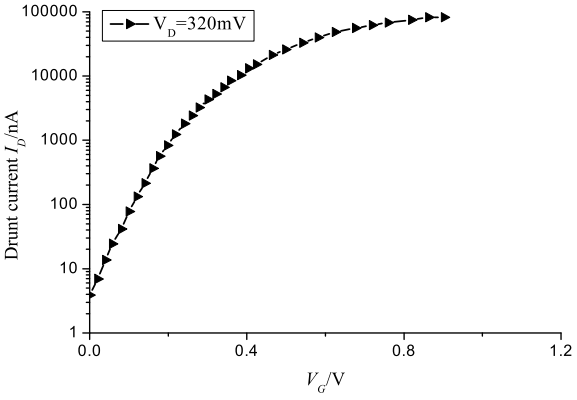

Fig. 11 Transition characteristic of the sample with the bias of V_D = 310 mv

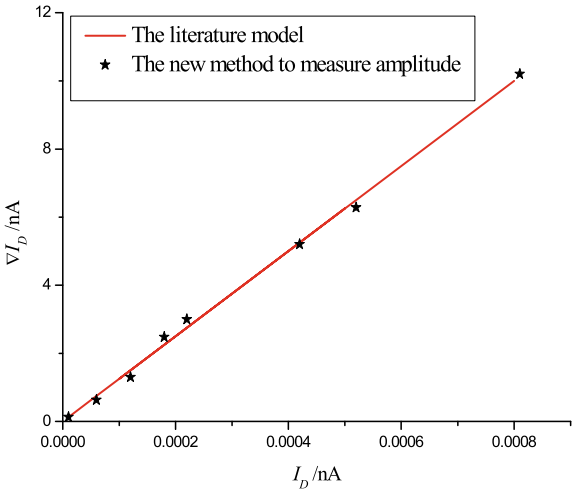

Fig. 12 Literature model and the new way to measure results

$$\Delta I_{\mathrm{D}} = \frac{4r_c^2}{WL - 2r_cL + 4r_c^2} I_{\mathrm{D}} \tag{10}$$

where W is the channel width, L is the channel length, r_c—is the distance between trap charge and channel (Fig. 12).

5 Conclusions

In this paper, NSP method and k-order median filter are used to identify RTN, It can judge the basic information such as RTN level value and center position of noise point. At the same time according to the error of relative value $e(n)$ $e(n-1)$, a improved LMS algorithm is proposed for the detection. The experimental measurements show that the following conclusions:

(a) The new method is in conformity with the mathematical model in the process of amplitude parameter extraction from RTN.
(b) The new method can reduce 40% under the same precision error,Compared with the traditional extraction algorithm of RTN time parameter.
(c) Improved error accuracy by 10%, Compared with the related literature proposed by difference equation.
(d) The new method solved the shortcomings of traditional algorithm existed in sensitive to noise.

Acknowledgements This work was supported by a grant from National Natural Science Foundation of China (NSFC 61271115). The authors would like to thank Xinxin Fan for excellent technical support and Professor Xiaojuan Chen for critically reviewing the manuscript.

References

1. Kola SR, Li Y, Thoti N (2020) Random telegraph noise in gate-all-around silicon nanowire MOSFETs induced by a single charge trap or random interface traps. J Comput Electron 19 (1):12–16
2. Fan XX, Yang LY, Chen XG et al (2018) Detection and analysis of random telegraph signal noise in P-MOSFET. Dian zi Jishu Yingyong 44(8):44–46
3. Möhle C, Zota CB, Hellenbrand M et al (2017) 1/ f and RTN in InGaAs Nanowire MOSFETs. Microelectron Eng 36(6):52–55
4. Cai XJ (2020) Quantum depraving induced by non-markovian random telegraph noise. Sci Rep 10(1):18–20
5. Both TH, Croon JA, Silva MD et al (2017) Autocorrelation analysis as a technique to study physical mechanisms of MOSFET low-frequency noise. IEEE Trans Electron Devices 18 (6):1–8
6. Fried JP, Bian XY, Swett JL et al (2020) Large amplitude charge noise and random telegraph fluctuations in room-temperature graphene single-electron transistors. Nanoscale 12(2):26–29
7. Ishida HK, Kagawa KC, Takashi ZB et al (2018) Multi-aperture-based probabilistic noise reduction of random telegraph signal noise and photon shot noise in semi-photon-counting complementary-metal-oxide-semiconductor image sensor. Sensors 8(4):26–32
8. Li Z, Sotto M, Liu FY et al (2018) Random telegraph noise from resonant tunneling at low temperatures. Sci Rep 8(1):4–9
9. Yian YC, Potirakis SM, Stavrinides SG et al (2019) Intermittency-induced criticality in the random telegraph noise of nanoscale UTBB FD-SOI MOSFETs. Microelectron Eng 16 (8):216:219
10. Martin J, Rodrigue R, Nafria M et al (2014) New weighted time lag method for the analysis of random telegraph signals. IEEE Electron Device Lett 35(4):479–481

11. Ban M (2020) Decoherence of a two-quite system interacting with initially correlated random telegraph noises. Quant Inf Process 19(2)
12. Saraza PC, Martin JM, Castro RL et al (2019) A detailed study of the gate/drain voltage dependence of RTN in bulk NMOS transistors. Microelectron Eng 19(8):215–217
13. Awano H, Hiromoto M, Sato T (2015) An efficient method for calculating RTN-induced failure probability of an SRAM cell. Design Autom Test 16(2):346–349
14. Markus H, Pekka O, Johannes K et al (2019) Low-frequency noise in nanowire and planar III-V MOSFETs. Microelectron Eng 26(16):215–220

Evaluation of Interactive WebSIR Using Software Usability Measurement Inventory (SUMI)

Mohd Suffian Sulaiman and Azri Azmi

Abstract The classical studies of information retrieval such as precision, recall, accuracy and F-measure, detached the human out from the model of evaluation. As this study have proposed a model that would engage with the user, the assessment must also take into account the experiences that exist between users and systems. In this paper, the Software Usability Measurement Inventory (SUMI) is used to evaluate a semantic image retrieval application namely as WebSIR. WebSIR is a web-based application that developed using Java programming language, Liferay and Jena. A collection of questions derived from the SUMI instrument were used. The results demonstrated that 85% evaluation test of respondents are satisfied and they considered this application is easy to be used.

Keywords SUMI · Liferay · Semantic image retrieval · Interactive information retrieval

1 Introduction

The evaluation is performed to further evaluate the efficiency of the program proposed. A good information retrieval system has a better strategy and offers a better classified list to satisfy the information needs of the user. According to the Cranfield paradigm, a document collection (the document may be in the form of articles or images), a set of queries (or topics) and relevant judgements identified for the document collection are needed to determine the quality of the retrieved results provided by a retrieval system [1]. Generally, the evaluation performance for

M. S. Sulaiman (✉)
Faculty of Computer and Mathematical Sciences, Universiti Teknologi MARA (UiTM), Shah Alam, Selangor, Malaysia
e-mail: Suffian@tmsk.uitm.edu.my

A. Azmi
Razak Faculty of Technology and Informatics, Universiti Teknologi Malaysia (UTM), Kuala Lumpur, Malaysia

Z. Zakaria and S. S. Emamian, *Advances in Electrical and Electronic Engineering and Computer Science*, Lecture Notes in Electrical Engineering 741,
https://doi.org/10.1007/978-981-33-6490-5_10

information retrieval studies such as precision, recall, F-measure and accuracy were used [2, 3]. This form of evaluation, however, is still insufficient to determine whether the consumers are pleased with using it before the program can be handed over to the consumer. In other words, the classical evaluation of information retrieval usually asks the question, can this program get relevant documents? While the interactive evaluation of information retrieval raises the question of whether people should use this program to access relevant documents [4].

2 Related Work

The user acceptance is very critical otherwise the program or product produced does not make any sense for the users. Therefore, an evaluation must be carried out before a product can be delivered to the consumer. 24 questionnaires evaluations can be used since the late 1980s until today and five of them have been shortlisted based on the highest number of quality criteria as shown in Table 1 [5]. The five questionnaires are Questionnaire for User Interface Satisfaction (QUIS) [6], Usefulness, Satisfaction and Ease of Use Questionnaire (USE) [7], Software Usability Measurement Inventory (SUMI) [8], Technology Acceptance Model questionnaire (TAM) [9] and Purdue Usability Testing Questionnaire (PTUQ) [10].

The QUIS is a method designed to measure subjective satisfaction of users with particular aspects of the interaction between the person and computers.

Table 1 Usability criteria

Usability criteria		QUIS	TAM	SUMI	PUTQ	USE
ISO 9421-11 criteria [11]	Effectiveness	X		X		X
	Efficiency		X	X		
	Satisfaction	X		X		X
ISO 9241-112 criteria [12]	Detectability	X	X	X		
	Discriminability	X		X	X	
	Appropriateness			X	X	
	Consistency	X		X	X	X
	Comprehensibility	X	X	X	X	
Scapin and Bastien criteria [13]	Guidance	X		X	X	X
	Workload			X	X	X
	Explicit control			X	X	
	Adaptability	X	X	X	X	X
	Error management	X		X	X	X
	Consistency	X		X	X	X
	Significance of codes	X		X	X	
	Compatibility			X	X	

A multi-disciplinary research team at the University of Maryland Human-Computer Interaction Lab, created it in 1987. The QUIS is currently available in version 7.0 with a demographic questionnaire, a 6-scale indicator of overall device efficiency and 9 different design factors. The USE measures a product or service's subjective usability. It has a 30-item survey that examines four usability dimensions: utility, ease of use, ease of learning and satisfaction. This metric applies to different usability assessment scenarios because it is non-proprietary and technology-agnostic. Items in the USE also have good face validity with a clear and appropriate description. The SUMI is a rigorously tested and validated tool for assessing the usability of a computer from end-users. SUMI also used to assess the user experience when it first appeared in the 1990s. The TAM was one of the most prominent technologies acceptance models, with two key factors shaping an individual's intent to use modern technology: perceived user-friendliness and perceived usefulness while the PTUQ was developed at the University of Purdue, based on eight human factors related to the usability of the program. It is derived from the experimental and theoretical basis outlined in the published literature. PTUQ has strong construct validity and content validity. The usability questionnaire will eventually be used to extract usability index measurements for each application. Thus, the emphasis on the user-friendly design of computer software systems would be further increased.

Based on five shortlisted questionnaires, the SUMI was selected to evaluate the program because it was rigorously tested and proven method of measuring software quality from the end user's point of view and fulfil all the usability criteria as shown in Table 1 that adapted from Assila et al. (2016). A set of questions that are taken from SUMI instrument was used. Compared to other evaluation questionnaires, SUMI cover all the usability criteria such as effectiveness, efficiency, satisfaction, detectability, discriminability, appropriateness, consistency, comprehensibility, guidance, workload, explicit control, adaptability, error management, consistency, significance of codes and compatibility.

3 Methodology

WebSIR is an application developed by using Java programming language, Liferay enterprise portal technology [14] and Jena toolkit [15] that provide an application programming interface (API) for Resource Description Framework (RDF) [16]. It has four functional requirements which are input text query, view the initial result, select related properties and view the filtered result as illustrated in Fig. 1 [17]. The use case diagram showing a series of use cases and actors and their relations; use case diagrams describe a system's static use case view [18]. In WebSIR, the user needs to enter a natural language query inside the search text box. Then, the user can view the initial result once the submit button clicked. Next, the user needs to mark related properties to filter the initial result that is dynamically displayed with the initial queried results. The dynamic means the list of properties can flexibly

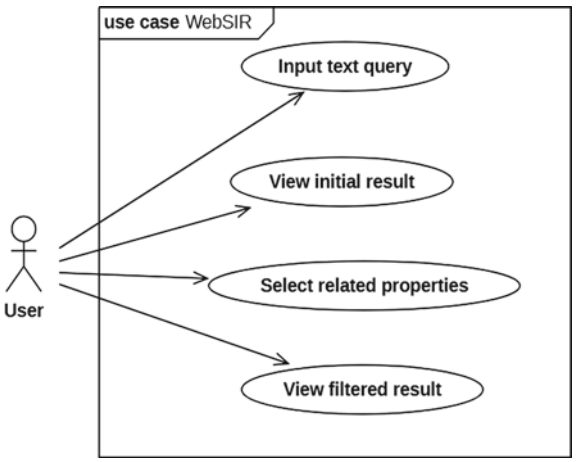

Fig. 1 Use case diagram of WebSIR

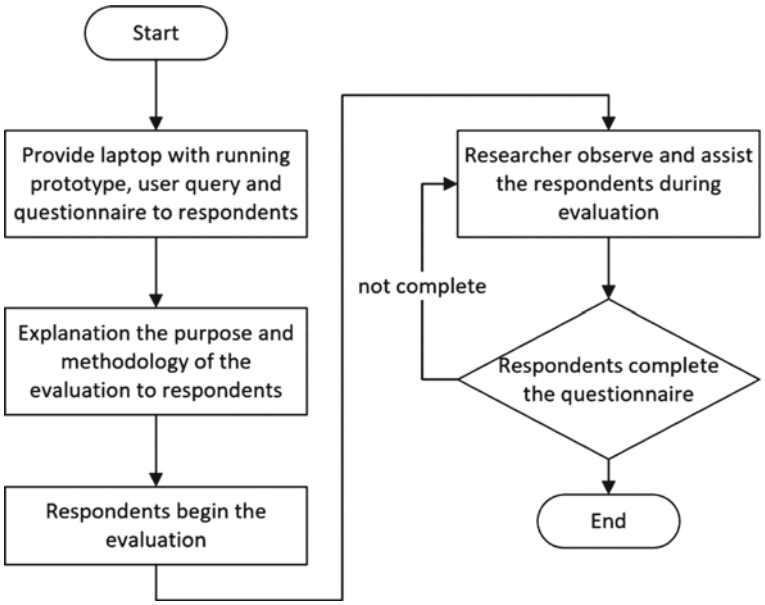

Fig. 2 Flow chart of SUMI evaluation

change depending on the retrieval query. Then, the marked properties are fed back into the system as a new redefined query for the following cycle of the retrieval process to obtain the better queried result [19].

The usability evaluation of the program was done by meeting the respondents physically and the flow of SUMI evaluation can be illustrated in Fig. 2. During the meeting, the laptop with running program, user query and the questionnaires are provided. The researcher met with the respondents for 10 min to explain the

purpose of the measurement and explain the methodology of SUMI evaluation. The respondents received the verbal instructions from the researcher, throughout the evaluation session. The researcher was present to help with any difficulties with the questionnaire and to answer questions asked from respondents. For next phase the users were asked to complete the SUMI questionnaire for user-interaction satisfaction. The evaluation sessions lasted around 20 min each.

The program and questionnaire were tested by ten individuals. All of them are an undergraduate student from Faculty of Applied Sciences, Universiti Teknologi MARA (UiTM), Shah Alam, Selangor, Malaysia. As part of the evaluation process, we ensured that all respondents had some basic knowledge to search the herbal medicinal plant information using a web browser.

4 Result and Discussion

The 20 SUMI questionnaires were selected from 50 items which the respondents need to select one of three responses ("Agree", "Undecided" and "Disagree") [20]. For the analysis purpose, a certain value is assigned for each scale as shown in Table 2. The average is collected from the summation of input from the respondents. If the result is between 1.00 and 1.99, it shows the user agreed with the specific measurement of the program. If the result is between 2.00 and 2.99, it shows the user is undecided and if the result is between 3.00 and 4.00, it shows the user disagrees with the program. Table 3 shows the details of the result.

Table 2 Attribute in the evaluation form

Scale	Agree	Undecided	Disagree
Value	1.00–1.99	2.00–2.99	3.00–4.00

Table 3 Result of evaluation test

No.	Questions	Result (Average)
1	The software reacts quicker to input	1.17
2	The directions and prompt are beneficial	1.12
3	Simple to learn how to use the software	1.16
4	The support information is really helpful	1.2
5	Spend less time mastering the software	1.17
6	The software is compliant	1.18
7	Information presented is transparent and comprehensible	2.45
8	Enough on-screen details if needed	2.57
9	The software is reliable	1.14
10	Can understand and act on the supplied information	1.12
11	The software is not awkward	2.44

(continued)

Table 3 (continued)

No.	Questions	Result (Average)
12	Less to learn before you can use the software	1.2
13	Operation can be carried out right away	1.28
14	The software is not frustrating	1.24
15	The software had fixed the problem	1.21
16	Menu structure is rational	1.13
17	Can be economical of keystroke	1.23
18	Few required action	1.16
19	Simple to make software exactly what you want	1.15
20	The software provided correct results	1.24

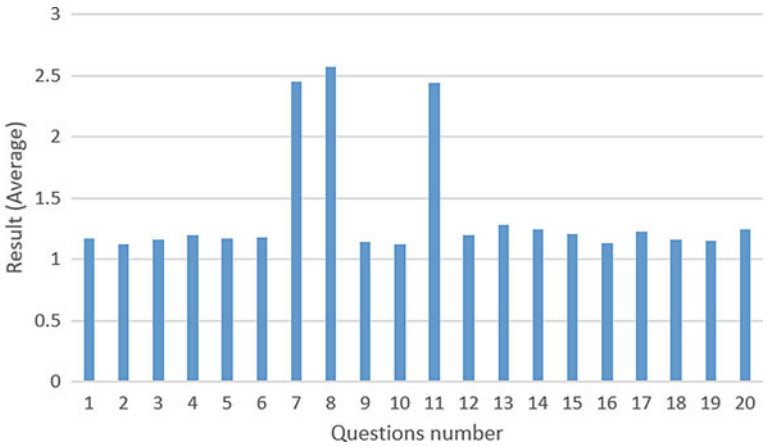

Fig. 3 Result of evaluation test graph

Figure 3 shows the respondent's feedback that can be categorized into two categories namely as agree and undecided. No feedback goes to disagree category. From the 20 questions, the respondents could not indicate the feedback in three questions which are information presented is transparent and comprehensible, enough on-screen details if needed and the software is not awkward. This is because the program dealing with the variety of datatype properties, which the respondents need to be understood before they can proceed with the searching enhancement process.

5 Conclusions

This paper presents interactive WebSIR evaluations using SUMI. Overall, the results show that the respondents are satisfied with the program and they considered it possible to use the program even though the issue of bias can be happening when

involving with human interaction. The result indicates that 85% evaluation test are satisfied by respondents. For future study enhancement, the coverage of metadata can be extended not only for the public user but to the entire related user. It will provide the real user in this domain with a more comprehensive dataset.

Acknowledgements The authors gratefully acknowledge the funding support received from Faculty of Computer and Mathematical Sciences, Universiti Teknologi MARA (UiTM), Malaysia.

References

1. Jones KS, Willett P (1997) Readings in information retrieval, 1st edn. Morgan Kaufmann Publishers, Inc.
2. Del Bimbo A (1999) Visual information retrieval, 1st edn. Morgan Kaufmann, California, USA
3. Manning CD, Raghavan P, Schutze H (2008) An introduction to information retrieval. Cambridge University Press, New York, USA
4. Kelly D (2009) Methods for evaluating interactive information retrieval systems with users 3 (1–2)
5. Assila A, De Oliveira K, Ezzedine H (2016) Standardized usability questionnaires: features and quality focus. J Comput Sci Inf Technol 6(1):15–31
6. Chin JP, Diehl VA, Norman KL (1988) Development of an instrument measuring user satisfaction of the human-computer interface. Conf Hum Factors Comput Syst Proc, Part F1302:213–218. https://doi.org/10.1145/57167.57203
7. Lund AM (2001) Measuring usability with the USE questionnaire. Usability Interface 8(2):3–6. https://doi.org/10.1177/1078087402250360
8. Kirakowski J, Corbett M (1993) SUMI: the software usability measurement inventory. Br J Educ Technol 24(3):210–212. https://doi.org/10.1111/j.1467-8535.1993.tb00076.x
9. Davis FD (1989) Perceived usefulness, perceived ease of use, and user acceptance of information technology. MIS Q 13(3):319–340
10. Lin HX, Choong YY, Salvendy G (1997) A proposed index of usability: a method for comparing the relative usability of different software systems. Behav Inf Technol 16(4–5):267–277. https://doi.org/10.1080/014492997119833
11. ISO 9241-11 (1998) Ergonomic requirements for office work with visual display terminals (VDTs): guidance on usability
12. ISO 9241-112 (2017) Ergonomics of human-system interaction—Part 112: principles for the presentation of information
13. Bastien JMC, Scapin DL (2006) Ergonomic criteria for the evaluation of human-computer interfaces to cite this version: HAL Id: inria-00070012
14. Yuan JX (2010) Liferay portal 6 enterprise intranets. Packt Publishing
15. McBride B (2002) Jena: a semantic web toolkit. IEEE Internet Comput 6(6):55–58
16. Sulaiman MS, Nordin S, Jamil N (2017) An object properties filter for multi-modality ontology semantic image retrieval. J Inf Comun Technol 16(1):1–19
17. Sulaiman MS, Nordin S, Jamil N, Halin AA (2014) Multi-modality ontology for herbal medicinal plant semantic based image retrieval. In: Knowledge Management International Conference (KMiCE)

18. Sulaiman MS, Ghani MKA (2011) Software requirement, analysis and design. Object Oriented Approach UML, Penerbit UTeM
19. Sulaiman MS, Nordin S, Jamil N (2015) Enhancing the performance of multi-modality ontology semantic image retrieval using object properties filter. In: International conference on computing and informatics (ICOCI)
20. Mansor Z, Kasirun Z, Yahya S, Arshad N (2012) The evaluation of webcost using software usability measurement inventory (SUMI). Int J 2(2):197–201

Raspberry Pi Based Wireless Interface System for Automated Microfabrication in the Context of Industry 4.0

Yih Bing Chu and Weng Kent Yap

Abstract The context of Industry 4.0 emphasizes on networking of manufacturing stations to a remote server for process planning and visualization. Especially for electronics production which is sensitive to process variations, networking of the manufacturing stations facilitates the monitoring of manufacturing stations remotely. In contrast with manual look up of the machines, the aforementioned approach allows prompt notification in real-time to manufacturer for immediate resolution and as a result, breakdown time of the production can be minimized. Therefore, this paper presents a wireless interface system for electronics microfabrication stations. Each microfabrication stations are interfaced with a WiFi module for wireless data transmission to a remote server established on Raspberry Pi. The experimental setup and testing of the developed system is presented in this paper for public interest.

Keywords Industry 4.0 · Microfabrication · Photolithography · Raspberry Pi · Wireless interface system

1 Introduction

In current electronics manufacturing industry, patterns of the devices are transferred using photolithography techniques. Association of various stations such as coating stations to deposit photoresist film on wafer, ultraviolet lighting station for transferring the device pattern onto the photoresist film and etching station to remove the excessive metal layers are essential to form the final electronic devices [1]. However, often due to the small aspect ratio of the metal layers, the dimension or feature size of the fabricated device is often subjected to unwanted deviation during the entire microfabrication processes. Hence, networking of the stations are

Y. B. Chu (✉) · W. K. Yap
Tunku Abdul Rahman University College, Kuala Lumpur, Malaysia
e-mail: allan.chu.y.b@gmail.com

Z. Zakaria and S. S. Emamian, *Advances in Electrical and Electronic Engineering and Computer Science*, Lecture Notes in Electrical Engineering 741,
https://doi.org/10.1007/978-981-33-6490-5_11

required to communicate the process discrepancies between each other and coordinate the production of electronic devices systematically.

In accordance to the current industry revolution, the interconnection of machines to a centralized network facilitate the transfer and processing of production data. In this context, the remote server is responsible to interpret, control and provides data visualization of the manufacturing process to interested parties outside of the manufacturing stations. This mechanism assists manufacturer to manage more effectively the fabrication compared to manual look up of the production machine and in addition allows real-time notification for prompt action should breakdown occurs. Despite the inception of Industry 4.0, the development of such system especially for the aforementioned microfabrication process has yet been reported. In view of this, the development of such system is both strategic in time and advantageous. Therefore, the objective of this research is to design an interconnected interface between the microfabrication stations which allows the data to be communciated to a remote server for real-time visualization. In this work, WeMos WiFi ESP8266 is used to implement the wireless interface between the production stations and Raspberry Pi microcontroller is applied as the embedded server for remote visualization. The microfabrication stations should transfer the production status and able to be visualized at the remote server.

The remainder of this paper is structured as follows: Sect. 2 outlines the proposed methodology; Sect. 3 describes the initial implementation of the system and an evaluation of the proposed system; Sect. 4 draws the conclusion, limitation and future improvement of the work.

2 Methods

In electronics manufacturing, most devices are patterned in two steps; patterning of photoresist film on top of the functional material and transferring the photoresist pattern onto the functional material. Photolithography has been the forerunner among the patterning techniques for microfabrication of miniature devices such as microelectronics, micro devices and micro-electro-mechanical-system (MEMS). The technology involves making a mask and then project the mask pattern via ultraviolet (UV) light onto a photoresist-coated wafer. Lastly, the wafer is developed and etched to remove the excessive photoresist and metal layers respectively and form the final electronics pattern. The first portable and low-cost photolithography station was reported by Huntington et al. in 2011 however for small scale production and laboratory use [2]. The configuration recorded a resolution of 200 nm feature size at the consumption of 0.2% power of the mercury-vapor lamps used in the industrial mask aligner system. Similarly, a portable UV lighting station will be constructed along with tailor-made microfabrication stations. For simplicity, commercial 4 inches copper board readily coated with copper layers will be used for testing of the proposed system. Figure 1 shows the general microfabrication processes for microfabrication of electronic devices.

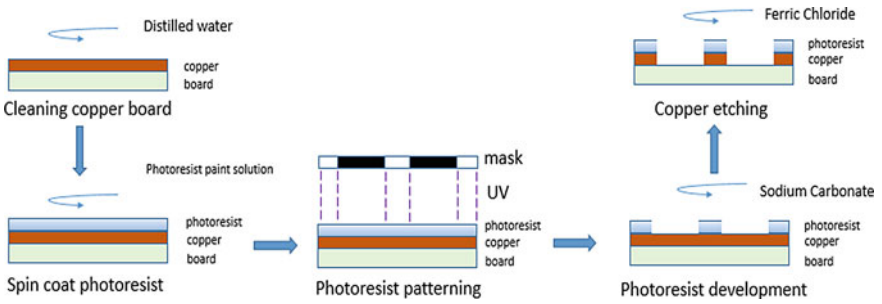

Fig. 1 Microfabrication processes for electronic devices

In this work, WiFi module ESP 8266 is applied as communication interface of the stations with the remote server. The WiFi module utilizes Message Queuing Telemetry Transport (MQTT) data transfer protocol which is suitable for light-weight data transmission and wireless sensing application [3]. In recent years, the WiFi module has been used in application such as smart home monitoring [4], heart rate monitoring [5] and monitoring of oyster mushroom cultivation [6]. The proposed system consists of spin coater for cleaning and coating of photoresist onto the copper board, UV lighting station to form patterns onto the coated photoresist layer and robotic arm handler to transfer the copper board between the spin coater and UV lighting station. All of these stations are installed with Wemos and communicated to a remote computer (Raspberry Pi). In this work, the spin coater station is applied to perform cleaning of the copper board, coating of photoresist and wet etching. The experiments and testing of the proposed system are conducted in room

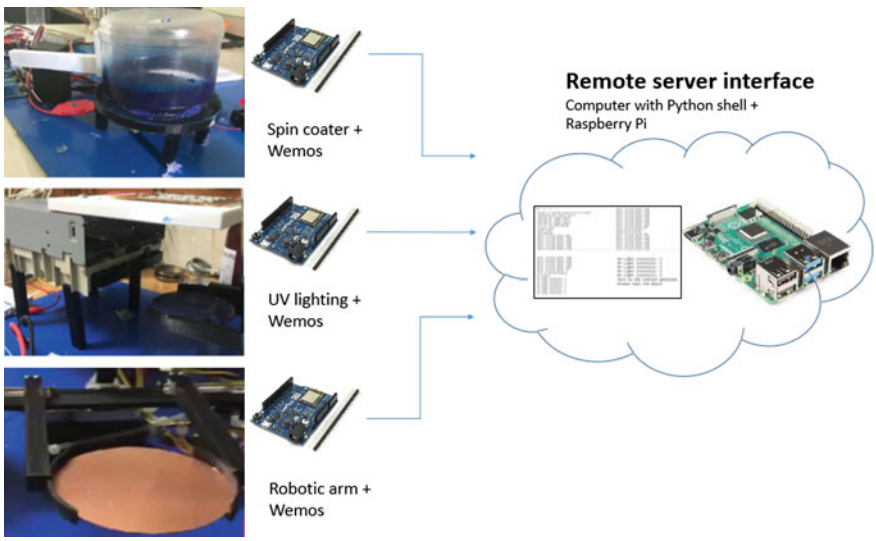

Fig. 2 Design of the proposed system

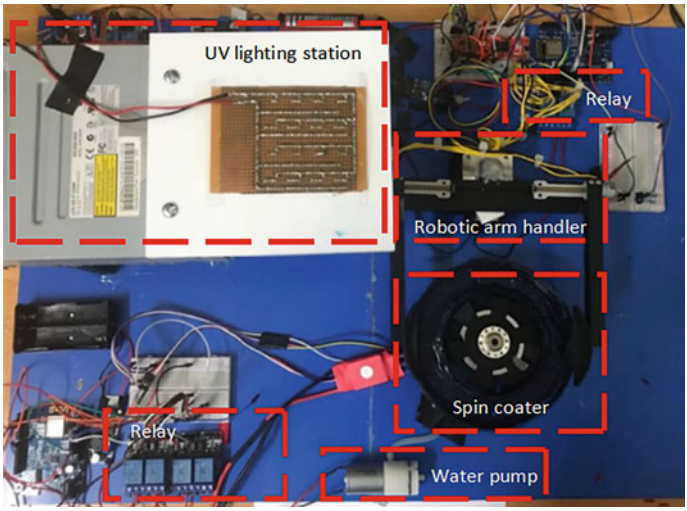

Fig. 3 The proposed setup (top view); spin coater removed casing

temperature condition. Figures 2 and 3 shows the design and overall setup of the proposed system respectively.

The spin coater is built-in with encoder sensor (tcrt5000 optical sensor) to determine the speed of rotation. The encoder will then feedback the speed measurement to the motor to spin till a desirable speed is achieved. Such system is also termed as close-loop control system. In this work, 1,000 rpm is set as default spinning speed for all the processes under the spin coater operation. For the UV patterning station, 16 pieces of UV LED (each connected in series with a 100 Ohm resistor) is aligned in square fashion and connected to a 5 V power supply. Similarly, a VEML 6070 UV intensity sensor is built-into the station to feedback the desireable UV intensity. The mask for patterning is printed in black colour on a transparent sheet using commercially available printer.

3 Results and Discussions

Firstly, the robotic arm handler transfers the coper board from its initial position to the spin coater. Then, the nozzle at the top of the spin coater casing sprays distilled water to clean the surface of the copper board. The cleaning process ends after drying of the copper board via spinning. After this, photoresist paint is dipped onto the surface of copper board and spinned to form the photoresist dry film. After that, the robotic arm handler transfers the cleaned copper board to UV lighting station to form the desired pattern onto the coated photoresist film. Subsequently, the robotic handler transfers the copper board from the UV lighting station back to the spin

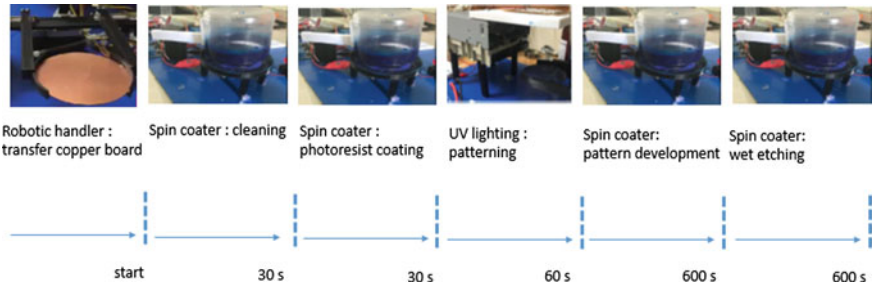

Fig. 4 Timing sequence of the overall processes

Fig. 5 Patterning mask (left); Copper board after development (mid); copper board after etching (right)

coater. The spraying cum spinning process continues at the spin coater with developer solution (1 g sodium carbonate per 1,000 ml distilled water) and copper etchant (ferric chloride) to form the final electronic patterns on the copper layer. Figure 4 shows the timing sequence of the overall processes.

The proposed system was tested for feature patterning on the 4 inches copper board based on the design shown in Fig. 5 (left). However, the surface of the coated photoresist after the spin coating process was found uneven and the surface roughness was found technically difficult to be approached due to the nature of the photoresist material used (photoresist paint). Despite being diluted in different solutions using distilled water, deionized water and acetone respectively, never the less, due to the viscosity of the photoresist paint, the dilution is difficult to curb the surface roughness and unevenness of the coated layer. The problem persists in the development and etching process, where the coated photoresist layer was still not able to be removed. The complete development of the photoresist layer was not formed even after 10 minutes has collapsed. Therefore, the remainder of the photoresist layer has to be removed by means of manual brushing before etching of the copper layers. Figure 5 shows the copper board after developed (mid) and etched (right).

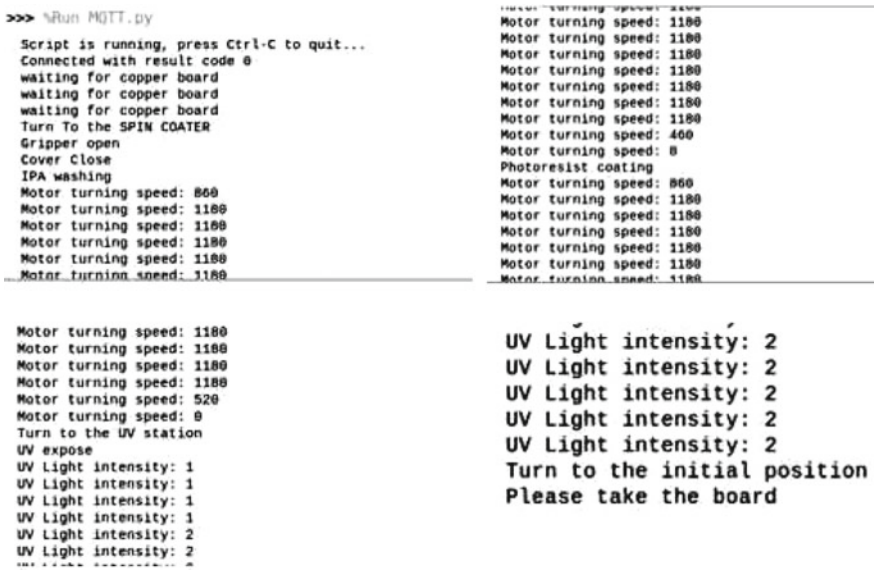

Fig. 6 Visualization of the manufacturing processes on python shell

In spite of the technical difficulty encountered, the microfabrication stations were able to communicate and interact with the remote server hosted on Raspberry Pi. Figure 6 shows visualization of the manufacturing processes displayed on python shell of the remote computer (Raspberry Pi).

4 Conclusions

The work proposed development of wireless interface system for microfabrication stations to a remote server for real-time process visualization. Compared with traditional machine look up, the developed system enables monitoring of all the machines and prompts manufacturer for immediate resolution in real-time. Especially in large scaled production, the mechanism is essential for safeguarding manufacturing down time and ensures the production is able to be delivered on time. The developed system can be easily implemented on any existing stations. Despite of the successful implementation, further experimentation is still required to standardize the application in actual production field. Limitation of the proposed system such as uneven surface thickness due to the use of viscous photoresist solution and in-line process monitoring of the feature size of the devices under fabrication should be included as future improvement of the work.

Acknowledgements The authors wish to thank Ms. Khairun Nisak and Department of Electrical and Electronics Engineering, Tunku Abdul Rahman University College (TARUC) for the support provided to this work.

References

1. Pimpin A, Srituravanich W (2011) Review on micro- and nanolithography techniques and their applications. Eng J 16(1):37–56
2. Huntington MD, Odom TW (2011) A portable, benchtop photolithography system based on a solid-state light source. Small 7(22):3144–3147
3. Tukade TM, Banakar R (2018) Data transfer protocols in IoT—an overview. IJPAM 118 (16):121–138
4. Syafaah L, Minarno AE, Sumadi FDS, Mukti GW (2019) Distance measurement of ESP8266 for control and monitoring in smart home application. J Phys Conf Ser 1381:012058
5. Hamidi EAZ, Effendi MR, Ramdani F (2019) Heart rate monitoring system based on website. J Phys Conf Ser 1402:044003
6. Mohammed MF, Azmi A, Zakaria Z, Tajuddin MFN, Isa ZM, Azmi SA (2018) IoT based monitoring and environment control system for indoor cultivation of oyster mushroom. J Phys Conf Ser 1019:012053